Doctoral Dissertations   Student Theses and Dissertations

Fall 2014

Part I: In-situ fluorometric quantification of microalgal neutral lipids Part II: Thermal degradation behavior of investment casting polymer patterns

Hongfang Zhao

Follow this and additional works at: https://scholarsmine.mst.edu/doctoral_dissertations

Part of the Chemistry Commons

Department: Chemistry

Recommended Citation

PART I: IN-SITU FLUOROMETRIC QUANTIFICATION OF MICROALGAL

NEUTRAL LIPIDS

PART II: THERMAL DEGRADATION BEHAVIOR OF INVESTMENT CASTING

POLYMER PATTERNS

by

HONGFANG ZHAO

A DISSERTATION

Presented to the Faculty of the Graduate School of the

MISSOURI UNIVERSITY OF SCIENCE AND TECHNOLOGY

In Partial Fulfillment of the Requirements for the Degree

DOCTOR OF PHILOSOPHY

In

CHEMISTRY

2014

Approved by

Paul K. Nam, Advisor
Von L. Richards, Co-Advisor
Yinfa Ma
V. Prakash Reddy
Jeffrey G. Winiarz
K. Chandrashekhara

PUBLICATION DISSERTATION OPTION

This dissertation consists of the following five articles that have been published or will be submitted for publication as follows:

Paper I (pages 33-48) is intended for submission to ALGAL RESEARCH.

Paper II (pages 49-62) is intended for submission to the JOURNAL OF APPLIED PHYCOLOGY.

Paper III (pages 63-80) has been submitted to the INTERNATIONAL JOURNAL OF METALCASTING.

Paper IV (pages 81-94) is intended for submission to TRANSACTIONS OF THE AMERICAN FOUNDRY SOCIETY.

Paper V (pages 99-119) as Appendix A was published in TRANSACTIONS OF THE AMERICAN FOUNDRY SOCIETY.

ABSTRACT

Research described in this dissertation covers two topics. Part-I is focused on in-situ determination of neutral lipid content of microalgae using a lipophilic fluorescent dye. The traditional Nile red stain-based method for detecting microalgal intracellular lipids is limited due to varying composition and thickness of rigid cell walls. In this study, the addition of dilute acid and heating of solution, were found to greatly enhance staining efficiency of Nile red for microalgal species evaluated. Oil-in-water (O/W) microemulsion stabilized by a non-ionic surfactant was employed as a pseudo-standard that mimics lipid-bearing microalgal cells suspended in water. The average neutral lipid contents determined were very close to the results obtained by traditional gravimetric method and solid phase extraction.

Part II of the dissertation explores thermo-physico-chemical properties of polymeric pattern materials, including expanded polystyrene (EPS) foam, polyurethane foam, and epoxy stereolithography (SLA) patterns, that are used in investment casting. Density, elastic modulus, expansion coefficient, thermal degradation behavior, *etc*. were experimentally investigated for their effects on metal casting quality. The reduction in toxic hydrogen cyanide (HCN) generated during thermal decomposition of polyurethane pattern was achieved by increasing either oxidant level or residence time in heated zone. Thermal degradation kinetics of the pattern materials were examined with a thermogravimetric analysis and activation energies were determined by Kissinger and Flynn-Wall-Ozawa methods.

ACKNOWLEDGMENTS

I would like to express my deepest gratitude to my advisor Dr. Paul Nam for his financial support, guidance and encouragement through the course of pursuing my PhD. His creative thinking and critical attitude improved my research skills and prepared me for future challenges. I also extend my sincere gratitude to my co-advisor Dr. Von Richards for his financial support and constructive criticism during my graduate study. My personality has been highly influenced by his valuable insights and wisdom. Special thanks are also given to Dr. Keesoo Lee from Lincoln University for her continuous encouragement, guidance and help with my study and research.

I extend my gratitude to my other committee members, Dr. Yinfa Ma, Dr. V. Prakash Reddy, Dr. Jeffrey Winiarz, and Dr. K. Chandrashekhara for their time and assistance with my graduate study and research work.

I would like to thank my former and current lab members, Dr. Ganesh, Dr. Dayananda, Nick, and Pengpeng from the Department of Chemistry, Haifeng from the Department of Mechanical and Aerospace Engineering; Simon, Mingzhi, Samrat, and Wesley from the Department of Material Science and Engineering for their help with my research work.

I am truly indebted to my parents for their unconditional love, inspiration, and spiritual guidance in my lifetime. My deepest gratitude must be given to my husband, Dr. Rongpeng Wang and our children, Ella and Aiden for their constant love, understanding and encouragement.

TABLE OF CONTENTS

LIST OF ILLUSTRATIONS

xii

LIST OF TABLES

SECTION

1. INTRODUCTION

1.1. WHAT IS MICROALGAE

Any organism with chlorophyll a and a thallus not differentiated into roots, stems and leaves is regarded as an alga[1]. Algae are photosynthetic organisms that use energy from the sun to combine water with carbon dioxide (CO_2) to produce biomass. Macroalgae, or seaweed, are found in both marine and freshwater environments and can grow to considerable size up to 60m in length. Microalgae, known to biologists as phytoplankton, refer to microscopic algae. Microalgae are primarily distributed in not only aquatic but also terrestrial environmental conditions because they have either a unicellular or a simple multicellular structure. A large variety of microalgal species (50,000) exists in the world today. Of these 50,000, approximately 30,000 have been studied and analyzed[2]. With an increased emphasis on the production of natural oil for biodiesel, microalgae has become the exclusive focus of research as it offers many advantages over other available feedstocks[3-12].

Microalgae can be classified into the following four categories (in terms of abundance) according to their pigmentation, life-cycle, and basic cellular structure:

- **Diatoms (Bacillariophyceae)** Algae dominate the phytoplankton found in the ocean. Some can even be found in both fresh and brackish water. These unicellular organisms exhibit a very conspicuous number of golden brown colors. The storage product is chrysolaminarin (β-1.3-lined glucn). Lipids are also present.

- **Green algae (Chlorophyceae)** Green algae form one of the largest groups of algae (approximately 7500 species). These algae are abundant in freshwater. They contain chlorophyll a and chlorophyll b pigments, giving the algae green color. Their primary storage compound is starch (α-1,4-linked glucan). They can also produce a considerable amount of lipids under certain growth conditions.

- **Blue-green algae (Cyanophyceae or Cyanobacteria)** The presence of phycocyanin and phycoerythrin in the blue-green algal structure mask the chlorophyll pigmentation. The primary storage product is glycogen (α-1,4-linked glucan). These algae play an important role in fixing nitrogen from the atmosphere.

- **Golden algae (Chrysophyceae)** Golden algae exist primarily in freshwater, particularly in oligotrophic water that is low in calcium. These algae can appear either yellow, brown, or orange in color. Their storage products are chrysolaminarin (β-1.3-lined glucan) and lipid, which is similar to the diatoms.

1.2. ADVANTAGES OF USING MICROALGAE FOR BIODIESEL PRODUCTION

As the world's transportation and energy consumption continue to increase, the environmental damage produced by the emission of greenhouse gas (GHG) becomes even more severe[13]. GHG contributes not only to global warming but also to the environmental contamination and human being life's threat. Energy security is another important driving force behind the development of biofuels technology. Petroleum cost continues to increase due to reduction of crude oil reserves and difficulties in their extraction and processing[14]. The United States currently imports approximately two-

thirds of its petroleum and the U.S. Department of Energy (DOE)'s Energy Information

Administration paints a dismal picture of growing dependence on foreign oil[5,15]. These

issues reveal the importance and urgency of deploying renewable fuels for the entire

society.

Biodiesel and bio-ethanol are the two most common biofuels available today that

can replace diesel and gasoline, respectively. Biodiesel in the EU represents 82% of total

biofuels production and is still growing in Europe, Brazil, and United States based on

political and economic objectives[9]. As the same as other oilseed crops such as rapeseed

(in Europe) and soybean oil (in the U.S.), the natural oil made by algae is in the form of

triacylglycerols (TAGs), which have three long chains of tatty acids attached to a glycerol

backbone. The modification of TAGs through chemical reaction (transesterification) into

biodiesel is described as in the following reaction (Fig. 1.1):
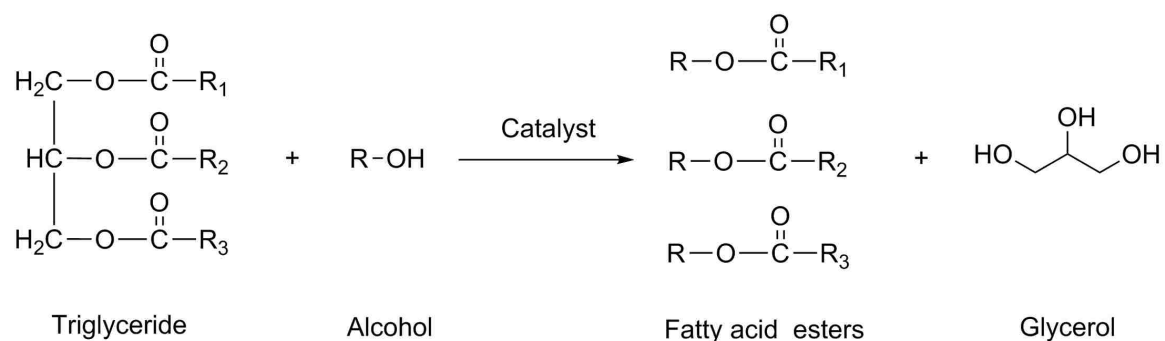
Fig. 1.1 Transesterification process of TAGs to produce biodiesel

After reaction of triglyceride with an alcohol in the presence of either an acid or a

base catalyst, fatty acid esters are formed. These fatty acid esters are known generically

as biodiesel, whose properties are very close to those of petroleum-based diesel fuel.

Algal biomass may offer significant advantages over other traditional feedstocks toward producing these biofuels. They require much less cultivation land area than other biodiesel feedstocks that have an agricultural origin; up to 49 or 132 times less when compared to rapeseed or soybean crops, respectively, for a 30% (w/w) of oil content in algal biomass[6]. Oleaginous microalgae have also demonstrated much higher growth rates and productivity, producing higher oil yields than that from oilseed crops (see Table 1.1). Certain algal species could produce at least 60 times higher oil yields than soybean can produce per acre of land on an annual basis[9].

Table 1.1 A comparison of oil yields from biomass feedstocks[15]

Crop	Oil Yield (Gallons/Acre/Yr)
Soybean	48
Camelina	62
Sunflower	102
Jatropha	202
Oil palm	635
Algae	1,000-6,500

Microalgae as a renewable biofuel feedstock has several unique advantages toward producing advanced biofuels:

- Microalgae have high growth rates with requirements of only sunlight and simple nutrients and can produce significant biomass yields per acre of cultivation[16-18].

- Microalgae can grow in a variety of environmental conditions, including harsh conditions. Thus they can minimize and possibly even avoid competition with

arable land and nutrients used for conventional agriculture, independent of seasonal changes.

- Microalgae can utilize NH_4^+, NO_3^-, and PO_4^{3-} in waste water, produced water, and saline water as nutrients to accumulate biomass during the removal treatment process[19,20].

- Microalgae can recycle carbon as CO_2 through biofixation during growth from industrial flue gases (*e.g.*, from power plants) and thus reduce greenhouse gas emissions[21].

- Microalgal biomass provides various high-value biological derivatives with many possible commercial applications, including biofuels, cosmetics, pharmaceuticals, nutrition and food additives, aquaculture, and pollution prevention[22-25].

1.3. MICROALGAL SPECIES SCREENING

The development of a simple screening procedure to estimate the lipid contents of microalgal cell is used to determine which strains have the best potential as biofuel production organisms. It is also critical to apply a significant effort toward microalgal isolation and screening in order to identify and maintain promising algal specimens for cultivation and strain development. Several factors must be considered in the sampling and selection process, including growing rate, lipid content, resistance to environmental condition changes, nutrient availability, and possibility of obtaining other valuable chemicals[26-28]. For commercial-scale biodiesel production, a high productivity of desired biofuel feedstocks such as lipids (primarily triacylglycerols), is an essential

characteristic[29]. The term "high lipid productivity" refers two main important factors: a high lipid content and a high growth rate of selected microalgal strains.

A number of studies have investigated applicable methods for lipid determination of microalgae. The most commonly used method for total lipid quantification is gravimetric measurement, which involves solvent extraction and weighing according to the Bligh and Dyer method or modified by Kates and Volcani or Folch method[30-32]. Each of these methods requires at least 10-15 mg of dry algal biomass for extraction so that a sufficient amount of lipid is extracted for accurate weighing. In addition to being both time consuming and labor intensive, these methods extract not only neutral lipids but also other lipids, including glycolipids, phospholipids, and sterols, which are not suitable for biodiesel production. Thin layer chromatography (TLC) has been reported as a rapid and reproducible semi-quantitative method to separate major lipid into several fractions, such as triglycerides, waxes, and free fatty acids [33, 34]. Other quantitative analysis methods, such as high performance liquid chromatography (HPLC), gas chromatography (GC), and the combination of these methods with mass spectrometry, have also been used to analyze lipid molecular species[35-37]. However, these separation techniques still have numerous steps and are time-consuming and not suitable for high-throughput screening. In an attempt to develop a rapid, easy-to-use, and reproducible screening procedure to identify microalgal strains with high lipid content, Cooksey introduced a direct spectrophotometric measurement using lipophilic dye Nile Red (9-diethylamino-5H-benzo[α]phenoxazine-5-one) as an ideal stain for detecting neutral lipids in microalgal cells[38]. Greenspan and Fowler first isolated Nile red from Nile blue and found that the Nile red would only fluoresce in a nonpolar environment at a yellow-green range

(excitation, 450-500 nm; emission, > 528 nm)[39]. Nile red staining was originally established for microalgae to provide either a qualitative or semi-quantitative determination of neutral lipid content[40-42]. Nile Red staining method is most useful during rapid screening of microalgae for their neutral lipid content since the method is quick.

The average lipid content varies between 1 and 70% for many microalgae. Some can even reach 90% of dry weight under certain conditions[3, 4, 6, 43]. Table 1.2 illustrates the lipid content and lipid productivities of different marine and freshwater microalgal species. Most common microalgae (*Chlorella*, *Cylindrotheca*, *Dunaliella*, *Isochrysis*, *Nannochloris*, *Nannochloropsis*, *Neochloris*, *Nitzschia*, *Phaeodactylum*, *Porphyridium*, *Schizochytrium*, and *Tetraselmis*) have a lipid content ranging from 20 to 50%. They also have a higher lipid productivity. Although *Botryococcus braunii* can reach a higher lipid level (75%), it is associated with low productivity. Therefore, lipid content, lipid productivity, and others factors, such as nutrient availability and cultivation conditions, should be considered simultaneously in the selection of either microalgal species or strains for biodiesel production.

Table 1.2 Lipid content and productivities of different microalgal species[2, 4, 6, 9, 18, 43-52]

Marine and freshwater microalgal species	Lipid content (% dry weight biomass)	Lipid productivity (mg/L/day)
Ankistrodesmus sp.	24.0-31.0	-
Botryococcus braunii	25.0-75.0	-
Chlorella emersonii	25.0-63.0	10.3-50.0
Chlorella sorokiniana	19.0-22.0	44.7
Chlorella vulgaris	5.0-58.0	11.2-40.0

Table 1.2 Lipid content and productivities of different microalgal species (cont.)

Chlorella sp.	10.0-48.0	42.1
Chlorella pyrenoidosa	2.0	-
Chlorella	18.0-57.0	18.7
Chlorococcum sp.	19.3	53.7
Dunaliella salina	6.0-25.0	116.0
Dunaliella primolecta	23.1	-
Dunaliella tertiolecta	16.7-71.0	-
Dunaliella sp.	17.5-67.0	33.5
Ellipsoidion sp.	27.4	47.3
Euglena gracilis	14.0-20.0	-
Haematococcus pluvialis	25.0	-
Isochrysis galbana	7.0-40.0	-
Isochrysis sp.	7.1-33.0	37.8
Monodus subterraneus	16.0	30.4
Nannochloris sp.	20.0-56.0	60.9-76.5
Nannochloropsis oculata.	22.7-29.7	84.0-142.0
Nannochloropsis sp.	12.0-53.0	37.6-90.0
Scenedesmus obliquus	11.0-55.0	-
Scenedesmus quadricauda	1.9-18.4	35.1
Scenedesmus sp.	19.6-21.1	40.8-53.9
Skeletonema sp.	13.3-31.8	27.3
Skeletonema costatum	13.5-51.3	17.4
Spirulina platensis	4.0-16.6	-
Spirulina maxima	4.0-9.0	-
Tetraselmis suecica	8.5-23.0	27.0-36.4
Tetraselmis sp.	12.6-14.7	43.4

1.4. MICROALGAL PROCESSING

A number of additional stages must be followed after microalgal species screening is complete before biofuels can be produced (Fig. 1.2). These processing steps are presented and discussed in the following subsections.

```
┌─────────────────────────────┐
│ Microalgae species isolation │
│        and screening         │
└─────────────────────────────┘
   Light, water │ │ CO₂, Nutrients
               ⇓
┌─────────────────────────────┐
│          Cultivation         │
└─────────────────────────────┘
               ⇓
┌─────────────────────────────┐
│      Harvesing and Drying    │
└─────────────────────────────┘
               ⇓
┌─────────────────────────────┐
│       Lipid extraction       │
└─────────────────────────────┘
               ⇓ Lipids and free fatty acids
┌─────────────────────────────┐
│      Biodiese production      │
└─────────────────────────────┘
```
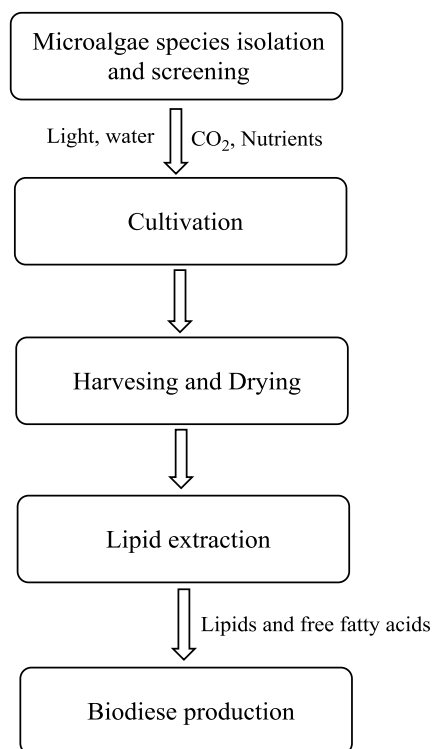
Fig. 1.2 Schematic of processing steps of microalgal biofuels

1.4.1. Cultivation. Several factors impact microalgal growth: light, temperature, nutrient concentration, O_2, CO_2, pH, salinity, and biological contaminants (other microalgae, bacteria, fungi, yeast, mould, and viruses). Operational factors, such as shear produced by mixing, dilution rate, depth, harvest frequency, and the addition of bicarbonates, can also affect their growth[52-54]. For biomass production, microalgae

require a sufficient supply of a carbon source and light to carry out photosynthesis. The energy conversion efficiencies from incoming sunlight to biomass can reach as high as 5%. This high yield, combined with different growing conditions, is why many researchers refer to microalgae as the "third generation biomass"[11].

   1.4.1.1 Metabolisms. Broadly speaking, microalgae can be cultivated via either autotrophic (or phototrophic), heterotrophic or mixotrophic metabolisms; and are capable of a metabolic shift as a response to changes in environment conditions, including pH[44].

   Autotrophic metabolism is the most commonly used cultivation condition for microalgal growth[49, 55, 56]. This metabolism occurs when microalgae use light (*e.g.*, sunlight) as the energy source and convert inorganic carbon dioxide (the carbon source) to glucose through photosynthetic reactions[57]. The requirement of using only CO_2 as a carbon source for both cell growth and oil production is the major advantage of using this cultivation method for microalgae. Autotrophic cultivation also experiences fewer contamination problems than do other types of cultivation. It is easy to scale-up and has a potential to utilize CO_2 from flue gases of factories, like power plant[58].

   Heterotrophic metabolism is another microalgal cultivation method, in which organic carbon is used as both energy and carbon source for biomass growth and lipid production without light[59]. A variety of organic carbon sources, such as glucose, acetate, glycerol, fructose, sucrose, lactose, galactose, and mannose, can be utilized for microalgal growth[60]. This type of cultivation method can avoid the problems associated with limited light that hinder high cell density in large-scale photobioreactors during autotrophic cultivation[57]. It yields a higher biomass productivity and higher lipid content than that obtained under autotrophic cultivation condition[61]. However, cost of an organic

carbon source is the main concern not only from commercial aspect, but also the exploitation of organic substrate (*e.g.*, lignocellulosic sugars) is competing for feedstocks with other biofuel technologies. Heterotrophic cultivation can also be contaminated very easily, particularly in open systems[58].

Mixotrophic metabolism is a cultivation method in which microalgae simultaneously use light for photosynthesis and both an organic and an inorganic carbon source (CO_2) for growth. As a result, microalgae can grow under either autotrophic conditions or heterotrophic conditions, or both[44]. Although lipid productivity is higher than other cultivation methods when mixotrphic cultivation is used, it is rarely used in microalgal oil production[60, 62].

1.4.1.2 Cultivation systems. Microalgal cultivation systems are broadly classified into open systems (such as lakes or ponds) and closed systems (known as photobioreactors; PBRs). Open ponds or raceways are the most common cultivation systems used worldwide to commercially produce microalgae.

In open ponds systems, an algal culture is directly exposed to the environment. Here, paddle wheels are used to mix and circulate the microalgal culture (Fig.1.3). This culture system is typically less expensive to build and operate than are photobioreactors. United States Department of Energy has extensively evaluated the large-scale production of microalgal biomass in raceway ponds for the purpose of making biodiesel[5]. Although they may produce large quantities of microalgal biomass, these large-scale productions require an extensive amount of land. The cultures are also easy to be contaminated by unwanted algae or bacteria. Open ponds are more susceptive to weather conditions, thus making it difficult to control water temperature, evaporation, and light.

Fig. 1.3 Open ponds/raceways used for microalgal cultivation[63]

Both closed ponds and PBRs are closed to the atmosphere (Fig.1.4). Thus, they can to some extent protect microalgal culture. They can either greatly reduce or in some instance eliminate the contamination and water evaporation of the culture. PBRs are flexible systems that offer better control of culture conditions and growth parameters (*e.g.*, pH, temperature, mixing, CO_2, and O_2). They also allow for higher microalgal densities (cell concentrations) and volumetric productivities. The application of PBRs in commercial plants and tested pilot level has been described elsewhere[64, 65]. However, very few PBRs have been developed for large-scale microalgal biomass production for a

number of reasons, including overheating, bio-fouling, oxygen accumulation, difficulty in

scaling-up, high cost of construction and operating, cell damage by shear stress, and the

deterioration of materials used for the photo-stage[44].

Fig. 1.4 Closed photobioreactors used for microalgal cultivation[58]

Many believe that a combination of PBRs and open ponds will promote

microalgal bulk cultivation [9,51]. Open pond technology cannot provide a sustainable

production of microalgal species although it has the advantage of industrial-scale

cultivation. Closed-system PBRs allow users to control sterility while also permitting the

continuous cultivation of a wide variety of species. However, their application has been limited to small-scale industrial production. The coupled PBRs and open ponds cultivation systems could resolve these issues.

1.4.2. Harvesting and Dewatering. Microalgae harvesting involves biomass recovery from a culture media, which is an essential component for the production of almost all microalgal products. The harvesting process may contribute to 20-30% of total biomass production costs[66]. The cell concentration of a microalgal culture is very low; it generally lies within the range of 0.1-4.0g/L ash free dry weight[67]. An efficient harvesting method is needed to remove the large quantities of water from the microalgae culture. This method may involve one or more steps of applying physical, chemical or biological ways. Depending on particles properties (size, specific gravity, zeta-potential), fluid properties (i.e. composition, nutrients, ionic strength, salinity and pH) and desired product quality, a suitable harvesting method should be selected. The harvesting method includes sedimentation, centrifugation, filtration, ultra-filtration, and sometimes with an additional flocculation step or with a combination of flocculation-flotation.

Flocculation is used to aggregate the microalgal cells and thus increase the effective particle size. Doing so then enhances sedimentation efficiency, centrifugal recovery, and filtration[66]. Flocculation leading to sedimentation occurs naturally in many older algal cultures. In some cultures, however, forced flocculation is necessary to promote sedimentation during harvest. Many different flocculation methods have been studied, including chemical additives (i.e., cellulose, polyacrylamide polymers, surfactants, chitosan, and other man-made fibers), autoflucculation, bioflocculation and electroflocculation[68-75]. Centrifugation is suitable for rapidly and effectively

concentrating any type of microorganisms. It widely used in recovery of high-value

products such as for food or aquaculture applications. The employment of centrifugation

as a harvesting method must be considered in conjunction with the product's scale and

values due to high capital and operational costs. Filtration processes operate under

gravity, pressure, or vacuum for recovering large quantities of microalgal biomass.

However, when the particles are slimy or very fine, the filtration can be relatively slow

due to the formed dense and impermeable cake plug the filter media. Therefore, filtration

is better suited for larger size of microalgae[66]. Filamentous microalgae, including

Spirulina, are often recovered by filtration under either gravity or low pressure[67]. Other

alternative recovery methods, such as membrane microfiltration and ultra-filtration, are

more suitable for fragile cells and small-scale production.

1.4.3. Drying. In general, 75-90% of water remains in the microalgal biomass

when the mechanical dewatering processes are completed. For the requirement of higher

biomass concentration, such as the production of biofuel, additional drying is needed

prior to biomass processing. The biomass solid concentration can then reach higher than

85% after drying. Several systems, including spray-drying, drum-drying, freeze-drying,

and sun-drying have been employed to dry the microalgae, such as Chlorella,

Scenedesmus, and Spirulina2. Higher water content within the microalgal biomass

makes sun-drying difficult. The sun-drying also requires both extra space as well as a

considerable amount of time. Spray-drying is a rapid and continuous drying process.

Small biomass droplets with a high surface area are brought into continuous contact with

hot air in a large chamber. Freeze-drying (lyophilization) is the most gentle drying

method available for microalgal biomass. This method involves the process of direct

sublimation of ice crystals to vapor from the frozen microalgal biomass by slight warming without thawing. The application of lyophilization at the commercial level may be considered for high market-value products only because of the high capital and energy costs.

1.4.4. Lipid Extraction and Biodiesel Production. Lipids or oil must be extracted from a microalgal biomass for biodiesel production. Lipid extraction is largely within the realm of laboratory-scale processes, such as physical methods, chemical methods, and supercritical methods.

Solvent extraction is fast and efficient and has proved to be the most approachable method. Several organic solvents such as hexane, ethanol, hexane-ethanol mixture, hexane-isopropanol mixture, and a chloroform-methanol-water co-solvent were used to extract lipids from microalgae[2, 30]. The principles of organic solvents extraction can be explained as "like dissolving like". The ideal solvent be volatile (for easy water removal), free from toxic or reactive impurities (to avoid reaction with the lipids), able to form a two-phase system with water (to remove non-lipids), and ineffective for the extraction of undesirable components (*e.g*., proteolipid protein)[76]. Two critical factors must be considered when a co-solvent system is chosen for lipid extraction. First, the more polar co-solvent has the ability to disrupt the cell membrane, making it sufficiently porous. Second, a less polar co-solvent needs to match the polarity index of the lipids being extracted. When ethanol is used in lipid extraction, it can also extract cellular contaminants, such as sugars, amino acids, salts, hydrophobic proteins, and pigments, which are not desirable for biofuel production. The Bligh and dyer method, which uses a ternary system (chloroform: methanol: water in a ratio 1:2:0.8; v/v/v), is the most reliable

and commonly employed system for the extraction of total lipids from microalgae at an analytical level. The yield recovery of total lipids could reach to above 95% when the Bligh and Dyer method is applied during extraction[77]. The extracted lipids (primarily the TAGs) are subjected by transesterification to produce biodiesel (discussed in detail in Section 1.2).

Recent studies investigated the direct transesterification of wet and dry microalgal biomass to produce fatty acid methyl ester (biodiesel) without employing the initial extraction step[78]. Direct transesterification involves both lipid extraction and transesterification process to be catalyzed by acid in a single step. This method reduces cost and operating time compared to lipid extraction followed by transesterification, although more intensive operating conditions are employed (1h at 60 $^{\circ}$C or 8 h at room temperature).

The biodiesel from a renewable resource is miscible with petroleum based diesel at certain blend levels, reduce the most regulated exhaust emissions, is biodegradable and has little or no sulfur and aromatics content. Biodiesel is an excellent alternative to conventional petroleum-derived diesel fuel.

1.5. INVESTMENT CASTING PROCESS

Investment casting, or lost wax casting, is one of the most widely used methods in the automotive, aerospace and biomedical industries for the production of complex metal shapes[79,80]. The investment casting process can be dated back to 4000-6000 BC when Early Man employed the method to produce rudimentary tools[81]. It is a cheaper alternative than forging and machining since the waste material is kept to a minimum[82].

In investment casting process, a die as the permanent tooling for a cast component is produced first. The die material could be steel, brass, aluminium alloy, polymer, plasters or rubber. Then a molten wax is introduced into the die from an injection machine. In this step, a full replica of wax pattern is produced. The wax patterns are attached to a sprue and feeder system, with the result of known as a pattern cluster. Then the cluster is coated with a layer of refractory slurry or primary slurry by spraying, dipping or pouring. This primary layer is used to give a smooth surface of the casting. The coated pattern is dried and stuccoed by applying a fluidized bed or rainfall sender to build up multiple layers of a mold shell. After the coating drying, the wax pattern is removed by steam autoclave or flash firing in a furnace, leaving a hollow shell. The shells are fired in an oven to build strength and remove any residue volatiles. In the casting stage, molten metal is poured into the heated shells and solidified inside the shells to form the castings. The ceramic shell is removed by mechanical or chemical methods during knockout process.

The wax pattern could be replaced by a polymer pattern due to the latter's lower creep under self-loading, lower tooling cost for low production quantities and in some cases ease of handling due to lighter weight than wax[83]. Several alternative polymer patterns those can be used in investment casting will be discussed in the following section.

1.6. ALTERNATIVE PATTERN MATERIALS FOR INVESTMENT CASTING

1.6.1. Expanded Polystyrene (EPS) Foam. Expanded polystyrene (EPS) is the most common polymer used for production of a casting. Polystyrene is a long chain hydrocarbon and can be obtained from the polymerization of styrene monomers through

four different chain-growth initiations, including free radical, cationic, anionic or

coordination.

   Figure1.5 shows the schematic of polymerization of styrene monomers. Typically,

a chain of polystyrene comprises a few thousand monomers and gives a molecular weight

of 100,000- 400,000. EPS is a closed-cell, light weight and rigid plastic foam[84]. It is

usually produced by a process known as steam molding. In the process, expandable

polystyrene beads are loaded into a pre-expander and heated by steam until soft. The

entrapped blowing agent is expanded to reduce density of EPS beads. After pre-

expansion, the beads are filled in a mold to be heated again by steam to further expand

into voids and fuse together into a rigid pattern. The rigid EPS pattern material can be

easily shaped, machined and fabricated by gluing to form any desired complex shapes

and used in an investment casting process as a casting pattern. For a larger volume EPS

foam pattern, it can be made by injection molding method.
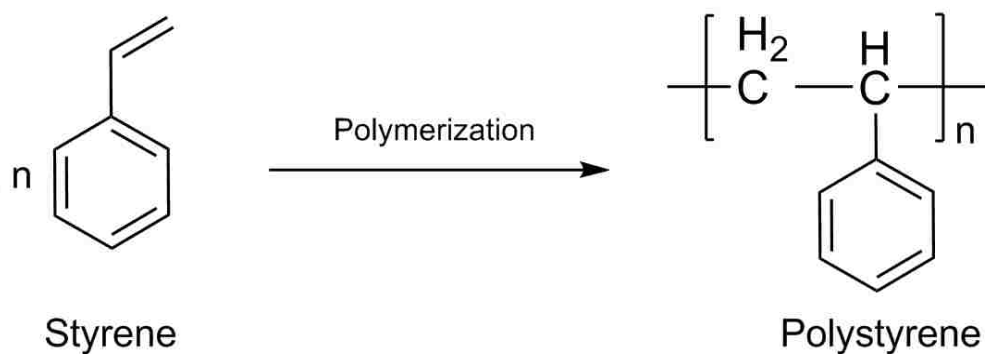
Fig. 1.5 Schematic of polymerization of styrene monomers to polystyrene

1.6.2. Polyurethane (PU) Foam. Polyurethane (PU) foam has also been developed in investment casting but to a much smaller extent. PUs are thermosetting polymers those are produced by the reaction of isocyanate (R-N=C=O), such as diphenylmethane diisocyanate (MDI), toluene diisocyanate (TDI), hexamethylene diisocyanate (HDI) or isophorone diisocyanate (IPDI) with polyester or polyether polyols, which containing at least two active hydroxyl groups (R-OH-). Other additives including catalyst, blowing agent, and surfactant are necessary for production of PU foams. This material has low thermal conductivity, high strength, and no shrinkage[85]. Typically a PU foam pattern is produced by foaming in a metal die. PU foam pattern used in investment casting can produce high quality castings of good surface finish. PU foam pattern also provides dimensional stability over a range of temperatures and removability by ashless burnout from the shell mold formed thereon without cracking the shell mold[86].

1.6.3. Epoxy Resin. An epoxy based thermosetting polymer is another polymer pattern that can be employed in investment casting. Most common and important class of epoxy resins in industry are diglycidyl ethers of bisphenol A, which are formed from a reaction between epichlorohydrin and bisphenol A. Epoxy resin may be cured (cross-links and polymerizes) either by themselves (homopolymerization) or with a curing agent. The common used curing agents include polyfunctional amines, acids (and acid anhydrides), phenols, alcohols, and thiols.

Epoxy resin pattern used in investment casting can be built precisely by the Stereolithography process (SLA) - one of modern rapid prototyping (RP) technologies. Its capabilities of high accuracy and good surface finish make it a preferred choice for designer models. SLA makes use of laser-induced polymerization for building of solids

objects starting from three-dimensional CAD models. The process involves a laser beam

drawing cross section of the model onto the surface of liquid UV-curable epoxy resin.

The three main steps of the process include CAD design, interface with software

equipment and stereolithography build process[87]. By using SLA machine, QuickCast 2.0

build styles create a quasi-hollow epoxy resin pattern with an internal architecture of

hexagonal honeycombs[88, 89]. The solid SLA geometry with a honeycomb structure

removes up to 90 percent of the mass and makes a drop in material costs and lead time[90].

The hollow structure allows the pattern to collapse inward during the pattern removal

process and thus prevents expansion forces from cracking the shell[91]. The mostly hollow

build style also makes the pattern's burnout to occur more easily in investment casting.

1.6.4. Bio-based Polymers. Advances in petroleum-based polymers have

benefited mankind in numerous ways. However, due to the limitation of petroleum

resources thus resulting in continuous price rising of the petroleum and greenhouse gas

(CO_2) emission from process of fossil fuel combustion, it is critical to find alternative

ways for sustainable world development. Bio-based materials from renewable resources

are possible to partially replace petroleum-based products. This can reduce materials

dependence on petroleum and enhance global sustainability. In addition, bio-based

materials can biodegrade or be recycled, and be beneficial to the environment.

Three major renewable resources, protein, oil and carbohydrates have great

potential to produce bio-based polymers in industry. This section only focuses on oil-

based polymers derived from renewable resources. The oil (lipid) is mainly made up of

triglyceride (glycerol esters of fatty acids), which have the structure shown in Fig.1.6. In

triglyceride structure, three fatty acids chains varying from 14 to 22 carbons in length

with 0 to 3 double bonds per fatty acid are joined at a glycerol backbone. The double

bonds of the triglyceride are used to functionalize the triglyceride with various chemical

groups to form polymers.

triglyceride

palmitic acid (C16:0)

stearic acid (C18:0)

oleic acid (C18:1)

linoleic acid (C18:2)

linolenic acid (C18:3)
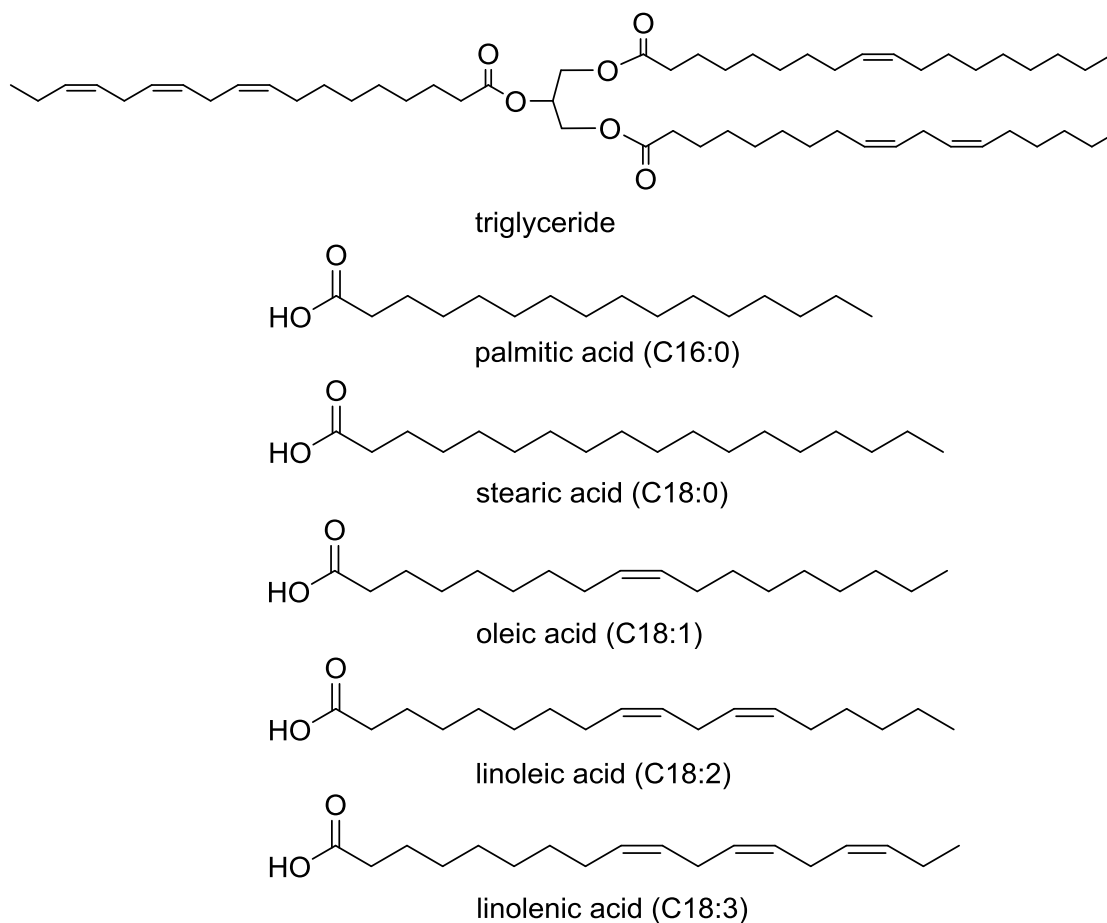
Fig. 1.6 Triglyceride and fatty acids molecule structures

Figure 1.7 illustrates three main pathways for functionalization of triglyceride to

synthesis polymers, which are possible to be considered as patterns in investment casting.

The unsaturation part (double bonds) from the triglyceride structure can be converted to

epoxy[92-94]. The epoxy resin from soybean oil shows relatively low strength and

elongation while epoxidized linseed oil can give somewhat harder materials with glass

transition in the range 40-60 $^{\circ}$C, and of higher tensile strength[95]. The epoxidized

triglycerides have been successfully employed for production of polyols used for

polyurethane foams, whose mechanical and thermal properties are comparable to those of

petroleum-based PUs[96]. The transformation from epoxy functional triglyceride with

acrylic acid makes it possible to produce acrylated epoxidized polymers[97]. These

acrylated polymers can be used as substitution of petroleum-based polyacrylates or

blended with various amount of styrene to produce polymers with desired properties,

such as different moduli and glass transition temperature to reach a range acceptable for

structural applications.
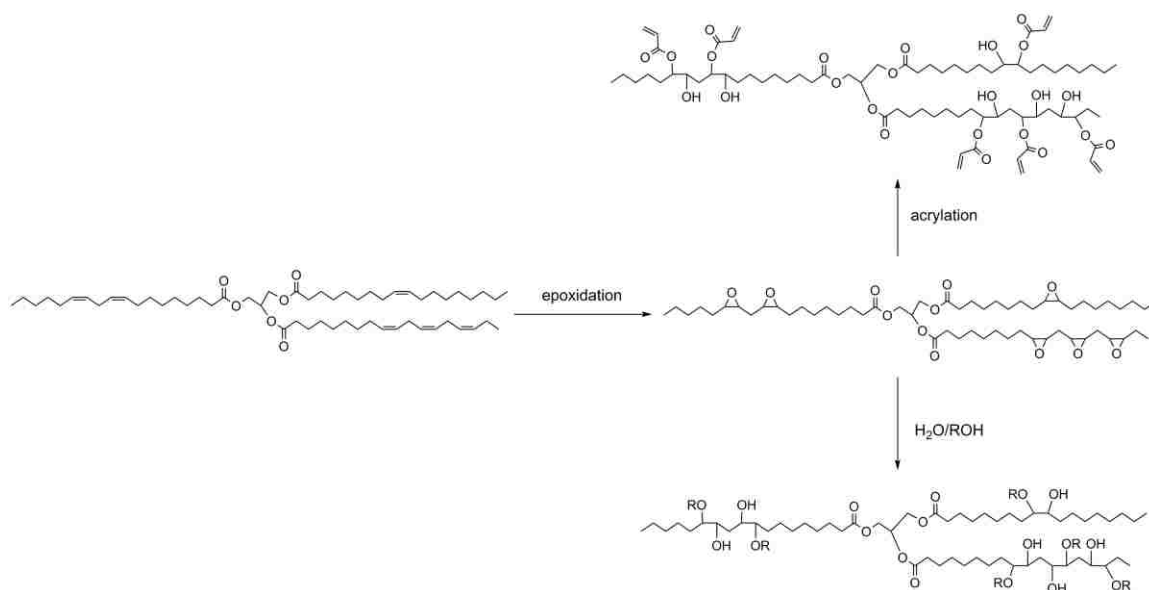
Fig. 1.7 Synthetic pathways leading to polymers from triglyceride molecule[98]

Microalgae have demonstrated a higher oil yield besides their higher growth rates

and productivity, as discussed in previous sections. Most microalgal oils are mainly

composed of triglyceride, which can be utilized for production of all of those bio-

polymers through functionalization of the double bonds. Therefore, microalgae are great alternative resource for making bio-based polymers those may be applicable in production of polymer patterns for investment casting.

1.7. THERMAL DEGRADATION OF PATTERNS IN INVESTMENT CASTING PROCESS

In investment casting process, a polymer pattern undergoes thermal degradation when it is removed by steam autoclave or flash firing in a furnace. The thermal degradation of patterns may involve both combustion and pyrolysis processes in investment casting. The heating temperature and atmospheric environment around the polymer pattern can significantly affect its decomposition, including degradation rate, degree, and products; and then influence casting quality in investment casting.

Several thermal analysis methods have been employed in study of thermal degradation of polymers. Thermogravimetric analysis (TGA) is one of the most common used techniques to determine degradation temperature, thermal stability, residual levels, moisture and volatiles content, and decomposition kinetics of a polymer or composite material. Differential scanning calorimetry (DSC) is another widely used thermoanalytical technique for polymeric materials to determine their thermal transitions, such as melting points, glass transition temperature, crystallization, polymer curing, and sample purity. Some other furnaces or heating devices may also be used for study of thermal degradation behaviors (decomposition products and kinetics) of polymers under a wide range of temperatures.

2. OBJECTIVE OF THIS RESEARCH

2.1. RESEARCH OBJECTIVE-PART 1

A direct spectrophotometric measurement using Nile red dye provides the simple method to determine the oil content of microalgae and allows the rapid identification of high oil-bearing microalgae. However, the applications of Nile red lipid staining in a number of green algal species has been hindered due to the composition and structure of the thick and rigid cell walls resulting in the permeation difficulty of Nile red through the cell walls and subsequently dissolving in the intracellular neutral lipid. Various physical and chemical treatments, including adding DMSO, ethanol as stain carrier and combination of DMSO and microwave irradiation have been studied to improve the fluorescence intensity of the lipid. Nevertheless, the organic solvent was included and several steps were involved in microwave-assisted staining.

This part of the dissertation focused on optimization of the conventional Nile red method with two assisted methods, including heating and diluted H_2SO_4 treatment to enhance the staining efficiency and improve the fluorescence intensity of microalgal lipid. Optimum procedures were successfully applied to five different green microalgal species. These two fast and simple methods to determine the microalgal neutral lipid content could potentially be used in the investigation of large scale lipid production from other microalgal biomass.

The spectrophotometric measurement using Nile red provided a qualitative or semi-quantitative analysis data in the determination of lipid content. One limitation of using this fluorescence method is the fluorescence intensity, which is relative to compare or estimate the intercellular lipid contents in microalgae; it is not an absolute content.

Staining of lipid standards and staining of algal cells resulting in different fluorescence responses due to the different hydrophobicity and size are other drawbacks.

This dissertation also involves the employment of a series of oil-in-water microemulsion standards stabilized by a non-ionic surfactant. This prepared pseudo standards can mimic microalgae cells suspended in water. The fluorescence intensity of neutral lipid from microalgae species was obtained by comparing with the O/W microemulsion standards curves and then the actual neutral lipid contents of microalgae were calculated. The established calibration standards method provided a reliable and fast way in the determination of the neutral lipid in microalgae. It can be used as a sensitive, quantitative, and high throughput method for screening of cellular neutral lipid content in green algae as well as other classes of algae.

2.2. RESEARCH OBJECTIVE-PART 2

This part of the dissertation was to explore polymers' thermal and chemical properties which affect application of different polymer patterns materials in the investment casting process. Three polymeric materials, including EPS foam produced from expanded polystyrene using a blowing agent; FOPAT foam pattern made from a water blown polyurethane and an epoxy resin based SLA pattern with an internal honeycomb structure were characterized in the research. Thermal degradation behavior and glass transition temperatures of these polymers were characterized by using TGA and DSC techniques, respectively. Generation of HCN from thermal decomposition of FOPAT pattern under different experimental conditions in lab-scaled muffle furnace and tube furnace was discussed.

Thermal degradation kinetics of epoxy resin pattern material were investigated by using various kinetic models (differential and integral) based on TGA data. These kinetic equations were applied to studies concerning the epoxy resin pattern's reaction to fire (ignition process, flame propagation, evaluation of amount of toxic products generated, etc.) and to the reactor design and optimization of the operating conditions in the thermochemical processing of the material. Flynn-Ozawa-Wall and Kissinger methods were used to calculate kinetic parameters of thermal decomposition of the epoxy resin pattern. Degradation mechanisms were estimated by Coates-Redfern analytical fitting method.

REFERENCES

1. R. E. Lee, *Phycology*, Cambridge University Press, 2008.

2. A. Richmond, *Handbook of Microalgal Culture: Biotechnology and Applied Phycology*, Wiley-Blackwell, 2004.

3. Y. Li, M. Horsman, B. Wang, N. Wu and C. Lan, *Appl Microbiol Biotechnol*, 2008, 81, 629-636.

4. Y. Li, M. Horsman, N. Wu, C. Q. Lan and N. Dubois-Calero, *Biotechnology Progress*, 2008, 24, 815-820.

5. J. Sheehan, T. Dunahay, J. Benemann and P. Roessler, *A Look Back at the U.S. Department of Energy's Aquatic Species Program—Biodiesel from Algae*, NREL/TP-580-24190, National Renewable Energy Laboratory, USA, 1998.

6. Y. Chisti, *Biotechnology Advances*, 2007, 25, 294-306.

7. A. B. M. S. Hossain, A. Salleh, A. N. Boyce, P. chowdhury and M. Naqiuddin, *American Journal of Biochemistry and Biotechnology*, 2008, 4, 250-254.

8. Q. Hu, M. Sommerfeld, E. Jarvis, M. Ghirardi, M. Posewitz, M. Seibert and A. Darzins, *The Plant Journal*, 2008, 54, 621-639.

9. L. Rodolfi, G. Chini Zittelli, N. Bassi, G. Padovani, N. Biondi, G. Bonini and M. R. Tredici, *Biotechnology and Bioengineering*, 2009, 102, 100-112.

10. J. N. Rosenberg, G. A. Oyler, L. Wilkinson and M. J. Betenbaugh, *Current Opinion in Biotechnology*, 2008, 19, 430-436.

11. P. Schenk, S. Thomas-Hall, E. Stephens, U. Marx, J. Mussgnug, C. Posten, O. Kruse and B. Hankamer, *Bioenerg. Res.*, 2008, 1, 20-43.

12. K. Tsukahara and S. Sawayama, *Journal of the Japan Petroleum Institute*, 2005, 48, 251-259.

13. "World Energy Outlook 2007: China and India Insights," http://www.worldenergyoutlook.org/media/weowebsite/2008-1994/weo_2007.pdf, accecssed July 2014.

14. J. Laherrère, Forecasting production from discovery, ASPO Lisbon 2005 conference.

15. J. Ferrell and V. Sarisky-Reed, *National Algal Biofuels Technology Roadmap*, Energy Efficiency & Renewable Energy, U.S. Department of Energy, 2010.

16. S. Aslan and I. K. Kapdan, *Ecological Engineering*, 2006, 28, 64-70.

17. J. Pratoomyot, P. Srivilas and T. Noiraksar, *Songklanakarin Journal of Science and Technology*, 2005, 27, 1179-1187.

18. S. M. Renaud, L.-V. Thinh and D. L. Parry, *Aquaculture*, 1999, 170, 147-159.

19. B. Wang, Y. Li, N. Wu and C. Lan, *Appl Microbiol Biotechnol*, 2008, 79, 707-718.

20. N. Mallick, *Biometals*, 2002, 15, 377-390.

21. "DIRECTIVE 2003/30/EC OF THE EUROPEAN PARLIAMENT AND OF THE COUNCIL of 8 May 2003," http://www.energy-community.org/pls/portal/docs/36290.PDF, accessed July 2014.

22. R. Raja, S. Hemaiswarya, N. A. Kumar, S. Sridhar and R. Rengasamy, *Critical Reviews in Microbiology*, 2008, 34, 77-88.

23. H. Milner, *J Am Oil Chem Soc*, 1951, 28, 363-367.

24. M. J. Geoghegan, *Nature*, 1951, 168, 426-427.

25. H. A. Spoehr, *Carnegie Institution Washington Yearbook*, 1948, 47, 100-103.

26. W. R. Barclay, K. L. Terry, N. J. Nagle, J. C. Weissman and R. P. Goebel, *Journal of the World Aquaculture Society*, 1987, 18, 218-228.

27. B. Barclay, N. Nagle, K. Terry and P. Roessler, 1985, SERI/CP-23-2700, 52-68.

28. A. Belay, *Mass culture of Spirulina outdoors-the earthrise farms experience*, Taylor & Francis, London, 1997.

29. M. Griffiths and S. L. Harrison, *J Appl Phycol*, 2009, 21, 493-507.

30. E. G. Bligh and W. J. Dyer, *Canadian journal of biochemistry and physiology*, 1959, 37, 911-917.

31. M. Kates and B. E. Volcani, *Biochimica et Biophysica Acta*, 1966, 116, 264-278.

32. J. Folch, M. Lees and G. H. S. Stanley, *Journal of Biological Chemistry*, 1957, 226, 497-509.

33. B. Fried and J. Sherma, *Thin-layer chromatography*, CRC Press, Boca Raton, 1999.

34. R. G. Ackman, Application of thin-layer chromatography to lipid separation: neutral lipids, In *Analyses of Fats, Oils and Derivatives*, edited by Edward G. Perkins, The American Oil Chemists Society, Champaign, Illinois, 1991. ch. 3, pp. 60-82

35. W. W. Christie, *Journal of Lipid Research*, 1985, 26, 507-512.

36. E. D. Hudson, R. J. Helleur and C. C. Parrish, *Journal of Chromatographic Science*, 2001, 39, 146-152.

37. K. MacDougall, J. McNichol, P. McGinn, S. B. O'Leary and J. Melanson, *Anal Bioanal Chem*, 2011, 401, 2609-2616.

38. K. E. Cooksey, J. B. Guckert, S. A. Williams and P. R. Callis, *Journal of Microbiological Methods*, 1987, 6, 333-345.

39. P. Greenspan, E. P. Mayer and S. D. Fowler, *The Journal of Cell Biology*, 1985, 100, 965-973.

40. D. Elsey, D. Jameson, B. Raleigh and M. J. Cooney, *Journal of Microbiological Methods*, 2007, 68, 639-642.

41. W. Chen, C. Zhang, L. Song, M. Sommerfeld and Q. Hu, *Journal of Microbiological Methods*, 2009, 77, 41-47.

42. S. Lee, B.-D. Yoon and H.-M. Oh, *Biotechnology Techniques*, 1998, 12, 553-556.

43. P. Spolaore, C. Joannis-Cassan, E. Duran and A. Isambert, *Journal of Bioscience and Bioengineering*, 2006, 101, 87-96.

44. T. M. Mata, A. A. Martins and N. S. Caetano, *Renewable and Sustainable Energy Reviews*, 2010, 14, 217-232.

45. S.-Y. Chiu, C.-Y. Kao, M.-T. Tsai, S.-C. Ong, C.-H. Chen and C.-S. Lin, *Bioresource Technology*, 2009, 100, 833-838.

46. A. Demirbas, *Energy Conversion and Management*, 2009, 50, 14-34.

47. M. Morais and J. Costa, *Biotechnol Lett*, 2007, 29, 1349-1352.

48. N. Eriksen, *Biotechnol Lett*, 2008, 30, 1525-1536.

49. L. Gouveia and A. Oliveira, *J Ind Microbiol Biotechnol*, 2009, 36, 269-274.

50. E. Molina, F. G. Acién Fernández, F. García Camacho, F. Camacho Rubio and Y. Chisti, *J Appl Phycol*, 2000, 12, 355-368.

51. M. Huntley and D. Redalje, *Mitig Adapt Strat Glob Change*, 2007, 12, 573-608.

52. A. M. Illman, A. H. Scragg and S. W. Shales, *Enzyme and Microbial Technology*, 2000, 27, 631-635.

53. W. H. Thomas, T. G. Tornabene and J. Weissman, *Screening for lipid yielding microalgae: activities for 1983*, Solar Energy Research Institute, U.S. Department of Energy,SERI/STR-231-2207, 1984.

54. Z.-Y. Liu, G.-C. Wang and B.-C. Zhou, *Bioresource Technology*, 2008, 99, 4717-4722.

55. S. Mandal and N. Mallick, *Appl Microbiol Biotechnol*, 2009, 84, 281-291.

56. C. Yoo, S.-Y. Jun, J.-Y. Lee, C.-Y. Ahn and H.-M. Oh, *Bioresource Technology*, 2010, 101, S71-S74.

57. G. Huang, F. Chen, D. Wei, X. Zhang and G. Chen, *Applied Energy*, 2010, 87, 38-46.

58. E. Sforza, PhD, Universitàdegli Studi di Padova, 2012.

59. K. Chojnacka and A. Noworyta, *Enzyme and Microbial Technology*, 2004, 34, 461-465.

60. Y. Liang, N. Sarkany and Y. Cui, *Biotechnol Lett*, 2009, 31, 1043-1049.

61. H. Xu, X. Miao and Q. Wu, *Journal of Biotechnology*, 2006, 126, 499-507.

62. O. Perez-Garcia, F. M. E. Escalante, L. E. de-Bashan and Y. Bashan, *Water Research*, 2011, 45, 11-36.

63. "Climate Tech Wiki," http://climatetechwiki.org/technology/algae, accessed July 2014

64. A. P. Carvalho, L. A. Meireles and F. X. Malcata, *Biotechnology Progress*, 2006, 22, 1490-1506.

65. M. R. Tredici, *Biofuels*, 2009, 1, 143-162.

66. E. Molina Grima, E. H. Belarbi, F. G. Acién Fernández, A. Robles Medina and Y. Chisti, *Biotechnology Advances*, 2003, 20, 491-515.

67. S. Pahl, A. Lee, T. Kalaitzidis, P. Ashman, S. Sathe and D. Lewis, in *Algae for Biofuels and Energy*, eds. M. A. Borowitzka and N. R. Moheimani, Springer Netherlands, 2013, vol. 5, ch. 10, pp. 165-185.

68. Lee, Kim, Kim, Kwon, Yoon and Oh, *Letters in Applied Microbiology*, 1998, 27, 14-18.

69. R. M. Knuckey, M. R. Brown, R. Robert and D. M. F. Frampton, *Aquacultural Engineering*, 2006, 35, 300-313.

70. J. R. Pan, C. Huang, Y.-C. Chuang and C.-C. Wu, *Colloids and Surfaces A: Physicochemical and Engineering Aspects*, 1999, 150, 185-190.

71. A. Sukenik and G. Shelef, *Biotechnology and Bioengineering*, 1984, 26, 142-147.

72. A. Lavoie and J. de la Noüe, *Biotechnology and Bioengineering*, 1987, 30, 852-859.

73. G. Chen, *Separation and Purification Technology*, 2004, 38, 11-41.

74. M. Y. A. Mollah, P. Morkovsky, J. A. G. Gomes, M. Kesmez, J. Parga and D. L. Cocke, *Journal of Hazardous Materials*, 2004, 114, 199-210.

75. E. Poelman, N. De Pauw and B. Jeurissen, *Resources, Conservation and Recycling*, 1997, 19, 1-10.

76. E. Grima, M. González and A. Giménez, in *Algae for Biofuels and Energy*, eds. M. A. Borowitzka and N. R. Moheimani, Springer Netherlands, 2013, vol. 5, ch. 11, pp. 187-205.

77. W. W. Christie, *Lipid Analysis, 2nd edn.*, Pergamon Press, New York, 1982.

78. B. D. Wahlen, R. M. Willis and L. C. Seefeldt, *Bioresource Technology*, 2011, 102, 2724-2730.

79. S. O. Barnett, *Foundry Trade Journal International*, 1988, 11, 33-37.

80. P. Aubertin, S. Cockcroft, J. Fernihough, A. Mitchell and A. Schmalz, presented in part at the Proceedings of the 10th World Conference on Investment Casting, Monte Carlo, 2000.

81. P. R. Taylor, An illustrated history of lost wax casting. *Proceedings of the 17th Annual BICTA Conference*, September,1983.

82. S. Jones and P. M. Marquis, *British Ceramic Transactions*, 1995, 94.

83. H. Zhao, M. Xu, H. Li, W. Everhart, S. Lekakh, V. Richards, K. Chandrashekhara and P. Nam, Characterization of Low Density Polymer Pattern for Large Steel Investment Casting. *58th Annual Technical Conference and Equipment Expo*, Investment Casting Institute, Covington, KY2011.

84. *Introduction to Expandable Polystyrene*, Huntsman Technical Bulletin 11.0, July 2001.

85. P. L. Jain, *Principles of Foundry Technology, Fourth Edition*, Tata McGraw-Hill Education, 2003.

86. US6481490, 2002.

87. P. F. Jacobs, *Stereolithography and Other RPM Technologies*, Society of Manufacturing Engineering, Dearborn, MI, 1996.

88. G. Tromans, *Developments in Rapid Casting*, Professional Engineering Publishing, Bury St Edmunds, 2003.

89. R. Hague, G. D' Costa and P. M. Dickens, *Rapid Prototyping Journal*, 2001, 7, 66-73.

90. *3D Systems Co., Application Guide, Investment Casting Using QuickCaste Build Style*, Rock Hill, SC, 2002.

91. P. F. Jacobs, Stereolithography 1993: epoxy resins, improved accuracy & investment casting. *Proc 4th International Conference on Rapid Prototyping*. Dayton, OH, June, 1993. p. 249-62, 14-17.

92. B. Rangarajan, A. Havey, E. Grulke and P. D. Culnan, *J Am Oil Chem Soc*, 1995, 72, 1161-1169.

93. F. A. Zaher, M. H. El-Mallah and M. M. El-Hefnawy, *J Am Oil Chem Soc*, 1989, 66, 698-700.

94. D. Swern, G. N. Billen, T. W. Findley and J. T. Scanlan, *Journal of the American Chemical Society*, 1945, 67, 1786-1789.

95. J. V. Crivello, R. Narayan and S. S. Sternstein, *Journal of Applied Polymer Science*, 1997, 64, 2073-2087.

96. A. Guo, I. Javni and Z. Petrovic, *Journal of Applied Polymer Science*, 2000, 77, 467-473.

97. J. Scala and R. Wool, *J Amer Oil Chem Soc*, 2002, 79, 59-63.

98. R. P. Wool, in *Bio-Based Polymers and Composites*, eds. R. P. Wool and X. S. Sun, Academic Press, Burlington, 2005, DOI: http://dx.doi.org/10.1016/B978-012763952-9/50005-8, pp. 56-113.

PAPER

I. ENHANCEMENT OF LIPOPHILIC DYE FLUORESCENCE IN MICROALGAE WITH HEATING OR DILUTED ACID TREATMENT

Hongfang Zhao,[1] Keesoo Lee,[2] and Paul Ki-souk Nam[1]

[1]Department of Chemistry, Missouri University of Science and Technology, 1870 Miner Circle, Rolla, MO, 65409, USA and [2]Department of Life and Physical Sciences, Lincoln University, 820 Chestnut St., Jefferson City, MO, 65101, USA

ABSTRACT

The Nile red fluorescence method has been employed to determine the amount of neutral lipid in microalgae. Several physical and chemical treatments, including addition of organic solvents and microwave assistance for lipid staining by Nile red have been applied to the thick and rigid cells. These cells are difficult to be quantified with the conventional unmodified Nile red method. In this study, the two optimization methods, heating and diluted acid treatments, were introduced into the microalgae staining process to improve the staining efficiency of Nile red. Four different microalgal species (*Botryococcus braunii*, *Chlorella pyrenoidosa*, *Haemetococcus pluvialis*, and *Scenedesmus quadricauda*) were included in this research. First, the heating treatment was employed to improve the fluorescence intensity of lipid from microalgae. The Nile red staining process was found to be affected by both temperature and durations of the heat applied. The optimum staining temperature and time were 60 $^\circ$C and 5 min, respectively for both *Botryococcus b.* and *Chlorella p.*. The fluorescence intensity of *Botryococcus b.* was improved more than ten times with the assistance of a heating

treatment at 60 $^{\circ}$C for 5 min. Moreover, the fluorescence microscopic images revealed that the neutral lipid with the heating treatment produced a stronger bright-yellow fluorescence than those without any treatment. The second method used was a treatment with addition of diluted sulfuric acid (H_2SO_4) during the Nile red staining process. With the assistance of H_2SO_4, the Nile red staining achieved a higher staining efficiency. The lipid fluorescence intensity for *Botryococcus b.* increased approximately 12 times at concentrations as low as 0.002% of H_2SO_4 comparing with the untreated one.

Key words: Nile red, Neutral lipid, Fluorescence, Algae, Heating treatment, Diluted acid treatment

1. INTRODUCTION

Microalgae have been widely investigated as an alternative feedstock for biodiesel production due to their great diversity, rapid growth rate, high lipid content, and carbon recycling potential[1,2]. Large numbers of algal strains and their growing conditions have been evaluated at various scales in an attempt to develop an economically feasible process for microalgae-based biodiesel production[3-5]. Traditional lipid extraction, combined with either the gravimetric or chromatographic method, is used for quantitative analysis of lipid composition. However, these methods can be both labor intensive and time-consuming[6,7].

A direct spectrophotometric measurement using lipophilic dyes is a simple method that can be used to determine the oil content of microalgae. This method also allows the rapid identification of high oil-bearing microalgae[8,9]. Greenspan and Fowler reported that Nile red as a stain on cultured aortic smooth muscle cells and peritoneal

macrophages[10]. They demonstrated Nile red fluoresces strongly only in a hydrophobic environment at yellow-green range (excitation, 450-500nm; emission, > 528nm). Nile red is preferred over other lipophilic dyes (i.e., Luminor 490PT, Sudan black B and Nile blue) in the determination of intracellular lipid[11]. When Nile red is used as a fluorescence probe, both smaller amount of sample and less time are needed than when gravimetric determination is used. Nile red has been frequently used in quantification of lipids from mammalian and microorganism cells (i.e., yeasts, zooplankton, and bacterial)[12-14].

Cooksey *et al.* introduced Nile red into the determination of neutral lipid of microalgae by using fluorescence microscopy, flow cytometry, and spectrofluorometry[8]. A qualitative or semi-quantitative analysis of lipid content from microalgae stained by Nile red has been reported[7, 9, 15]. Chen et al. reported that the applications of Nile red lipid staining in a number of green algal species has been hindered due to the composition and structure of thick and rigid cell walls[9]. This can result in the permeation difficulty of Nile red through the cell walls and subsequently dissolving in the intracellular neutral lipid. Variations in the fluorescence measurement of neutral lipid in microalgae are significantly affected by the algal species, environmental conditions, and Nile red staining process. Chen applied several physical and chemical treatments, such as the addition of DMSO, the use of ethanol as a stain carrier, and a combination of DMSO and microwave irradiation on improving the fluorescence intensity of the lipid[9]. Nevertheless, the organic solvent was included and several steps were involved in the microwave-assisted staining. Recently, a green lipophilic fluorescence dye, BODIPY 505/515 (4,4-difluoro-1,3,5,7-tetramethyl-4-bora-3a,4adiaza-s-indacene) was introduced to the lipid fluorescence determination. BODIPY has high oil/water partition coefficient,

which allows it to cross cell membranes easily[16, 17]. However, Siegler *et al*. concluded that the BODIPY 505/515 was unsuitable for the quantification of algal lipid because the binding of BODYPY 505/515 to the neutral lipid was either not proportional to the lipid content or the fluorescence background of BODIPY was too high[18].

In this study, the conventional Nile red method was optimized with two assisted methods, including heating and diluted H_2SO_4 treatments to enhance the staining efficiency and then improve the fluorescence intensity of algal lipid. Optimum procedures were successfully applied to five different green microalgal species. These two fast, simple methods that are used to determine the microalgal neutral lipid content could, potentially, also be used in the investigation of large scale lipid production from other microalgal biomass.

2. MATERIALS AND METHODS

2.1. ORGANISMS AND CULTURE CONDITIONS

Botryococcus braunii was purchased from the Integrated Energy Solutions Company. Both *Chlorella pyrenoidosa* (MC63AF2) and *Scenedesmus quadricauda* (MCF1) were obtained from the Lincoln University Culture Collection. *Haemetococcus pluvialis* was purchased from the Culture Collection of Algae at the University of Texas at Austin. *Chlorella p.* was maintained in BG-11 medium; other algal species were grown in f/2 culture medium. All of the algal strains were cultured in wide-mouth culture flasks at room temperature on a VWR orbital shaker that had an agitation speed of 100rpm.

The microalgae were harvested by decanting most water from the flask. The microalgal sediment was then placed in a tube to be centrifuged with an SNYO MISTRAL 3000i centrifuge at a speed of 2500 rcf for 10 minutes at the room temperature, so that the solids could be separated from with liquid. Finally, the dewatered microalgae slurry was dried with a Freeze Dryer (Refrigerated Vapor Trap, SAVANT). This drying process took approximatly one week for each ~3g dry weight sample. The dried microalgal pellets were stored in a desiccator for future use.

The Nile red (9-diethylamino-5-benzo[α] phenoxazinone) dye used in this study was purchased from the Acros Organics Company. Acetone (with an analytical grade) was purchased from Fisher Scientific. Sulfuric acid (with an analytical grade) was purchased from a commercial supplier.

2.2. STAINING OF MICROALGAE USING NILE RED

A Nile red stock solution of 0.1 mg/mL, prepared in acetone was stored in a refrigerator. Nile red, the concentrations ranging from 0.1 to 0.9 μg/mL was studied in the experiment in order to obtain the optimization concentration of Nile red in the lipid staining process. Optical density of all of the cell suspensions used for the analysis was 0.175 (OD_{680nm}) if the OD value was not mentioned specifically. A 35 μL Nile red stock solution was added to 5 mL of a microalgae culture. This culture was agitated vigorously on a vortex mixer for one minute and then placed in a dark area at room temperature. After 5 minutes, the solution was mixed for another one minute before it was measured. All of the experiments were performed at least three replicates. The background of the Nile red fluorescence in the medium was subtracted from the results.

2.3. HEATING TREATMENT OF NILE RED STAINING

After 35 µL Nile red was added to a 5 mL culture, the microalgal cells were placed in a preheated water bath. Nile red staining temperatures between room temperature and 70 $^\circ$C were maintained for 5 minutes. Various durations of the staining maintained at 55 $^\circ$C for *Botryococcus b.* were also performed to optimize the staining time. After the heating treatment was complete, the microalgal cells were agitated on a vortex mixer for one minute and then cooled to room temperature for fluorescence measurement.

2.4. FLUORESCENCE SPECTROPHOTOMETER

The fluorescence signals of Nile red-stained lipid from microalgae was measured on a Perkin-Elmer LS-5 fluorescence spectrophotometer. The excitation and emission wavelengths of 480 nm and 575 nm, respectively were selected, and both slits were set at 10nm. The spectrophotometer was warmed up for half an hour before measurement. The tested cuvette for placing sample is made of quartz material.

2.5. DILUTED ACID TREATMENT OF NILE RED STAINING

Diluted H_2SO_4 solutions with concentrations ranging from 0.001 to 1.0% (v/v) were introduced into the microalgae cells. The 5 mL acid treated microalgal cultures were stained by 35 µL Nile red and then agitated for one minute on a vortex mixer. The fluorescence emissions were recorded immediately.

3. RESULTS AND DISCUSSION

3.1. OPTIMIZATION OF NILE RED DYE CONCENTRATION

The microalgae *Scenedesmus q.* with an optical density of 0.66 (at 680 nm) was stained with Nile red with a heating treatment of 45 °C for 20 minutes. Fig.1 indicates that the fluorescence intensity for *Scenedesmus q.* increased with the Nile red concentration. Then it decreased when the Nile red concentration was higher than 0.7 µg/mL. The optimal concentration of Nile red of 0.7 µg/mL was applied to all of the experimental analysis. These results were found to be similar to the experimental values reported by Chen[9].
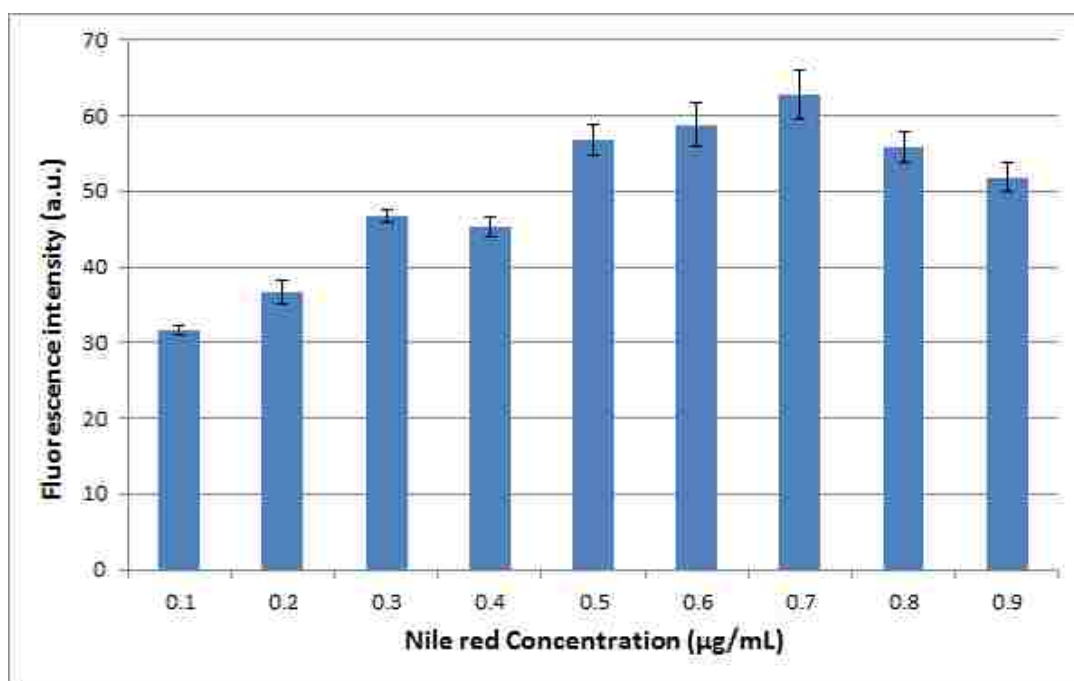
Fig. 1 The effect of Nile red concentration on the fluorescence intensity of the stained microalgae *Scenedesmus q.* with the heating treatment of 45 °C for 20 minutes. The OD of microalgae was 0.66 at 680nm. The excitation and emission wavelengths were 480 nm and 575 nm, respectively. Three replicate determinations were performed for each sample.

3.2. NILE RED STAINING WITHOUT TREATMENT

The same procedures described in section 2.2 were followed here. Based on the studies conducted here, optimized concentration of Nile red is 0.7 μg/mL. Four species of green microalgae, representing different classes, including *Botryococcus b.*, *Chlorella p.*, *Haemetococcus p.*, and *Scenedesmus q.* were investigated to evaluate the conventional Nile red fluorescence method. Three species, *Botryococcus b., Chlorella p.*, *and Scenedesmus q.* yielded very weak fluorescence signals (Fig.2). These low fluorescence emissions were indicative of either low neutral lipid contents or thicker cell walls that made the penetration of Nile red difficult during the current growth state. In contrast, the stained *Haemetococcus p.* exhibited a strong fluorescence intensity of 48 a.u..
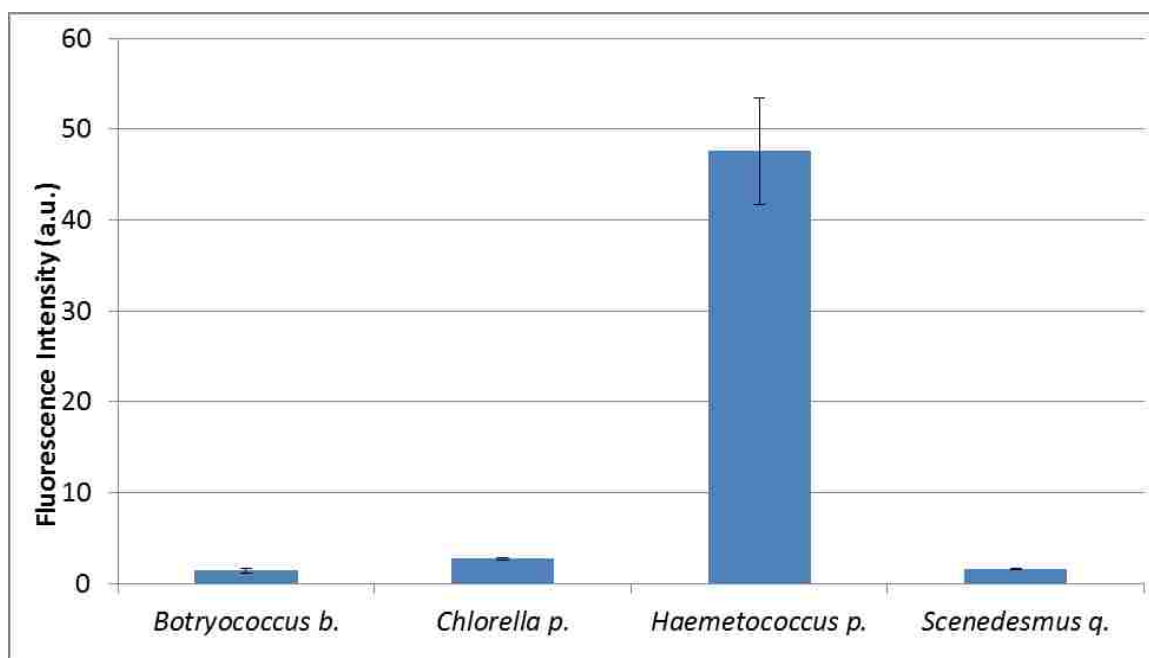
Fig. 2 Fluorescence intensity of Nile red stained microalgae without any treatment. The excitation and emission wavelengths were 480nm and 575nm, respectively. Three replicate determinations were performed for each sample.

3.3. NILE RED STAINING ASSISTED BY HEATING TREATMENT

The above conventional Nile red method was optimized with a heating treatment to determine whether or not the three algae species examined either had a low lipid content or thicker, rigid cells. Heating treatments between room temperature (control) and 65 °C were applied to the algae species. Heating durations were also considered.

3.3.1. Effects of Temperature and Time on Fluorescence Intensity

The fluorescence intensity of the algal cultures stained with Nile red were significantly affected by the staining temperature, as indicated in Fig. 3.
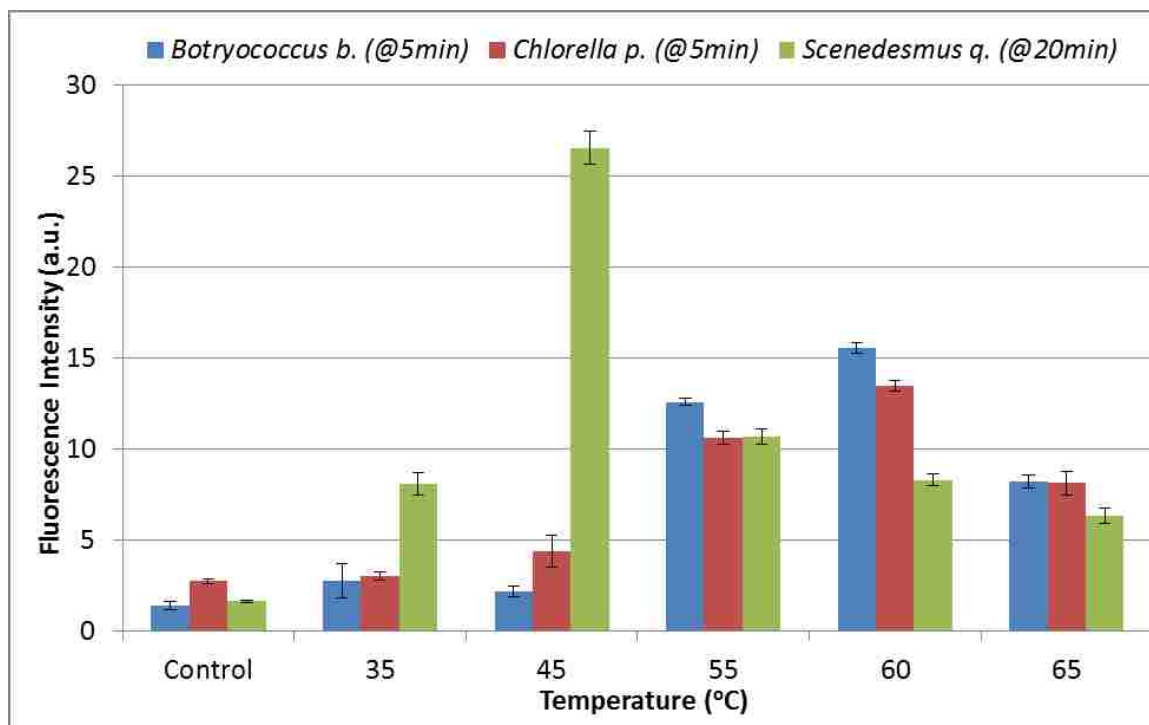
Fig. 3 The effect of staining temperature on fluorescence intensity of microalgae with various heating time. The excitation and emission wavelengths were 480 nm and 575 nm, respectively. Three replicate determinations were performed for each sample.

All of the algae species exhibited a higher fluorescence intensity as the heating temperature increased. The fluorescence signal of both *Scenedesmus q.* and *Botryococcus b.* with *Chlorella p.* decreased when the applied temperature exceeded 55 and 65 °C, respectively. The fluorescence emissions of stained *Scenedesmus q.* reached the highest level when the species was treated at 45 °C for 20 minutes. The optimum staining temperatures were approximately 60 °C for both *Botryococcus b.* and *Chlorella p.* The intensities were enhanced approximately 8 times for the *Botryococcus b.* comparing with the results from the conventional Nile red method. Therefore, the treatment of Nile red staining at a higher temperature (45- 55 °C) will accelerate the Nile red penetration rate of the *Botryococcus b.* cells. The heating treatment will also prompt the Nile red to penetrate the rigid and thick cell walls of the algae, as previously hypothesized.

Various staining time periods for *Botryococcus b.* stained with Nile red were examined to obtain the optimum heating treatment conditions. The effect of heating time on the staining efficiency of Nile red is illustrated in Fig. 4. A staining temperature of 55 °C was selected; the staining time varied between 5 and 50 minutes. The fluorescence intensity of stained *Botryococcus b.* reached the highest level when the heating duration was 10 minutes (see Fig. 3). The fluorescence intensity of *Botryococcus b.* then decreased gradually as the heating time increased, which may be due to the Nile red quenching in a culture solution for a longer time. When the heating temperature was set at 60 °C, the fluorescence intensity of *Botryococcus b.* dropped significantly when the heating time exceeded 5 minutes.
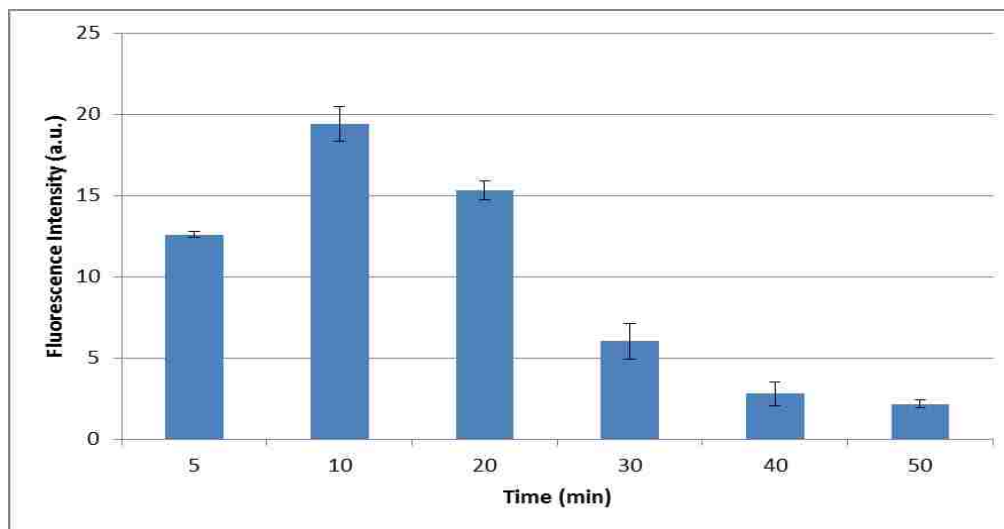
Fig. 4 The effect of staining time on fluorescence intensity for *Botryococcus b.* maintained at 55 °C. The excitation and emission wavelengths were 480nm and 575nm, respectively. Three replicate determinations were performed for each sample.

Overall, the penetration of Nile Red molecules into the microalgae cells and further disolved in the neutral lipid became slowly and difficultly for *Botryococcus b.*, *Chlorella p.*, and *Scenedesmus q.* due to their thick and rigid walls. A heating treatment with optimum conditions was employed to assist the Nile Red to penetrate through the cell walls. This simple and easy method was quite efficient in improving the fluorescence signal of the microalgae at their current growth status. Both temperature and time periods of the applied heat were also found to influence the Nile red staining efficiency of the algal species. These two factors must be controlled when this modified Nile red method is applied to the algae neutral lipid determination in order to obtain the maximum fluorescence intensity of the algal lipid.

3.3.2. Epifluorescent Microscopic Images of Algae

To verify the heating treatment did indeed improve the staining efficiency, the fluorescent microscopic images of *Botryococcus b.* were obtained from a Nikon Eclipse

E800 fluorescence microscope that had a TRITC filter set. Fig. 5a and 5b exhibited the microscopic image of *Scenedesmus* stained with Nile Red assisted by heating at 45 $^{\circ}$C for 20 min at red range and bright range, respectively. After heating, the nuetral lipid staining with Nile Red illuminated strong yellow-golden fluorescence signal at red range.
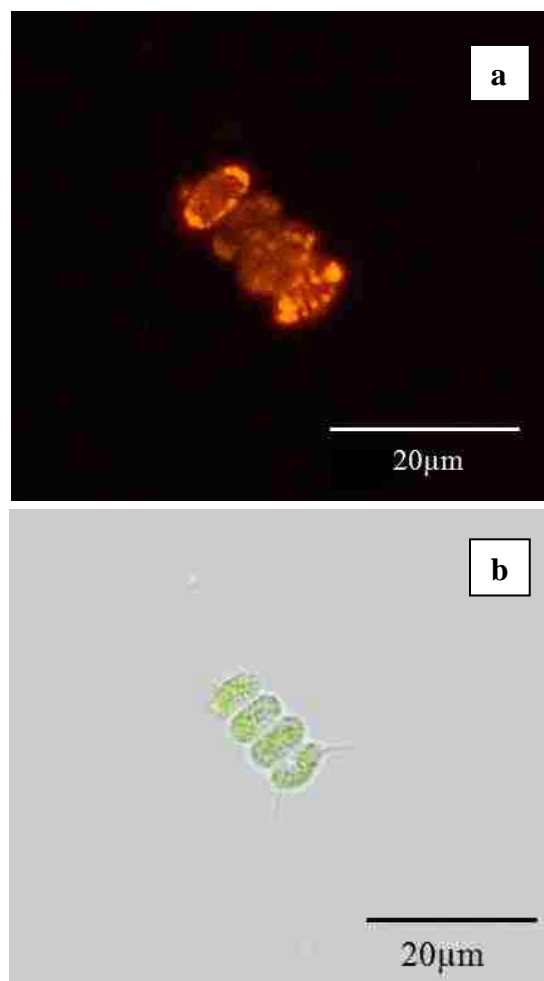
Fig. 5   Epifluorescent microscopic images of Nile red stained *Scenedesmus q.* with the heating treatment conditions of 45 $^{\circ}$C for 20 minutes at red range (a) and bright range (b)

Figure 6a and b indicated the microscopic images of *Botryococcus b.* stained with the conventional method and the heat-treated Nile red method at 55 $^{\circ}$C for 5 minutes,

respectively. It was observed that the Nile red-stained nuetral lipid assisted with heating treatment illuminated a stronger yellow-golden fluorescence than that without any treatment. This verified that the fluorescence intensity of neutral lipid from the microalgae was enhanced after a heating treatment.
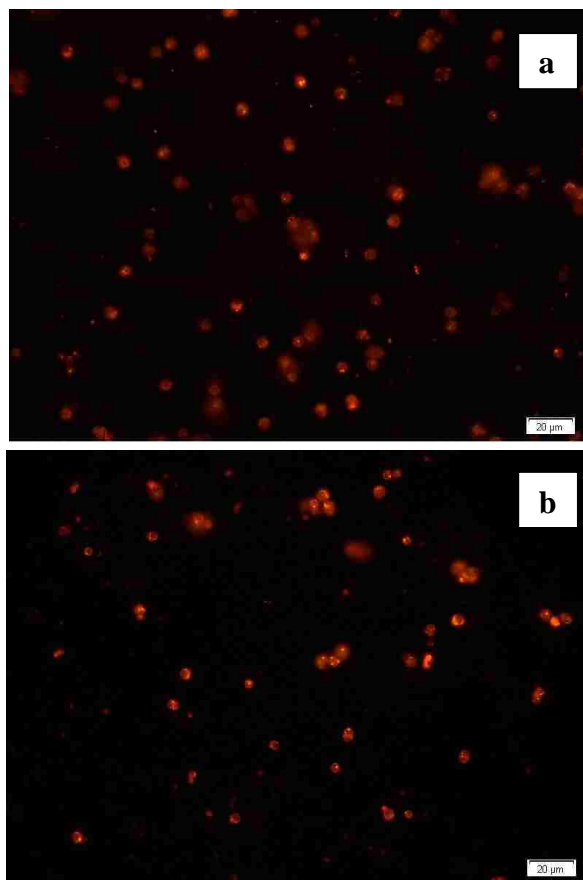
Fig.6   Epifluorescent microscopic images of Nile red stained *Botryococcus b.* by a) without a heating treatment and b) with a treatment at 55 °C for 5 minutes

3.4. NILE RED STAINING ASSISTED BY ACID TREATMENT

A series of different concentrations of diluted sulfuric acid (H_2SO_4) solution was added to three algae species (*Botryococcus b.*, *Chlorella p.*, and *Scenedesmus q.*) to improve the staining efficiency of Nile red and then enhance the fluorescence signal of

the stained neutral lipids. The H_2SO_4 concentration varying from 0.001 to 1.00% were considered in the present study

Figure7 illustrates changes in the microalgal fluorescence signals when the H_2SO_4 concentrations were varied. The Nile red staining efficiency of all three algal species improved. The *Botryococcus b.* treated by an H_2SO_4 solution exhibited 12 times increase of fluorescence intensity when the concentration of H_2SO_4 was as low as 0.002% as compared to the control. The H_2SO_4 treated *Chlorella p.* gave a significant rise of the fluorescence intensity when the concentration of diluted acid increased to 0.01%. Thereafter, the fluorescence intensity remained the same. Berglund reported that the lichen algal cells experienced stresses from sulfuric acid[19]. These cells treated at a pH of 4.5, had the highest mean fluorescence intensity. Cells treated with 5.5, 3.5, and 2.5 appeared to have a lower fluorescence intensity. The experimental results obtained during this study exhibited in the similar trends of fluorescence intensity of an algal culture treated by diluted H_2SO_4.
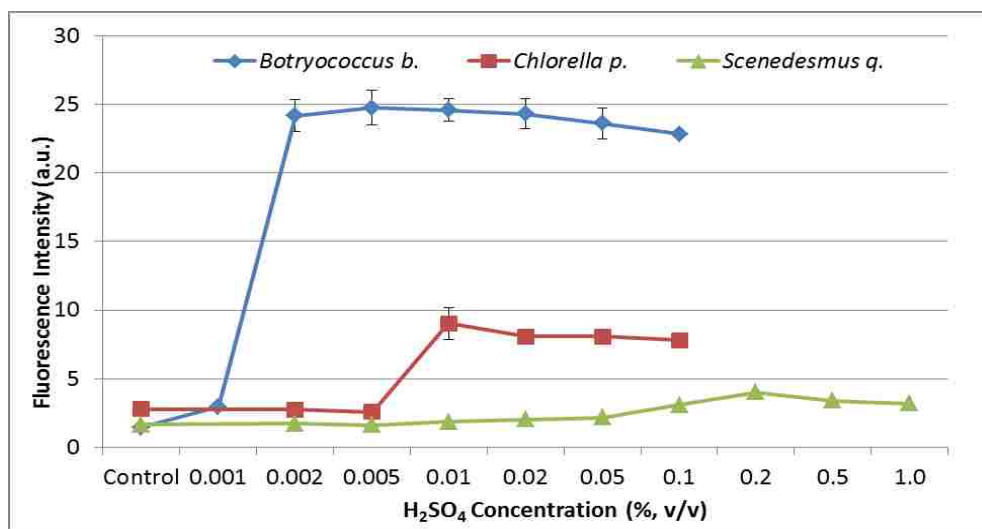
Fig. 7   The effect of H_2SO_4 concentrations on fluorescence intensity of the Nile red stained microalgae. Three replicate determinations were performed for each sample.

4. CONCLUSIONS

Nile red molecules penetration into microalgal cells and further disolving in neutral lipid was slow and difficult due to thick and rigid walls of microalgae. The optimized heated and diluted H_2SO_4 treated methods of lipids staining with Nile red successfully improved the fluorescence intensity of nuetral lipids for microalgae species of *Botryococcus b.*, *Chlorella p.*, and *Scenedesmus q..* The fluorescence intensity of *Botryococcus b.* was enhanced more than ten times by the assistance of a heating treatment at 60 $^{\circ}$C for 5 minutes as compared to the values obtained from the specie without any treatment. The lipid fluorescence intensity of the *Botryococcus b.* increased approximately 12 times at a concentration as low as 0.002% of H_2SO_4 when the specie was treated with H_2SO_4. These two optimized Nile red staining methods may have a potential to determine the neutral lipid content in other algal species and biomasses.

REFERENCES

1.   J. Day, E. Benson and R. Fleck, *In Vitro Cell.Dev.Biol.-Plant*, 1999, 35, 127-136.

2.   Q. Hu, M. Sommerfeld, E. Jarvis, M. Ghirardi, M. Posewitz, M. Seibert and A. Darzins, *The Plant Journal*, 2008, 54, 621-639.

3.   K. M. McGinnis, T. A. Dempster and M. R. Sommerfeld, *Journal of Applied Phycology*, 1997, 9, 19-24.

4.   A. R. Rao, C. Dayananda, R. Sarada and T. R. Shamala, *Bioresource technology*, 2007, 98, 560-564.

5.   Z. Y. Liu, G. C. Wang and B. C. Zhou, *Bioresource technology*, 2008, 99, 4717-4722.

6.   E. G. Bligh and W. J. Dyer, *Canadian journal of biochemistry and physiology*, 1959, 37, 911-917.

7. D. Elsey, D. Jameson, B. Raleigh and M. J. Cooney, *Journal of Microbiological Methods*, 2007, 68, 639-642.

8. K. E. Cooksey, J. B. Guckert, S. A. Williams and P. R. Callis, *Journal of Microbiological Methods*, 1987, 6, 333-345.

9. W. Chen, C. Zhang, L. Song, M. Sommerfeld and Q. Hu, *Journal of Microbiological Methods*, 2009, 77, 41-47.

10. P. Greenspan, E. P. Mayer and S. D. Fowler, *The Journal of Cell Biology*, 1985, 100, 965-973.

11. K. Kimura, M. Yamaoka and Y. Kamisaka, *Journal of Microbiological Methods*, 2004, 56, 331-338.

12. C. T. Evans, C. Ratledge and S. C. Gilbert, *Journal of Microbiological Methods*, 1985, 4, 203-210.

13. Y. Kamisaka, N. Noda, T. Sakai and K. Kawasaki, *Biochimica et Biophysica Acta (BBA) - Molecular and Cell Biology of Lipids*, 1999, 1438, 185-198.

14. J. Izard and R. J. Limberger, *Journal of Microbiological Methods*, 2003, 55, 411-418.

15. S. Lee, B.-D. Yoon and H.-M. Oh, *Biotechnology Techniques*, 1998, 12, 553-556.

16. M. S. Cooper, W. R. Hardin, T. W. Petersen and R. A. Cattolico, *Journal of bioscience and bioengineering*, 2010, 109, 198-201.

17. T. Govender, L. Ramanna, I. Rawat and F. Bux, *Bioresource technology*, 2012, 114, 507-511.

18. H. De la Hoz Siegler, W. Ayidzoe, A. Ben-Zvi, R. E. Burrell and W. C. McCaffrey, *Algal Research*, 2012, 1, 176-184.

19. L. D. Berglund and S. Eversman, *Cytometry*, 1988, 9, 150-155.

II. OIL-IN-WATER MICROEMULSIONS AS CALIBRATION STANDARDS FOR LIPOPHILIC DYE-BASED DETERMINATION OF MICROALGAL NEUTRAL LIPIDS CONTENT

Hongfang Zhao,[1] Keesoo Lee,[2] and Paul Ki-souk Nam[1]

Department of Chemistry, Missouri University of Science and Technology, 1870 Miner Circle, Rolla, MO, 65409, USA[1] and Department of Life and Physical Sciences, Lincoln University, 820 Chestnut St., Jefferson City, MO, 65101, USA[2]

ABSTRACT

A direct spectrophotometric measurement using lipophilic dyes such as Nile Red provides a simple method to determine oil content of microalgae and allows a rapid identification of high oil-bearing microalgae. However, the application of this method on varying microalgae strains is limited and yields only qualitative results due to lack of appropriate standards necessary for an accurate neutral lipid quantification. In this paper, oil-in-water (O/W) microemulsions were prepared in varying oil concentrations and employed as calibration standards for direct measurement of Nile Red-stained neutral lipids in microalgae using a fluorescence spectrophotometer. Four different microalgae species, including *Botryococcus braunii*, *Chlorella pyrenoidosa*, *Haemetococcus pluvialis* and *Scenedesmus quadricauda* were analyzed for neutral lipid contents through the O/W microemulsions standards. The average neutral lipid contents calculated from the O/W microemulsion calibration standards were very close to the results obtained by using gravimetric method and followed by SPE fractionation for *Botryococcus braunii*, *Haemetococcus pluvialis* and *Scenedesmus quadricauda*. This fast and reliable method

through the combination of lipophilic dye process and O/W microemulsions standards in order to determine an actual microalgal neutral lipid content could potentially be used in investigation of large scale lipid production from microalgal biomass.

Key words: Micoralgae, Oil-in-water microemulsion, lipid, SPE fractionation

1. INTRODUCTION

Accumulated natural lipid in microalgae has potential to be an ideal resource of alternative biofuel or biodiesel due to their rapid growth and high neutral lipid contents[1-5]. Utilization of greenhouse gas CO_2 and wastewater to grow microalgae photoautotrophically is another advantage for application of microalgae. Besides as energy sources, microalgae also can be used as source of pharmaceuticals and food for both human consumption and aquacultural use[6]. While intracellular lipid content varies with different environmental conditions and algal species, a rapid and on-site measurement of large scale neutral lipid in commercial production is required.

Traditional determination of intracellular lipid content involves solvent extraction and gravimetric determination. It requires large amounts of algal samples, and must ensure extraction is completed without decomposition and/or oxidation of the lipid. Time-consuming and labor-intensive are other major drawbacks for the traditional method. More accurate techniques are employed to determine FAME deriviations using gas chromatography-flame ionization detector (GC-FID) and gas chromatography-mass spectrometry (GC/MS). However, these separation techniques still have numerous steps and are time-consuming and not suitable for high-throughput screening. Therefore, one cost-effective and in situ measurement of cellular lipid content needs to be developed. A

direct spectrophotometric measurement using lipophilic dyes provides a simple method to determine the oil content of microalgae and allows a rapid identification of high oil-bearing microalgae. Greenspan and Fowler demonstrated Nile red fluoresces strongly only in hydrophobic environment and at yellow-green range (excitation, 450-500 nm; emission, > 528 nm)[7]. Cooksey et al. used Nile red for determination of neutral lipid of microalgae by using fluorescence microscopy, flow cytometry, and spectrofluorometry[8]. A qualitative or semi-quantitative analysis data in determination of lipid content from Nile red stained microalgae has been investigated[9,10]. However, the limitation of using this fluorescence method is the fluorescence intensity, which is relative to compare or estimate the intercellular lipid contents in microalgae; it does not provide an absolute content of the lipid. Staining of lipid standards and staining of algal cells resulting in different fluorescence responses due to the different hydrophobicity and size are other drawbacks.

In this study, a series of oil-in-water microemulsion standards stabilized by a non-ionic surfactant (Tween 80) were prepared as pseudo standards that mimic microalgae cells suspended in water. The fluorescence intensity of Nile red stained neutral lipids in four different microalgae species was compared with the O/W microemulsions standards curves for determination of neutral lipid contents of microalgae. The established calibration standards method provided a reliable and fast way in determination of the neutral lipid in *Botryococcus b.*, *Haemetococcus p.* and *Scenedesmus q.*

2. MATERIALS AND METHODS

2.1. MATERIALS

Botryococcus braunii was purchased from the Integrated Energy Solutions Company. *Chlorella pyrenoidosa* (MC63AF2) and *Scenedesmus quadricauda* (MCF1) were obtained from the Lincoln University Culture Collection. *Haemetococcus pluvialis* was from the Culture Collection of Algae at the University of Texas at Austin. *Chlorella p.* was maintained in BG-11 medium and the other microalgal species were grown in f/2 culture medium. All of the microalgal strains were cultured in wide-mouth culture flasks at room temperature on a VWR orbital shaker that had an agitation speed of 100rpm.

The microalgae were harvested by decanting most water from the flask. The microalgal sediment was then placed in a tube to be centrifuged with an SNYO MISTRAL 3000i centrifuge at a speed of 2500 rcf for 10 minutes at the room temperature, so that the solids could be separated from with liquid. Finally, the dewatered microalgae slurry was dried with a Freeze Dryer (Refrigerated Vapor Trap, SAVANT). This drying process took approximately one week for each ~3g dry weight sample. The dried microalgal pellets were stored in a desiccator for future use.

Nile red (9-diethylamino-5-benzo[α] phenoxazinone) dye used in this study was purchased from the Acros Organics Company. All of the organic solvents with certified ACS grade were purchased from Fisher Scientific. Polysorbate 80 (Tween 80) with analytical grade was obtained from ICI Americas, Inc.. Soybean oil was purchased from local grocery store with brand name of Crisco®. Silica gel (Activated) and FAMEs standards (35022/AOCS#1) were obtained from the Forcoven Products, Inc., TX and Pestek Corporation, PA, respectively.

2.2. PREPARATION OF OIL-IN-WATER (O/W) MICROEMULSIONS

A series of triglyceride standards were prepared to calibrate neutral lipid content in microalgae. The oil stock, Tween 80 stock and Nile red stock solutions were all prepared in acetone and their concentrations were 1.983 mg/mL, 2.000 mg/mL and 0.100mg/mL, respectively. Series of O/W microemulsion standards, which concentrations ranging from 0.001 to 0.100 mg/mL were prepared in the experiment. Table 1 showed the formulations of the O/W microemulsions standards. The mixture of oil, Tween 80 and water was agitated on a vortex mixer for two minutes at room temperature to form microemulsions. 25.00 μL Nile red stock solution was added to a 5 mL microemulsions and the mixture was agitated on the vortex mixer for another one minute to stain the lipid drops of the microemulsions before it was measured using fluorescence spectrophotometer.

Table 1 Formulations of O/W microemulsions standards

	Oil weight (mg)	Tween 80 stock sol. (mL)	Water (mL)	Oil Conc. (mg/mL)
1	0.030	0.10	30.00	0.00099
2	0.595	0.10	30.00	0.01957
3	1.487	0.10	30.00	0.04821
4	1.983	0.10	30.00	0.06376
5	2.974	0.10	30.00	0.09413

2.3. FLUORESCENCE SPECTROPHOTOMETER

The fluorescence signals of Nile red-stained lipid from microalgae and lipid standards were measured on a Perkin-Elmer LS-5 fluorescence spectrophotometer. The excitation and emission wavelengths of 480 nm and 575 nm were selected and both slits were set at 10nm. The spectrophotometer was warmed up for half an hour before measurement. The tested cuvette for placing sample is made of quartz material.

3. RESULTS AND DISCUSSION

3.1. GRAVIMETRIC DETERMINATION OF TOTAL LIPIDS

In gravimetric extraction method, solvent mixtures containing a polar (methanol) and a non-polar (chloroform) solvent extracted a great amount of lipids. In these cases, the polar solvent released the lipids from their protein-lipid complexes, and the lipids subsequently dissolve in the non-polar solvent[11].

The Fig.1 indicated the total lipids content of the dry biomass of four different microalgae, *Botryococcus b.*, *Chlorella p.*, *Haemetococcus p.*, and *Scenedesmus q.* by using the gravimetric extraction method. Both of *Chlorella p.* and *Scenedesmus q.* have about 18-19% total lipids of the dry biomass and *Haemetococcus p.* has about 8% total lipids.
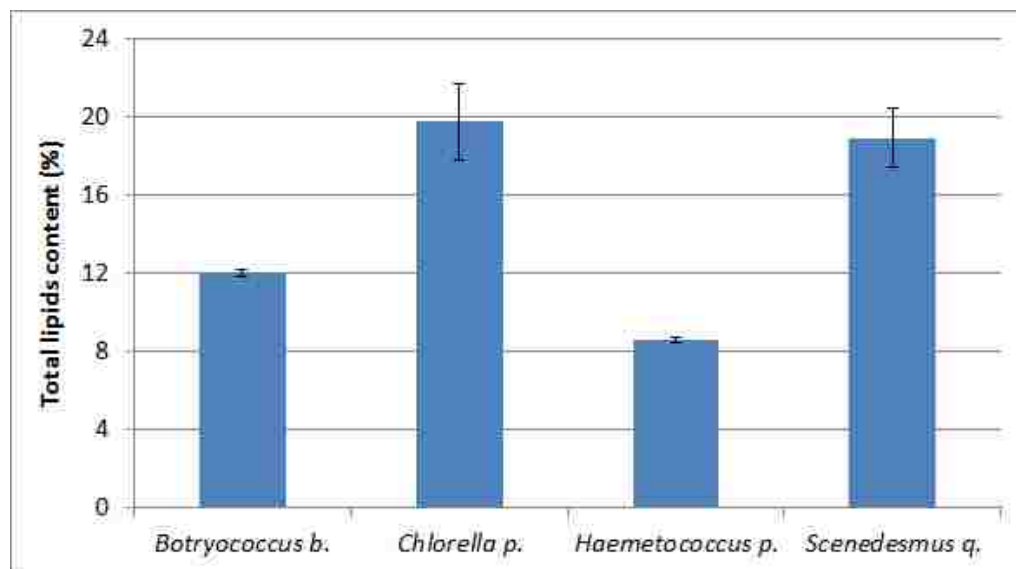
Fig. 1   Extracted total lipids content by using gravimetric method for four green microalgae, *Botryococcus b.*, *Chlorella p.*, *Haemetococcus p.*, and *Scenedesmus q.* Three replicate determinations were performed for each sample.

3.2. SPE FRACTIONATION OF TOTAL LIPIDS

SPE fractionation method was applied to the extracted total lipids obtained from the gravimetric method to determine non-polar lipid from microalgae. After subjecting with the SPE fractionation process of the total lipids, the percentages of neutral and polar lipids of the total lipid of microalgae were obtained and the results were showed in the Table 2.

The neutral lipids in *Haemetococcus p.* were 54.52%, which is higher than that in *Botryococcus b.*, *Chlorella p.*, and *Scenedesmus q.* containing 30.30%, 27.16%, and 26.00% of neutral lipids, respectively. The neutral and polar lipids compositions were found to be very similar with the results reported in a literature, whereas the neutral lipids occupied approximately 15-40% of the total lipids for most animal and microbial cellular lipids[12].

Table 2 Neutral and polar lipid compositions of microalgal species obtained from gravimetric extraction followed by SPE fractionation. Triplets determination were performed for each sample.

	Neutral lipids,% of dry biomass	Neutral lipids, % of total lipids	Polar lipids,% of dry biomass	Polar lipids, % of total lipids
Botryococcus b.	3.26±0.47	30.30	7.50±0.40	69.70
Chlorella p.	6.28±0.72	27.16	16.84±0.09	72.84
Haemetococcus p.	4.64±0.96	54.52	3.87±0.80	45.48
Scenedesmus q.	6.26±0.43	26.00	17.82±1.05	74.00

The neutral lipid content will be used to compare with the value that obtained from the prepared O/W microemulsions. This can be utilized to verify the efficiency of the O/W microemulsions as standards in the neutral lipid quantification of microalgae.

3.3. O/W MICROEMULSIONS STANDARDS

Surfactants have a characteristic molecular structure consisting of a chemical group that has very little attraction for the solvent (solvent-repellent), known as a lyophobic group, together with a group that has a strong attraction for the solvent (solvent-loving), called a lyophilic group. This is known as an amphipathic structure. Surfactant has the property of adsorbing onto the surfaces (interfaces when two immiscible phases are present) of the solution and decreasing the surface tension of the solution. In general, the HLB (hydrophile-lipophile balance) values of s surfactant ranges between 8 and 18 is recommended to make an oil-in-water emulsion and a value of 3-6 is the recommended range for water-in-oil emulsions[13]. Polysorbate 80 (Tween 80) possessing a HLB value at 15, is a nonionic surfactant and is often used in food and other

57

products as an emulsifier. In addition, Tween 80 is considered to be inherently

biodegradable and would not be expected to persist indefinitely in the environment. The

hydrophilic groups in Tween 80 are polyoxyethylene groups, which are also known as

hydrophilic heads, have highly polarity and are in contact with water. The alkyl chain as

hydrophobic or lipophilic tail in this compound assembles into an oil-like core to form an

oil-in-water micelle. The aggregates of micelles in aqueous solution form

microemulsions.

The O/W microemulsions in presence of a surfactant or emulsifier reduce the

interfacial tension once it is formed. Fig.2 showed the prepared five O/W

microemulsions standards, which were thermodynamically stable; and their

concentrations ranged from 0.001 to 0.01 mg/mL. The microemulsions solutions were

persistence and stable over several months from visual appearance.
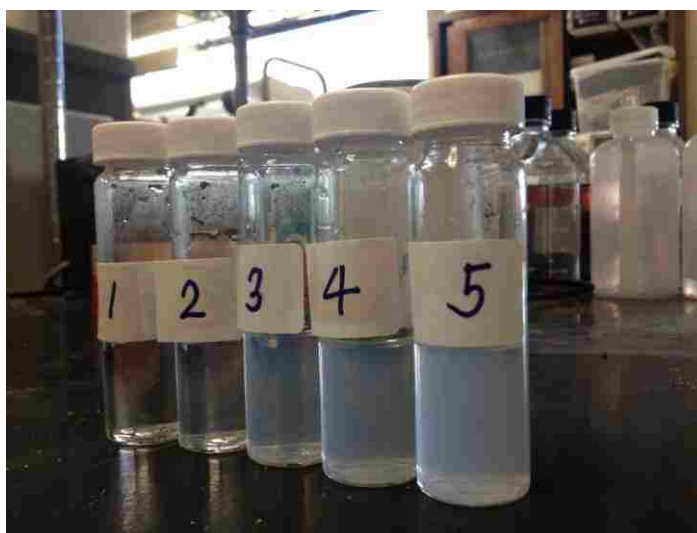
Fig. 2   Prepared O/W microemulsions standards solutions. (The oil concentrations
increased from the left side to the right side)

The fluorescence intensity of the O/W microemulsions standards was measured on a fluorescence spectrometer. The results gave rise to a very excellent linear relationship (R^2=0.9991) between fluorescence intensity and lipid standard solutions with high accuracy (Fig.3). This illustrated that the fluorescence spectrometer is applicable to the fluorescence emissions of Nile red stained-O/W microemulsions.
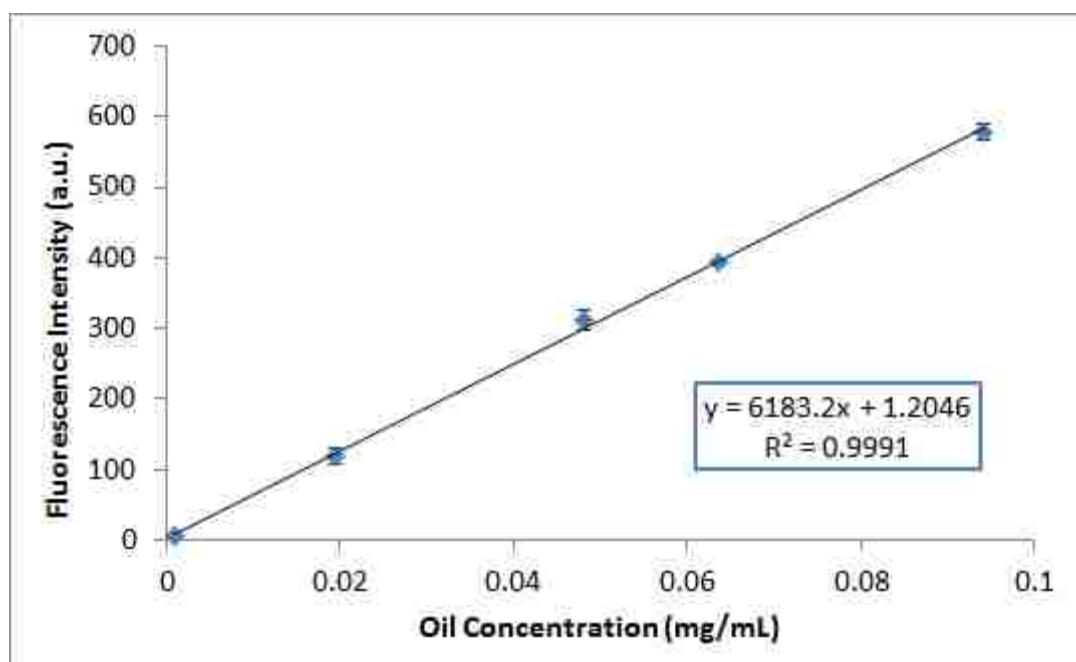
Fig. 3   Fluorescence intensity of the O/W microemulsions standards stained by Nile red. The fluorescence excitation was 480nm and fluorescence emissions were determined at 575nm. Both slits were set at 10nm. Three replicate determinations were performed for each standard.

3.4. COMPARISON OF NEUTRAL LIPID CONTENT DETERMINED BY O/W MICROEMULSIONS STANDARDS AND GRAVIMETRIC METHOD-SPE FRACTIONATION

The established O/W microemulsions standards were used to quantify the actual neutral lipid from microalgae in the experiment. The combination of gravimetric

extraction and SPE fractionation provides a reliable determination of neutral lipid content. The applicability and efficiency of the O/W microemulsions in determination of neutral lipid were demonstrated by comparing with the neutral lipid content obtained by using gravimetric extraction and followed by SPE fractionation method for four microalgal species *Botryococcus b.*, *Chlorella p. Haemetococcus p.*, and *Scenedesmus q.*.

The fluorescence intensity of neutral lipid from microalgae was measured under each optimized treatment condition for different microalgae species using fluorescence spectrometer. The treatment conditions for the microalgae have been discussed in the previous paper[14]. Before the measurement, *Botryococcus b.* was treated by 0.005% H_2SO_4; *Chlorella p.* and *Scenedesmus q.* were subjected heating at 55 $^{\circ}$C for 5min and 45 $^{\circ}$C for 20min, respectively. At last, the concentrations of neutral lipid from the microalgae were calculated according to the counterparts of the fluorescence intensity that obtained from the prepared O/W microemulsions standards.

The compared results of neutral lipid percentage of dry microalgal biomass from the two quantification methods, O/W microemulsion calibration standards method and gravimetric method followed by SPE fractionation method were given in the Fig.4.

The average neutral lipid contents calculated from the O/W microemulsion calibration standards were very close to the results obtained by using the gravimetric method followed by SPE fractionation for all of the microalgal species except *Chlorella p.*. Therefore, it illustrated that O/W microemulsions calibration method had abilities to provide an applicable and reliable way for a direct determination of actual neutral lipid contents from the microalgal species. The O/W microemulsions standards method may have the potential to be employed on other microalgal species or biomasses in

quantification of actual neutral lipid content if the fluorescence intensity of the sample

was reached the maximum level.
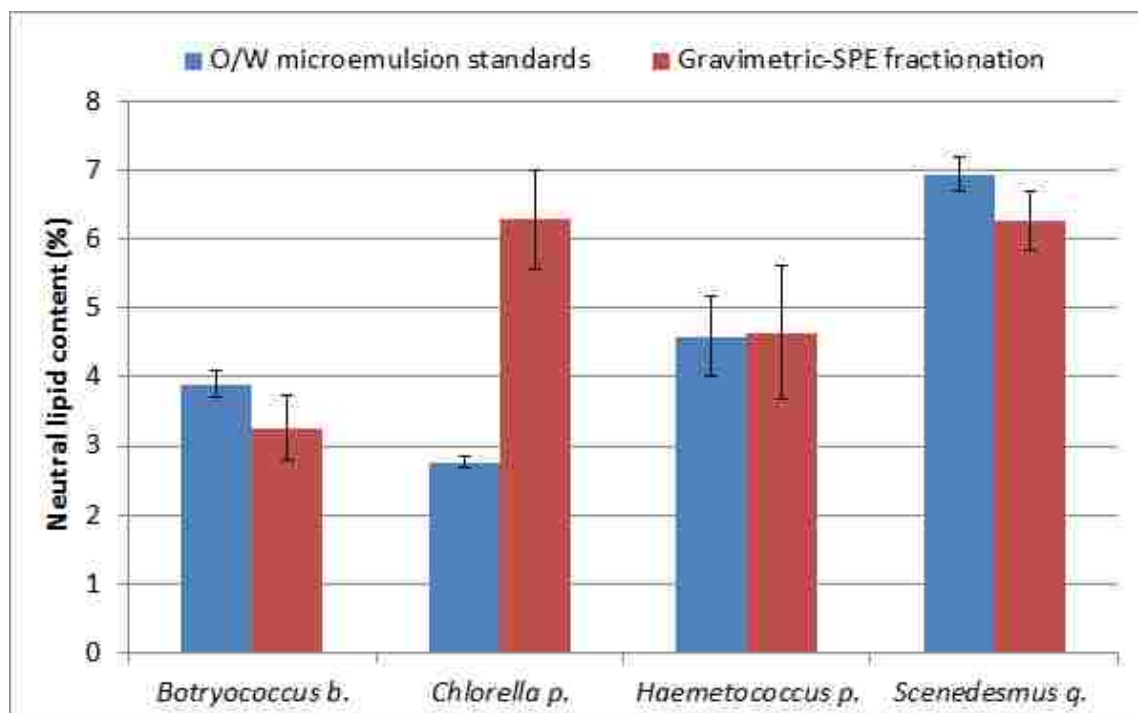
Fig. 4   A comparison of neutral lipid contents obtained with the O/W microemulsions calibration standards and with the gravimetric method followed by SPE fractionation for four microalgal species

Chlorella p. gave a significant difference of the neutral lipid content with using

these two methods. The presented discrepancy could be due to the difficult penetration

of Nile Red through the thick and rigid cell walls of *Chlorella p.*. This discrepancy may

be reduced or eliminated by enhancing the fluorescence intensity of Nile red-stained lipid

through other pretreatments.

4. CONCLUSIONS

Nile Red fluorescence allowed an *in situ* measurement of neutral lipid content with semi-quantitation of microalgae. In this study, a series of O/W microemulsions standards using triglyceride stabilizing with a non-ionic surfactant were prepared. It was demonstrated there was a linear fitting of the Nile Red fluorescence intensity vs. the O/W microemulsions standards with varying concentrations. It has been successfully employed to the determination of actual neutral lipid from microalgae under their optimized Nile red staining conditions. The pseudo-calibration standards had potential to be used as a sensitive, quantitative, and high throughput method for screening of cellular neutral lipid content in green algae as well as other classes of biomass.

REFERENCES

1. N. Kosaric and J. Velikonja, *FEMS Microbiology Reviews*, 1995, 16, 111-142.
2. J. Hill, E. Nelson, D. Tilman, S. Polasky and D. Tiffany, 2006.
3. J. Day, E. Benson and R. Fleck, *In Vitro Cell.Dev.Biol.-Plant*, 1999, 35, 127-136.
4. Y. Chisti, *Biotechnology Advances*, 2007, 25, 294-306.
5. Q. Hu, M. Sommerfeld, E. Jarvis, M. Ghirardi, M. Posewitz, M. Seibert and A. Darzins, *The Plant Journal*, 2008, 54, 621-639.
6. D. Elsey, D. Jameson, B. Raleigh and M. J. Cooney, *Journal of Microbiological Methods*, 2007, 68, 639-642.
7. P. Greenspan, E. P. Mayer and S. D. Fowler, *The Journal of Cell Biology*, 1985, 100, 965-973.
8. K. E. Cooksey, J. B. Guckert, S. A. Williams and P. R. Callis, *Journal of Microbiological Methods*, 1987, 6, 333-345.
9. S. Lee, B.-D. Yoon and H.-M. Oh, *Biotechnology Techniques*, 1998, 12, 553-556.
10. W. Chen, C. Zhang, L. Song, M. Sommerfeld and Q. Hu, *Journal of Microbiological Methods*, 2009, 77, 41-47.

11.   S. S. a. a. I. G. B. A. Intercomparison of Spanner, J.N. Hawthorne & R.M.C. Dawson, eds. Form and function of phospholipids, Amsterdam, Elsevier 43–65.

12.   E. Grima, M. Gonz ález and A. Gim énez, in *Algae for Biofuels and Energy*, eds. M. A. Borowitzka and N. R. Moheimani, Springer Netherlands, 2013, vol. 5, ch. 11, pp. 187-205.

13.   H. Y. Erbil, *Surface Chemistry of Solid and Liquid Interfaces*, Wiley-Blackwell, 2006.

14.   H. Zhao, K. Lee and P. K. Nam, *Intended for submission to Algal Research*.

III. THERMAL DECOMPOSITION STUDIES OF EPS, POLYURETHANE FOAM, AND EPOXY RESIN (SLA) AS PATTERNS FOR INVESTMENT CASTING

Hongfang Zhao[1], Paul Ki-souk Nam[1], Von L. Richards[2], Simon N. Lekakh[2]

[1]Department of Chemistry

[2]Department of Materials Science and Engineering

Missouri University of Science and Technology, Rolla, MO 65409, USA

ABSTRACT

Thermal and chemical characteristics of three different polymer pattern materials for investment casting, expanded polystyrene foam (EPS), polyurethane foam (FOPAT) at three densities of 0.12, 0.15 and 0.17 g/cm^3, and epoxy resin (SLA) were experimentally investigated. Thermal degradation behaviors of polymers were investigated by thermal gravimetric analysis (TGA). Glass transition temperatures of polymers were studied by differential scanning calorimetry (DSC). The TGA results indicated that the FOPAT pattern was decomposed completely at 700 $^\circ$C under air atmosphere while there was about 20% residual remaining at 800 $^\circ$C under N_2 atmosphere. Both of the EPS and SLA patterns were degraded more readily than the FOPAT pattern. The FOPAT pattern showed two glass transition temperatures (T_gs) at 56 $^\circ$C and 140 $^\circ$C. The EPS and SLA pattern showed a T_g at 106 $^\circ$C and 55 $^\circ$C, respectively. The potential generation of toxic gas, hydrogen cyanide (HCN) from thermal degradation of the FOPAT pattern was examined in a lab-built heating system. The HCN level depended on

the decomposition conditions, such as oxidant level and residence time. The experimental findings indicated that both of a higher oxidant level around the FOPAT sample and a longer residence time of the HCN in a hot zone of the furnace could reduce the HCN level.

Key words: EPS, Polyurethane, Epoxy, Thermal degradation, Hydrogen cyanide, Investment casting

1. INTRODUCTION

Investment casting, known as a lost-wax casting, has been widely employed to manufacture of high quality metal components due to its ability to produce accurate and complex castings. In investment casting, a wax pattern is dipped in ceramic slurry and stucco is applied by a rainfall sander or fluidized bed to build up multiple layers of a mold shell and then the pattern is removed by heating in an autoclave or flash firing in a furnace to create a mold. The mold shell is then fired to burn out residue and sinter. Liquid metal is poured in the mold and solidified to form a casting. Finally the ceramic shell is destroyed to release the metal part. While there are some limitations of wax pattern, such as distortion when storing and handling issues due to weight and brittleness. As dictated by technological or production level requirements, wax pattern could be replaced by a polymer foam pattern or printed pattern. The polymer foam pattern can provide lower tooling cost or the SLA pattern can provide low density printed structure for low production quantities and in either case ease of handling for low production dipping due to weight[1].

Expandable polystyrene (EPS) foam can be used in investment casting processing[2]. Polystyrene is a long chain hydrocarbon resulting from the polymerization of styrene monomers. EPS foam has a closed-cell foam structure. A rigid pattern can be manufactured by steam molding and can be modified by CNC (Computer Numerical Control) machining for rapid prototyping or very low quantity production without hard tooling. The small polystyrene beads are expanded to a desired density with a blowing agent. These expanded and/or machined pieces of foam pattern with complex geometry can be assembled into any desired shapes.

The SLA (Stereolithography apparatus) polymer pattern is a thermosetting polymer made from curing reaction (crosslinking) between epoxy resin and curing agent or "hardener". The diglycidyl ether of bisphenol A (DGEBA) structure, which is made from the reaction of bisphenol A and epichlorohydrin, is the most common, commercially available epoxy resin. SLA can be built precisely by a Stereolithography process- one of the modern rapid prototyping (RP) technologies. This overcomes the cost and lead time limitations of hard tooling for limited quantities of complicated castings[3]. The SLA pattern, having a honeycomb core structure, has the property of low density, which can produce less decomposition products and lead the SLA pattern to burn away readily during firing[4].

FOPAT (a FOam PATtern material) is a water blown polyurethane foam, which has been developed for investment casting process to produce high quality castings with good surface finish. This material offers many advantages, for example, lower cost per pattern, increased dimensional accuracy, increased temperature stability [5]. Polyurethanes are thermosetting polymers that are produced by the reaction of a hard segment,

isocyanate (R-N=C=O) with a soft segment that consists of compounds containing at least two active hydroxyl groups (R-OH-). Typically a FOPAT pattern is produced by foaming in metal die but a softer die (wood or rubber) or CNC machining could be used for low production volume.

It is well known that materials containing nitrogen in their chemical structure can be thermally degraded into highly toxic hydrogen cyanide (HCN), which is about thirty times more toxic than carbon monoxide (CO) on a volume basis[6]. Thus since 1970's much public attention has been directed toward the potential dangers of HCN to life and health, and numerous research studies were conducted to determine HCN which was released from the combustion of furnishings and structural materials containing nitrogen[7-12]. FOPAT pattern contains approximately 6 wt% of nitrogen in its chemical structure. Thus HCN could be produced during the pattern removal process in investment casting and could pose a hazard to workers especially when HCN reaches a certain concentration level in a working area. It has been suggested that decomposition of polyurethane includes three different reaction mechanisms (see scheme 1)[13-17]. The first one is the reversed reaction of formation of urethane group, giving isocyanate and alcohol. The second one is dissociation to amine, carbon dioxide, and olefin through a six-membered ring transition state. The last one is dissociation to secondary amine and carbon dioxide through a four-membered ring transition sate.

The objective of the current study was to explore the polymer pattern materials' thermal and chemical properties affecting the application in investment casting processing. Thermal degradation behavior and glass transition temperatures were characterized by using TGA and DSC techniques, respectively. Limiting the generation

of HCN from thermal decomposition of the FOPAT pattern material is also discussed in

this paper.
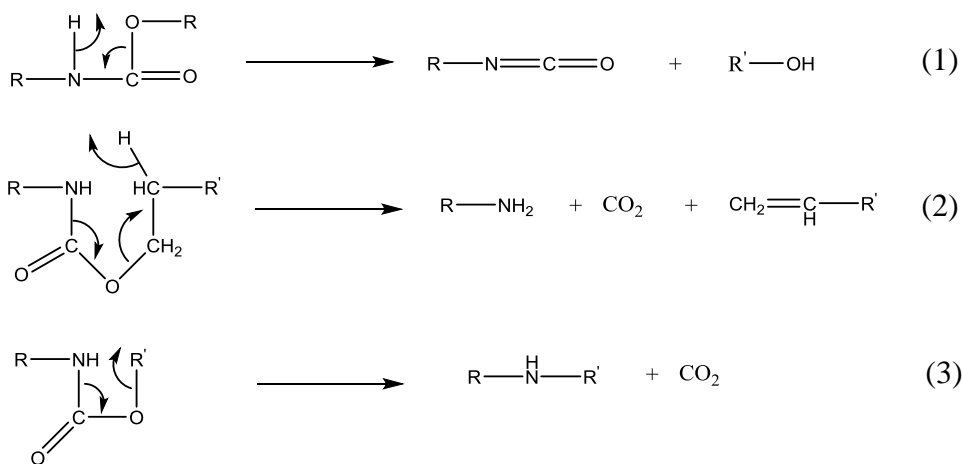
Scheme 1 Reaction mechanism of polyurethane decomposition

2. MATERIALS AND METHODS

2.1. MATERIALS

EPS foam (density, 0.025 g/cm^3) was purchased from the Austin Group LLC

(Montgomery, AL). FOPAT (three densities, 0.12, 0.15 and 0.17 g/cm^3) patterns were

provided by the Production Inc. (Miamisburg, OH). A commercial grade of WaterShed

XC 11122 SLA patterns (density, 0.2 g/cm^3) with honeycomb structure were from the

DSM Somos Company (Elgin, IL). Examples of investment casting patterns made from

these three different polymeric materials are given in Fig. 1(a-c).
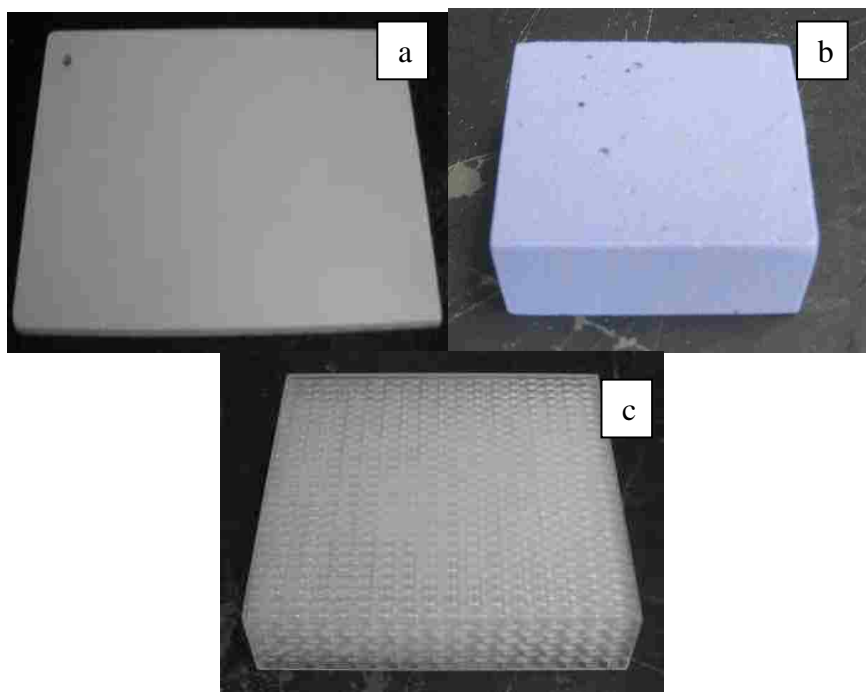
Fig. 1   Examples of investment casting patterns made from different polymeric materials:
a) EPS foam, b) FOPAT foam, and c) SLA with honeycomb internal structure

2.2. CHN ELEMENTAL ANALYSIS AND ASH CONTENT ANALYSIS

Elemental analysis of C, H, and N elements for EPS, FOPAT and SLA patterns

were performed on a Perkin Elmer 2400 machine. Ash content of EPS, FOPAT and SLA

patterns was analyzed according to the ASTM D5630-06 standard method. The

temperature of the muffle furnace was set at 800 $^\circ$C and the duration was 5min.

2.3. THERMOGRAVIMETRIC ANALYSIS (TGA)

Thermogravimetric analysis of EPS, FOPAT and SLA patterns were carried out

using a TGA instrument (TA-1000, New Castle, DE, USA) under both air and N_2

atmospheres. The scanning temperature ranged from room temperature to 600 $^\circ$C (EPS

and SLA patterns) or 800 $^\circ$C (FOPAT pattern) at a heating rate of 25 $^\circ$C/min.

2.4. DIFFERENTIAL SCANNING CALORIMETRY (DSC) ANALYSIS

A pre-weight sample was first preheated from room temperature to 180 °C at 20 °C/min to remove any previous thermal history, and then quenched to -40 °C. Heat flow was measured using DSC instrument (TA- Q2000, New Castle, DE, USA) over a temperature range from -38 °C to 210 °C at a heating rate of 20 °C/min under a nitrogen atmosphere. The glass transition temperatures of EPS, FOPAT and SLA patterns were obtained from the inflection temperature of the DSC curve.

2.5. ANALYSIS OF HCN RELEASED FROM FOPAT PATTERN DURING THERMAL DEGRADATION PROCESS

The generation of HCN from thermal decomposition of FOPAT patterns in a muffle furnace was studied. The procedures were performed according to the ASTM D7295-06 standard method. The FOPAT sample was coated with slurry to form a thin permeable refractory shell and an alumna tube was attached to the FOPAT (Fig. 2). The FOPAT samples without refractory shell were also studied in order to investigate the effect of oxidant/fuel ratio on the generated HCN level.
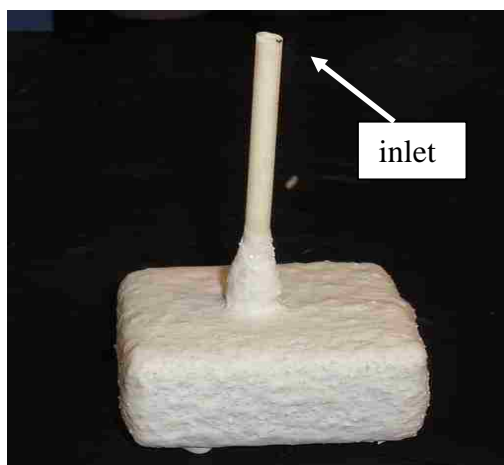
Fig. 2 Prepared FOPAT sample used for HCN analysis during thermal degradation process. The FOPAT sample was coated with a thin refractory layer. An alumina tube was attached to the sample and used to collect the HCN that formed inside of the shell.

2.5.1 Thermal Decomposition of FOPAT Pattern in Muffle Furnace

FOPAT samples (three densities, 0.12, 0.15 and 0.17g/cm^3) with dimensions of 2in (L) x 2in (W) x 1in (H) were studied. A HCN testing system was set up in the lab (Fig. 3). The generated HCN gas was trapped in an impinger vessel, which contained a 100mL of 0.1N sodium hydroxide (NaOH) solution. A 0.45 micron pore nylon filter was placed before the impinger vessel to remove any particulate products. A vacuum pump was connected to the impinger vessels to draw the HCN product at a flow rate of 160mL/min. The FOPAT sample was heated in the furnace at a temperature range of 25~ 800 $^{\circ}$C. After one hour of decomposition, the trapping solution was titrated with a 0.01M silver nitrate (AgNO$_3$) standard solution to determine the HCN content. Each experiment was performed in triplicate.
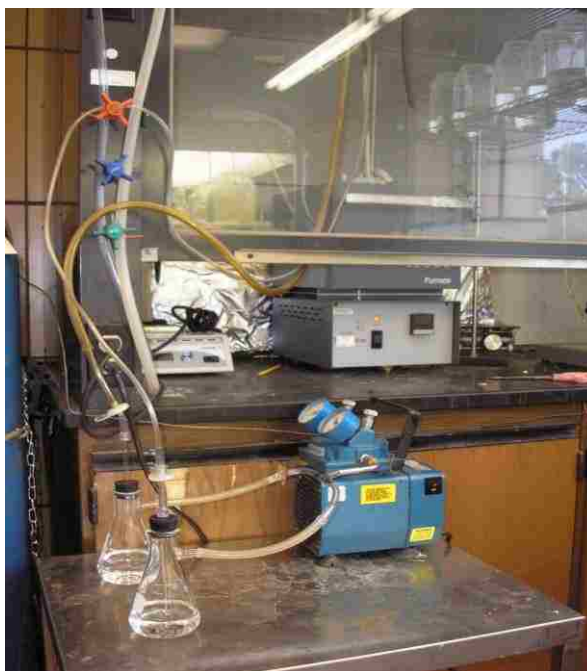
Fig. 3 Muffle furnace system (Thermolyne 47900) used for decomposing the FOPAT sample. Two long alumina tubes on top of the furnace were used to collect HCN gas generated from decomposition of the FOPAT sample. Two impinger solution vessels attaching with a vacuum pump were used to collect and trap the formed HCN gas.

In order to investigate the effects of oxidant level around the sample and

residence time of the decomposition product in a hot zone on the HCN level, three

different decomposition conditions were studied (Fig. 4-6),
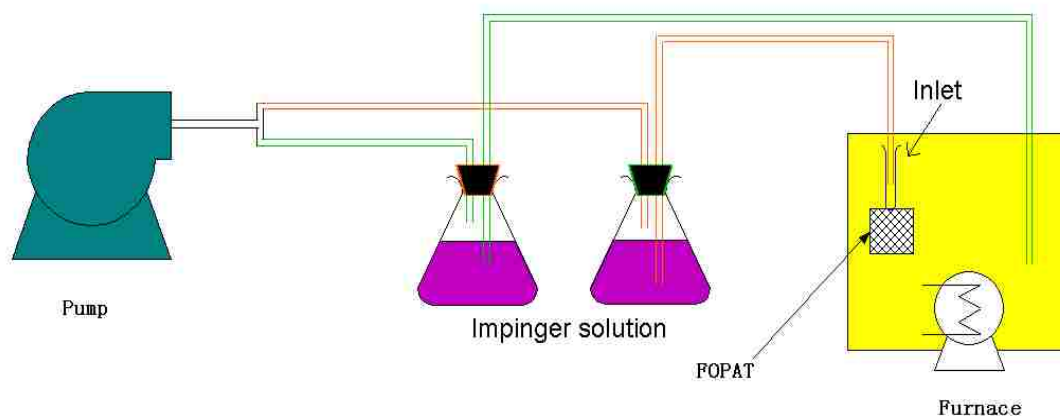
Fig. 4   FOPAT pattern coated with refractory shell and no air entering the shell from the inlet but by permeation only. One of the long alumina tubes was attached to the inlet of the FOPAT sample. This was used to collect HCN gas generated inside of the refractory shell of the FOPAT. The other long alumina tube was placed next to the FOPAT sample to collect the HCN gas penetrated from the shell of the FOPAT.
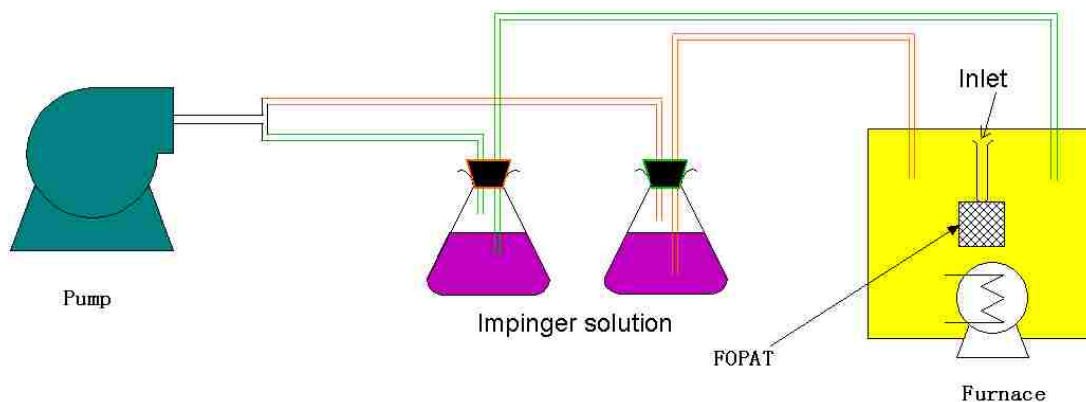
Fig. 5   FOPAT pattern coated with refractory shell and air entering the shell from the inlet and gas extracted by permeation. Both of the two long alumina tubes were placed next to the FOPAT sample. They were used to collect the HCN penetrated from the shell of the FOPAT sample. The short alumina tube that attached to the FOPAT sample was left open so more air entered in the shell.
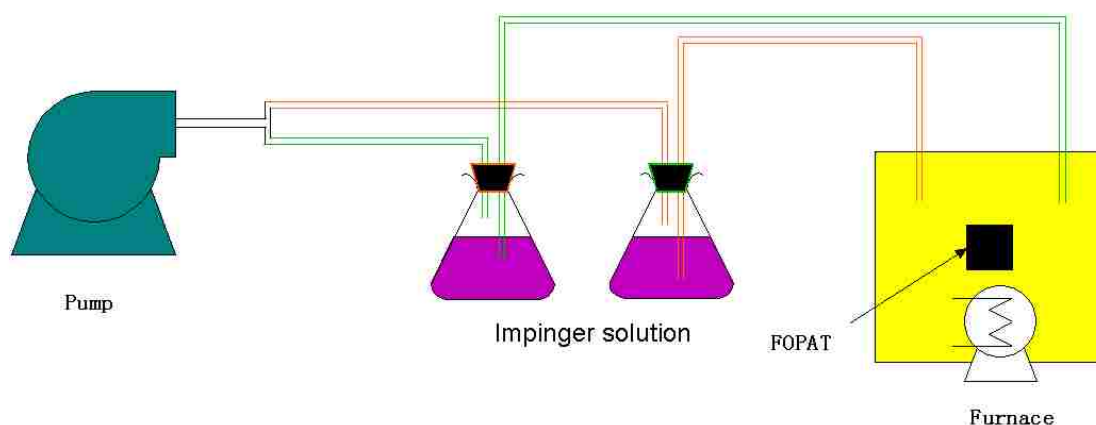
Fig. 6 FOPAT pattern no refractory shell. Both of the two long alumina tubes were placed next to the FOPAT sample to collect the HCN generated from the decomposition of FOPAT.

2.5.2. Quantification of Cyanides (CN) by Titration Using AgNO$_3$

The quantification of cyanides trapped in the impinger solutions was performed according to the ASTM D2036-09 standard method. In general, the CN$^-$ was titrated by using a 0.01N standard AgNO$_3$ solution. The end point of the titration was indicated as the color change of solution from yellow to salmon pink when the Rhodanine (p-dimethylaminobenzylidene) in acetone was used as an indicator. The concentration in milligrams of CN per litre in the original sample (impinger solution) was then calculated using the following equation:

mg CN/L = [(A – B)*N AgNO$_3$*0.052/mL original sample]*(250/mL aliquot used)*10^6

where:

A= AgNO$_3$ solution to titrate sample, mL, and

B= AgNO$_3$ solution to titrate blank, mL.

3. RESULTS AND DISCUSSION

3.1 ELEMENTAL AND ASH CONTENT ANALYSIS OF EPS, FOPAT, AND SLA PATTERNS

Table 1 shows the results of C, H, and N elemental analysis of EPS, FOPAT (three densities, 0.12, 0.15 and $0.17g/cm^3$), and SLA patterns. The composition of remaining content of the polymers could be approximated as oxygen. The FOPAT pattern contained approximately 6% of nitrogen of the total weight. The ash content of all of three polymer patterns after burning at 800 $^\circ$C for 5min in muffle furnace was negligible. Each sample was analyzed in triplicate.

Table 1 Elemental analysis of EPS, FOPAT and SLA patterns

	C%	H%	N%
EPS	91.6±0.3	5.4±0.5	1.9±0.1
FOPAT*	64.4±0.1	6.3±0.4	6.3±0.3
SLA	64.0±0.2	9.4±0.3	0.1±0.0

* FOPAT patterns with three different densities all have the same elemental compositions

3.2 TG ANALYSIS OF EPS, FOPAT, AND SLA PATTERNS

It is very important to understand thermal stability of patterns in order to reduce or avoid casting defects in investment casting. During pattern removal by flash firing, the pattern experiences both combustion and pyrolysis. In this study, TG analysis of EPS, FOPAT, and SLA patterns were studied in atmospheres of both air and N_2.

TGA curves of the polymer patterns are indicated in Fig. 7. The EPS patterns were decomposed completely at 450 $^{\circ}$C in both air and N_2. The SLA patterns were fully degraded at 600 $^{\circ}$C in both air and N_2. The FOPAT patterns at three different densities degraded completely at 700 $^{\circ}$C in air; and two distinct degradation stages were shown in the TGA curves. However, the FOPAT patterns had about 20% residue remaining at 800 $^{\circ}$C in N_2. As a consequence, casting defects resulting from the residue could be possible when the FOPAT pattern is applied to investment casting if the atmosphere is not adequately oxidizing. A high firing temperature (700 $^{\circ}$C or higher) and excess oxygen may be necessary to reduce or avoid defects of the castings during the FOPAT pattern removal.
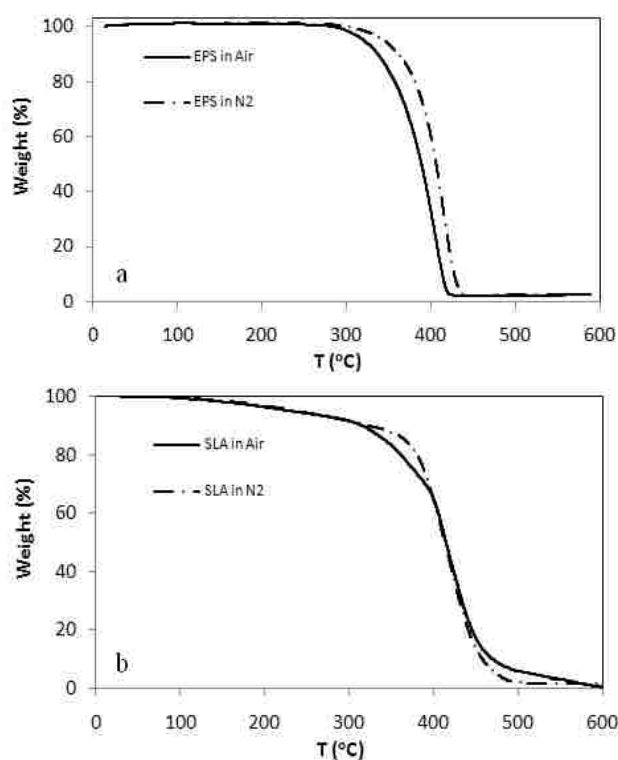
Fig. 7   TGA results of EPS, SLA, and FOPAT (three densities, 0.12, 0.15 and 0.17g/cm^3) patterns under both air and N_2 atmospheres at a heating rate of 25 $^{\circ}$C/min.
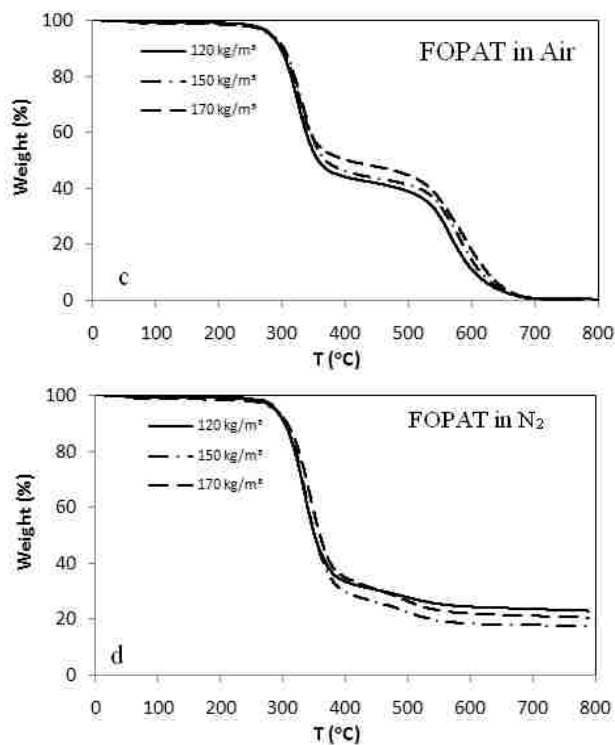
Fig. 7   TGA results of EPS, SLA, and FOPAT (three densities, 0.12, 0.15 and 0.17g/cm^3) patterns under both air and N$_2$ atmospheres at a heating rate of 25 °C/min (Cont.).

3.3 DSC ANALYSIS OF EPS, FOPAT, AND SLA PATTERNS

Glass transition temperatures (T_g) of the polymer patterns were obtained by using DSC. T_g is a transition of an amorphous material from a hard or glass-like non-crystalline state to a molten or rubber-like state during heating. Fig. 8 indicates the T_gs of the EPS, FOPAT and SLA polymer patterns. The T_g of the EPS pattern was at about 106 °C. The FOPAT pattern exhibited two glass transition temperatures at 57 and 140 °C. The first T_g at 57 °C was the glass transition temperature of the polyurethane; and the one at 140 °C was resulted from the state transition of the isocyanate segment present in the polyurethane. The SLA pattern gave a T_g at about 55 °C as indicated at the inflection point of the DSC curve. The glass transition temperatures of the three polymer patterns corresponded to the temperatures at which the patterns' thermal expansion occurred,

which has been discussed in the previous published papers[18,19]. This is because the

coefficient of thermal expansion shows a discontinuous change at this temperature[20].
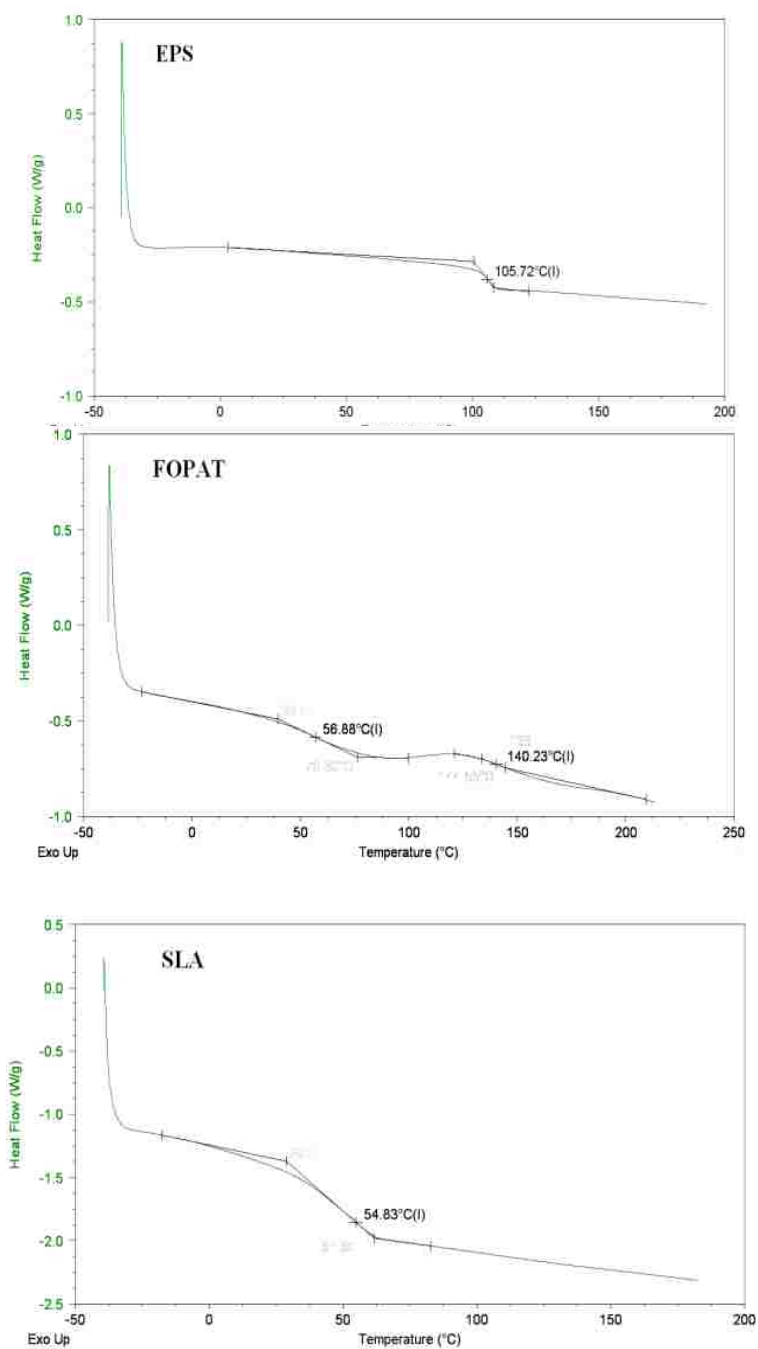
Fig. 8   DSC curves of EPS, FOPAT, and SLA polymer patterns. The T_g was shown at
the inflection temperature of the DSC curves.

3.4 ANALYSIS OF HCN CONTENT FROM THERMAL DEGRADATION OF FOPAT PATTERN

Table 2 shows the results of the HCN levels (wt% of the FOPAT sample) generated from the decomposition of the FOPAT patterns (three densities, 0.12, 0.15 and 0.17g/cm^3) under different decomposition conditions. About 0.05-0.11% HCN was produced from the decomposition of the FOPAT patterns with shell when only air entered the shell by permeation (Fig. 4). The HCN level was not significantly affected by density differences of the FOPAT pattern. The FOPAT pattern without shell (Fig. 6) produced about 0.017% of HCN, which was less than that obtained from the FOPAT pattern with shell. It was explained the FOPAT pattern without a shell had a larger contact area with air in the muffle furnace and thus less HCN was produced. When the FOPAT pattern was coated with shell and air can enter the shell through the inlet (Fig. 5), no significant HCN content was found. This was attributed to a higher level around the FOPAT sample because more air entered through the open inlet of the sample. And also a longer residence time of the products inside of the shell could be attributed to extraction of gaseous products being limited by permeation through the shell. The longer residence time enhanced decomposition of the HCN after its formation in the hot zone. Gordon found that HCN content produced from pyrolysis and combustion of polyacrylonitrile decreased when the oxidant/fuel ratio increased[21], which was in agreement with the experimental observations in the study.

The required minimum ventilation volume in cubic meters for 1kg FOPAT pattern decomposed was calculated according to the NIOSH Exposure limits (Table 2). Based on decomposition of 1 kg FOPAT pattern was under a less oxidant level (Fig.4), it would be harmful to human being's skin and health if the ventilation volume were

smaller than 108-270m^3 and 10-20m^3, respectively. At a higher oxidant level (Fig.6), the

required minimum ventilation volumes were only 34m^3 and 3m^3 to safety for people's

skin and health per 1kg FOPAT decomposed. Thus the volume of air change required for

a safe workplace can be estimated. The ventilation rates depend on the burnout rate used,

but safest practice could be greater than 227m^3 ventilation air for 1kg of foam burned out.

Table 2 HCN content (wt% of the FOPAT sample) from decomposition of the FOPAT
pattern and required ventilation volume in m^3 for 1kg FOPAT pattern decomposed under
three decomposition conditions. Each sample was performed in triplicate.

Decomposition condition	Density, kg/m^3	HCN% (wt) of FOPAT	Required ventilation volume (m^3) for 1kg FOPAT decomposed
a. FOPAT with shell and air entered through permeation of the shell	120	0.065 ±0.003	130 (REL) 12 (IDLH)
	150	0.054 ±0.003	108 (REL) 10 (IDLH)
	170	0.113 ±0.005	227 (REL) 20 (IDLH)
b. FOPAT with shell and air entered through inlet of the shell	120	-	-
	150	-	-
	170	-	-
c. FOPAT without shell	170	0.017 ±0.001	34 (REL) 3 (IDLH)

Note: "-" means the HCN content was negligible.
NIOSH (National Institute for Occupational Safety and Health) Exposure Limits:
REL (Recommended exposure limits): 5mg/m^3 or 4.7ppm [skin] in air
IDLH (Immediately dangerous to life or health): 55mg/m^3 or 50ppm in air

4. CONCLUSIONS

The properties which affect the applicability polymer pattern materials used in investment casting were experimentally investigated. The TGA study of the FOPAT pattern demonstrated that casting defects resulting from the residue was possibly formed if the atmosphere is not adequately oxidative in investment casting. The generation of toxic HCN gas from decomposition of FOPAT patterns under different decomposition conditions was studied. It indicated that HCN concentration could be reduced by increasing both oxidant level and residence time of the HCN in a hot zone of the furnace.

ACKNOWLEDGEMENT

REFERENCES

1. US 4655276, 1987.

2. D. Kline, S. Lekakh, C. Mahimkar and V. Richards, presented in part at the Technical and Operating Conference, Chicago, Illinois, 2009.

3. C. M. Cheah, C. K. Chua, C. W. Lee, C. Feng and K. Totong, *Int J Adv Manuf Technol*, 2005, 25, 308-320.

4. Y. Norouzi, S. Rahmati and Y. Hojjat, *Rapid Prototyping Journal*, 1995, 15, 255-263.

5. D. Neece, *Advanced Pattern Material for Investment Casting Applications*, Cleveland Tool and Machine, Brookpark, OH, Department of Energy, Washington, DC, 2006.

6. K. Sumi and Y. Tsuchiya, *Journal of Fire and Flammability*, 1973, 4, 15-22.

7. A. Alajbeg, *Journal of Analytical and Applied Pyrolysis*, 1987, 10, 215-224.

8. B. C. Levin, M. Paabo, M. L. Fultz and C. S. Bailey, *Fire and Materials*, 1985, 9, 125-134.

9. B. C. Levin, M. Paabo, J. L. Gurman and S. E. Harris, *Fundamental and Applied Toxicology*, 1987, 9, 236-250.

10. F. M. Esposito and Y. Alarie, *Journal of Fire Sciences*, 1988, 6, 195-242.

11. K. Yamamoto, *Journal of Combustion Toxicology*, 1977, 4, 69-78.

12. R. A. Anderson, I. Thomson and W. A. Harland, *Fire and Materials*, 1979, 3, 91-99.

13. E. Dyer and R. E. Read, *The Journal of Organic Chemistry*, 1961, 26, 4388-4394.

14. E. G. Bligh and W. J. Dyer, *Canadian journal of biochemistry and physiology*, 1959, 37, 911-917.

15. E. Dyer and G. E. Newborn, *Journal of the American Chemical Society*, 1958, 80, 5495-5498.

16. M. P. Thorne, *Canadian Journal of Chemistry*, 1967, 45, 2537-2546.

17. M. Boutin, J. Lesage, C. Ostiguy, J. Pauluhn and M. J. Bertrand, *Journal of Analytical and Applied Pyrolysis*, 2004, 71, 791-802.

18. W. Everhart, S. Lekakh, V. Richards, J. Smith, H. Li, K. Chandrashekhara, H. Zhao and P. Nam, presented in part at the Transactions of the American Foundry Society, 2012.

19. H. Zhao, M. Xu, H. Li, W. Everhart, S. Lekakh, V. Richards, K. Chandrashekhara and P. Nam, presented in part at the Investment Casting Institute, Covington, KY, 2011.

20. D. L. Beck, A. A. Hiltz and J. R. Knox, *Polymer Engineering & Science*, 1963, 3, 279-285.

21. S. Gordon and B. J. McBride, *NASA SP-273*, 1971.

IV. THERMAL DEGRADATION KINETICS OF EPOXY STEREOLITHOGRAPHY PATTERN FOR INVESTMENT CASTING PROCESS

Hongfang Zhao[1], Paul Ki-souk Nam[1], Von L. Richards[2], Simon N. Lekakh[2]

[1]Department of Chemistry

[2]Department of Materials Science and Engineering

Missouri University of Science and Technology, Rolla, MO 65409, USA

ABSTRACT

Thermal degradation behavior of epoxy stereolithography (SLA) pattern materials used in investment casting were studied by a conventional dynamic thermogravimetric analysis (TGA) at different heating rates between 5 and 40 $^{\circ}$C/min under nitrogen purge. The kinetics parameters of thermal degradation of the SLA pattern were determined by two different kinetics models, differential (Kissinger) and integral (Flynn-Wall-Ozawa) methods. A model-fitting method (modified Coats-Redfern) was used to evaluate the degradation mechanism of the epoxy SLA pattern. The activation energy corresponding to the mechanism *D*3 (diffusion) obtained from the fitting method was in good agreement with the value obtained by using the two kinetics models. The solid-state thermal degradation mechanism of the epoxy resin system was a diffusion process.

Key words: Epxoy resin, Investment casting, Kinetics, Thermal decomposition

1. INTRODUCTION

Investment casting, known as a lost-wax casting, has been widely employed to manufacture of quality metal components in automobile, aerospace and biomedical industries because of its ability to produce accurate and complex castings. In investment casting, a wax pattern is dipped in ceramic slurry and stucco is applied by a rainfall sander or fluidized bed to build up multiple layers of a mold shell and then the pattern is removed by heating in an autoclave or flash firing in a furnace to create a mold. The mold shell is then fired to burn out residue and sinter. Liquid metal is poured in the mold and solidified to form a casting. Finally the ceramic shell is destroyed to release the metal part. While there are some limitations of wax pattern, such as distortion when storing and handling issues due to weight and brittleness. As dictated by technological or production level requirements, wax pattern could be replaced by polymer pattern due to the latter's lower creep under self-loading, lower tooling cost for low production quantities and in some cases ease of handling due to lighter weight than wax[1].

Expanded polystyrene (EPS) foam is one of the most common pattern materials used in commercial practice. EPS experiences thermal degradation through chain scission during the pattern removal process. Thermal degradation behaviors of EPS pattern have been studied under oxidative and/or inert gas atmospheres[2,3]. However, EPS pattern may have distortion or even breaks during the dipping process in slurry due to low strength and density of the foam[4]. Epoxy is one novel candidate pattern material and can overcome the above issues in both iron and aluminum castings. Epoxy is a thermosetting epoxide polymer and photosensitive, which can be cured (cross-links and polymerizes) with a curing agent or "hardener". Stereolithography (SLA) Rapid

Prototyping process is mostly used to manufacture epoxy resin parts with high

dimensional stability and low cost for Investment Casting. The Rapid Prototyping

process is used to build three-dimensional epoxy pattern parts and developed to provide

dimensional accuracy and surface finish of epoxy resins. Most common and important

class of epoxy resins are formed from a reaction between epichlorohydrin and bisphenol-

A to form diglycidyl ethers of bisphenol A.

For Investment casting, one important aspect concerning the behavior of epoxy

resin during its thermal decomposition is the kinetic studies. The kinetic equations can

be applied to studies concerning its reaction to fire (ignition process, flame propagation,

evaluation of the amount of toxic products generated, etc.) and to the reactor design and

optimization of the operating conditions in the thermochemical processing of the

material[5]. Thermogravimetric analysis (TGA) has been extensively employed for study

of thermal degradation kinetics of different polymers and copolymers[6,7]. Experiments are

usually performed under nonisothermal conditions. The kinetics parameters such as

activation energy, preexponential factor, and reaction order may be obtained. The

objective of our work is to study the thermal degradation kinetics of epoxy resin pattern

using two kinetic models, Kissinger model (differential method) and Flynn-Ozawa-Wall

model (integral method). The two methods were used to calculate the kinetic parameters

of thermal decomposition of epoxy resin pattern. The degradation mechanisms were

estimated by Coates-Redfern analytical fitting method.

2. THEORETICAL BACKGROUND

2.1. KISSINGER'S METHOD

Kissinger method is another common non-isothermal and model-free technique.
It is used to determine the activation energy for a simple decomposition reaction
regardless of reaction order from differential thermal analysis for a series of experiments
at different heating rates. The Kissinger method is based on the study of the rate equation
at the maximum reaction rate. This method allows obtaining the kinetic parameters from
a plot of $\ln (\beta/T^2_m)$ against $1/T_m$. The equation is the following,

$$\ln \left(\frac{\beta}{T_m^2} \right) = \ln \left(\frac{AR}{E} \right) - \frac{E}{RT_m}$$

where β is the heating rate, A is the pre-exponential factor, E is the activation energy. R
is the gas constant. T_m is the temperature at the maximum rate occurs.

2.2. FLYNN-WALL-OZAWA METHOD

This method is derived from the integral iso-conversional method which the
kinetic parameters can be determined without knowledge of reaction model. The Flynn-
Wall-Ozawa method is useful to interpret the kinetics with complex reactions obtained
from the TGA data. By Doyle approximation, the integration equation after taking
logarithms is given as follows,

$$\log \beta = \log \left[\frac{AE}{Rg(\alpha)} \right] - 2.315 - 0.4567 \frac{E}{RT}$$

where α is the extent of conversion, $g(\alpha)$ is the integral function of extent of conversion
(α), T is the absolute temperature. β, A and E have the known meanings as mentioned
above.

The activation energy could be obtained by the calculation from the slope of the straight lines when $\log \beta$ is plotted against *1/T* at a fixed degree of conversion with different heating rates. If the determined activation energy varies with conversion, the complex reactions could be presented in the sample degradation. Otherwise the existence of a single-step reaction can be concluded.

2.3. COATS-REDFERN ANALYTICAL FITTING MODEL

To study the degradation mechanisms of the polymeric materials, Coats-Redfern method was employed to calculate the kinetic parameters of the process. Modified Coats-Redfern method, proposed by Burnham and Braun[7], is based on an approximate integrated form of a first-order reaction for a constant heating rate β. The equation is given as,

$$\ln \frac{g(\alpha)}{T^2} = \ln \left[\frac{AR}{\beta E} \left(1 - \frac{2RT}{E}\right)\right] - \frac{E}{RT}$$

When using an asymptotic approximation, $2RT/E << 1$[8], the equation is written as

$$\ln \frac{g(\alpha)}{T^2} = \ln \left(\frac{AR}{\beta E}\right) - \frac{E}{RT}$$

Table 1 give various expression of integral, $g(\alpha)$, models of the different solid state mechanisms. The model matching a given set of TGA data can specify the mechanism and yields the relevant kinetic parameters of thermal degradation of polymers.

Table 1 Kinetic mechanisms and expressions of solid-state processes[9-11]

Model	Symbol	$g(\alpha)$
Nucleation and nuclear growth		
Mampel unimolecular law	A1	$-\ln(1-\alpha)$
Avrami-Erofe'ev equation	A2	$[-\ln(1-\alpha)]^{1/2}$
Avrami-Erofe'ev equation	A3	$[-\ln(1-\alpha)]^{1/3}$
Avrami-Erofe'ev equation	A4	$[-\ln(1-\alpha)]^{1/4}$
Diffusion		
Parabolic law	D1	α^2
Valenci equation	D2	$\alpha + (1-\alpha)\ln(1-\alpha)$
Jander equation	D3	$[1-(1-\alpha)^{1/3}]^2$
Brounshtein-Ginstling equation	D4	$1-(2\alpha/3)-(1-\alpha)^{2/3}$
Phase boundary controlled equation		
One-dimensional movement	R1	α
Contracting area	R2	$1-(1-\alpha)^{1/2}$
Contraction volume	R3	$1-(1-\alpha)^{1/3}$

3. EXPERIMENTAL

3.1. MATERIALS

BPA-based epoxy resin for stereolithography (SLA) pattern was a commercial grade Somos® WaterShed XC 11122 from DSM Company (Elgin, IL). The SLA pattern with honeycomb structure had a density of 0.20 g·cm^{-3}.

3.2. THERMOGRAVIMETRIC ANALYSIS (TGA)

TGA measurements of SLA pattern were carried out using a TA Instruments TA-1000 analyzer (New Castle, DE) to study the non-isothermal degradation kinetics.

Approximately, 5mg pieces of polymer patterns were placed in a platinum pan and heated from room temperature to 600 $^{\circ}$C with nitrogen purge at a flow rate of 40 ml/min. Different linear heating rates of 5, 10, 25 and 40 $^{\circ}$C/min were applied and the corresponding sample weigh loss was recorded.

4. RESULTS AND DISCUSSION

The weight loss versus temperature curves from dynamic thermal degradation of the SLA pattern under various heating rates (5, 10, 25 and 40 $^{\circ}$C/min) are shown in Fig. 1. The results indicate that the major decomposition of the epoxy polymer starts above 300 $^{\circ}$C and completed at 475 $^{\circ}$C for all heating rates. The TGA curves corresponded to a single-stage decomposition reaction. Shifting of curves to the higher temperatures with increasing heating rates was observed due to the shorter time required for a sample to reach a given temperature at faster heating rates.
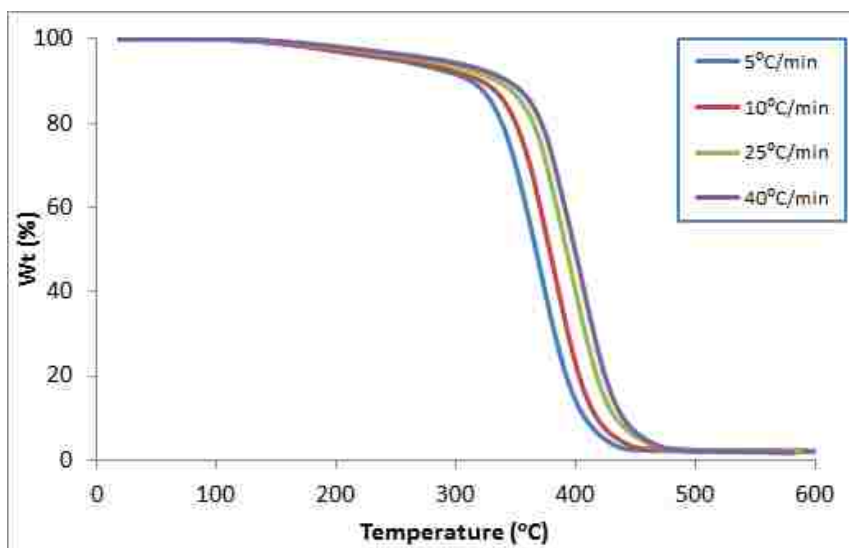

Fig.1   TGA curves of SLA pattern at different heating rates

The decomposition kinetic of SLA pattern was evaluated by Kissinger and Flynn-Wall-Ozawa methods. The Kissinger method allowed the activation energy to be determined by plotting ln (β/T^2_m) versus $1/T_m$. T_m is the inflection point temperature on the TGA curves obtained from different heating rates. The resulting curve was a straight line as shown in Fig. 2. The activation energy of 203.43kJ/mol was obtained from the plot.
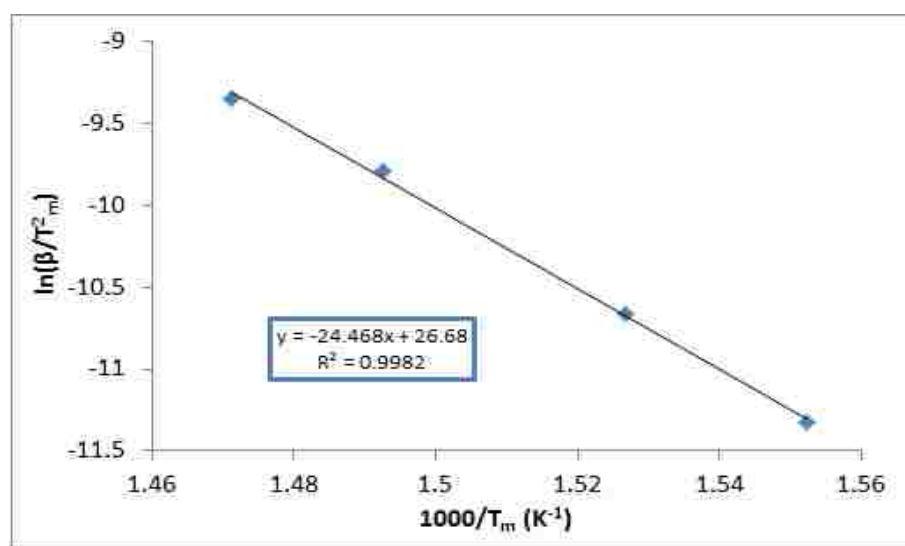
Fig.2   Kissinger plot of ln (β/T^2_m) against $1/T_m$ at different heating rates

The activation energy using Flynn-Wall-Ozawa analysis was obtained from a linear fitting of log β vs. 1000/T at different conversions (Fig. 3). The conversion values from 0.10- 0.90 were applied for the thermal decomposition of SLA pattern sample. The fitted straight lines for various heating rates were nearly parallel, which indicated the suitability of the method in the conversion range investigated. Activation energies corresponding different heating rates were calculated from the slope of these plots and

shown in Table 2. A mean value of 217.22kJ/mol was obtained. The increasing

activation energy with the higher conversion values was observed. It has been reported

that increasing dependencies of the activation energy on conversion are quite common for

degradation of polymers, including epoxy materials[12]. The Flynn-Wall-Ozawa method

yielded a slightly lower (13.79 kJ/mol) activation energy when compared with the value

determined by Kissinger's method.
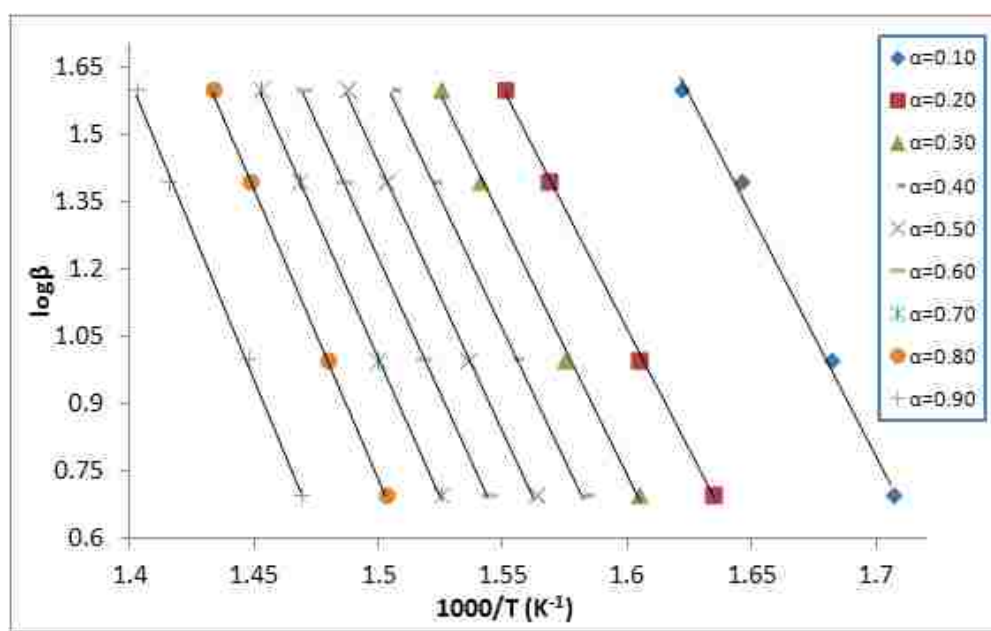
Fig.3.   Flynn-Wall-Ozawa plots of log β vs. 1000/T at conversion in the range of 0.10-0.90 in steps of 0.10

Both the Kissinger and Flynn-Wall-Ozawa models do not require the previous

knowledge of the reaction mechanisms in order to evaluate the activation energy.

Kissinger method only uses one point (the point of maximum rate) to calculate the

activation energy. Flynn-Wall-Ozawa method is applicable to the whole conversion

range. Therefore, it is regarded as a more satisfactory mathematical approach to establish

the kinetic parameters for the thermal degradation of SLA pattern as well as other materials.

Table 2 Activation Energies Obtained Using the Flynn-Wall-Ozawa Method

α	E_α (kJ/mol)	R^2
0.10	195.32	0.9957
0.20	195.88	0.9991
0.30	206.57	0.9972
0.40	212.45	0.9984
0.50	217.69	0.9987
0.60	221.26	0.9993
0.70	226.72	0.9994
0.80	235.00	0.9997
0.90	244.54	0.9983
Average	217.27	-

In order to determine the most probable degradation model of SLA pattern, a modified Coats-Redfern analysis with corresponding degradation mechanisms(Table 1) was employed. The activation energies and correlations at constant heating rates can be obtained by fitting ln [g(α)/T^2] versus 1/T plots. The conversion range of 10~90% and heating rate values of 5, 10, 25 and 40 ℃/min were used in this method. Table 3 shows the calculated energies and correlations by using the modified Coats-Redfern method. The results indicate that the activation energy strongly depend on the different reaction mechanism. It was found that the activation energies corresponding to the *D*3 mechanism are in good agreement with the values obtained by both the Kissinger method and the Flynn-Wall-Ozawa method at heating rates of 10, 25 and 40 $^{\circ}$C/min. The correlation factors (R^2) of *D3* are 0.9912, 0.9897 and 0.9915 at the heating rates of 10, 25

and 40 $^{\circ}$C/min, respectively. These correlation factors are higher compared with the other

models. It has been demonstrated that the thermal degradation behaviors of polymer

closely follows the mechanisms that have higher correlation factors[6]. Therefore, it is

suggested that the solid state thermal degradation mechanism for our epoxy system is

probably a diffusion (D3) process. The mean activation energy and pre-exponential

factor were 202.73 kJ/mol and 1.2×10^{14} K^2/s, respectively, based on the Coats-Redfern

analytical fitting model.

Table 3 Activation Energies Obtained Using the Coats-Redfern Method for different Solid-State Processes

Mechanism	E(kJ/mol)	R^2
(a) Heating Rate of 5 $^{\circ}$C/min		
A1	102.73	0.9944
A2	46.12	0.9931
A3	27.25	0.9913
A4	17.82	0.9886
D1	154.28	0.9766
D2	171.14	0.9851
D3	192.65	0.9923
D4	199.65	0.9881
R1	71.90	0.9728
R2	85.79	0.9881
R3	91.09	0.9913
(b) Heating Rate of 10 $^{\circ}$C/min		
A1	104.79	0.9905
A2	47.07	0.9885
A3	27.83	0.9858
A4	18.22	0.9818

Table 3 Activation Energies Obtained Using the Coats-Redfern Method for different Solid-State Processes (cont.)

D1	157.93	0.9806
D2	174.98	0.9868
D3	196.72	0.9912
D4	182.13	0.9888
R1	73.65	0.9775
R2	87.69	0.9885
R3	93.03	0.9902
(c) Heating Rate of 25 $^{\circ}$C/min		
A1	107.05	0.9894
A2	48.09	0.9871
A3	28.43	0.9840
A4	18.60	0.9794
D1	161.24	0.9782
D2	178.68	0.9848
D3	200.92	0.9897
D4	185.98	0.9870
R1	75.18	0.9747
R2	89.55	0.9865
R3	95.02	0.9885
(a) Heating Rate of 40 $^{\circ}$C/min		
A1	112.41	0.9923
A2	50.69	0.9907
A3	30.13	0.9885
A4	19.84	0.9854
D1	168.88	0.9782
D2	187.19	0.9857
D3	210.54	0.9915
D4	194.86	0.9882
R1	78.94	0.9749
R2	94.02	0.9881
R3	99.77	0.9905

5. CONCLUSIONS

The thermal degradation behavior of epoxy SLA patterns for the metal investment casting process is studied. The TGA curves shifted to higher temperatures when the heating rates were increased from 5 $^{\circ}$C/min to 40 $^{\circ}$C/min. It also showed a single-stage decomposition reaction. A difference of 13.79 kJ/mol for the activation energy values determined by the Kissinger's method and Flynn-Wall-Ozawa method was founded. The results of kinetic analysis demonstrate that the most probable degradation mechanism for the SLA pattern is in good agreement with the diffusion model (D3). The rate equation of the thermal degradation of the SLA pattern is given as:

$$ln\frac{[1-(1-\alpha)^{\frac{1}{3}}]^2}{T^2} = ln\left[\frac{4.92\times10^9}{\beta}(1 - 8.2 \times 10^{-5}T)\right] - \frac{2.4\times10^4}{T},$$

where α is conversion, β is heating rate in K/s and T is temperature in K.

REFERENCES

1. H. Zhao, M. Xu, H. Li, W. Everhart, S. Lekakh, V. Richards, K. Chandrashekhara and P. Nam, Characterization of Low Density Polymer Pattern for Large Steel Investment Casting. *58th Annual Technical Conference and Equipment Expo*, 2011, Investment Casting Institute, Covington, KY.

2. P. Kannan, J. J. Biernacki, D. P. Visco and W. Lambert, *Journal of Analytical and Applied Pyrolysis*, 2009, 84, 139-144.

3. J. D. Peterson, S. Vyazovkin and C. A. Wight, *Macromolecular Chemistry and Physics*, 2001, 202, 775-784.

4. W. Everhart, S. Lekakh, V. Richards, J. Smith, H. Li, K. Chandrashekhara, H. Zhao and P. Nam, presented in part at the Transactions of the American Foundry Society, 2012.

5. R. Bilbao, J. F. Mastral, J. Ceamanos and M. E. Aldea, *Journal of Analytical and Applied Pyrolysis*, 1996, 37, 69-82.

6. H. R. Azimi, M. Rezaei, F. Abbasi, A. Charchi and Y. Bahluli, *Thermochimica Acta*, 2008, 474, 72-77.

7. A. K. Burnham and R. L. Braun, *Energy Fuels*, 1999, 13, 1-22.

8. S. Mallakpour and M. Taghavi, *Iranian Polymer Journal*, 2009, 18, 857-872.

9. A. W. Coats and J. P. Redfern, *Nature*, 1964, 201, 68-69.

10. J. Šesták and G. Berggren, *Thermochimica Acta*, 1971, 3, 1-12.

11. S. Ma, J. O. Hilt and H. S., *Journal of thermal Analysis*, 1991, 37, 1161-1177.

12. S. Vyazovkin and N. Sbirrazzuoli, *Macromolecular Rapid Communications*, 2006, 27, 1515-1532.

SECTION

3. CONCLUSION

A direct spectrophotometric measurement using Nile red dye provides the simple method to determine the oil content of microalgae and allows the rapid identification of high oil-bearing microalgae. However, the applications of Nile red lipid staining in a number of green algal species has been hindered due to the composition and structure of the thick and rigid cell walls resulting in the permeation difficulty of Nile red through the cell walls and subsequently dissolving in the intracellular neutral lipid. Various physical and chemical treatments, including adding DMSO, ethanol as stain carrier and combination of DMSO and microwave irradiation have been studied to improve the fluorescence intensity of the lipid. Nevertheless, the organic solvent was included and several steps were involved in microwave-assisted staining.

This part of the dissertation focused on optimization of the conventional Nile red method with two assisted methods, including heating and diluted H_2SO_4 treatment to enhance the staining efficiency and improve the fluorescence intensity of microalgal lipid. Optimum procedures were successfully applied to five different green microalgal species. These two fast and simple methods to determine the microalgal neutral lipid content could potentially be used in the investigation of large scale lipid production from other microalgal biomass.

The spectrophotometric measurement using Nile red provided a qualitative or semi-quantitative analysis data in the determination of lipid content. One limitation of

using this fluorescence method is the fluorescence intensity, which is relative to compare or estimate the intercellular lipid contents in microalgae; it is not an absolute content. Staining of lipid standards and staining of algal cells resulting in different fluorescence responses due to the different hydrophobicity and size are other drawbacks.

This dissertation also involves the employment of a series of oil-in-water microemulsion standards stabilized by a non-ionic surfactant. This prepared pseudo standards can mimic microalgae cells suspended in water. The fluorescence intensity of neutral lipid from microalgae species was obtained by comparing with the O/W microemulsions standards curves and then the actual neutral lipid contents of microalgae were calculated. The established calibration standards method provided a reliable and fast way in the determination of the neutral lipid in microalgae. It can be used as a sensitive, quantitative, and high throughput method for screening of cellular neutral lipid content in green algae as well as other classes of algae.

This part of the dissertation was to explore polymers' thermal and chemical properties affecting application of different polymer patterns materials in investment casting processing. Three polymeric materials, including EPS foam produced from expanded polystyrene using a blowing agent; FOPAT foam pattern made from a water blown polyurethane and an epoxy resin based SLA pattern with an internal honeycomb structure were characterized in the research. Thermal degradation behavior and glass transition temperatures of these polymers were characterized by using TGA and DSC techniques, respectively. Generation of HCN from thermal decomposition of FOPAT pattern under different experimental conditions in lab-scaled muffle furnace and tube furnace was discussed.

Thermal degradation kinetics of epoxy resin pattern using various kinetic models (differential and integral) were investigated by using TGA. These kinetic equations were applied to studies concerning the epoxy resin pattern's reaction to fire (ignition process, flame propagation, evaluation of amount of toxic products generated, etc.) and to the reactor design and optimization of the operating conditions in the thermochemical processing of the material. Flynn-Ozawa-Wall and Kissinger methods were used to calculate kinetic parameters of thermal decomposition of the epoxy resin pattern. Degradation mechanisms were estimated by Coates-Redfern analytical fitting method.

APPENDIX A.

FOAM PATTERN AGING AND ITS EFFECT ON CRACK FORMATION IN INVESTMENT CASTING CERAMIC SHELLS

V. FOAM PATTERN AGING AND ITS EFFECT ON CRACK FORMATION IN INVESTMENT CASTING CERAMIC SHELLS

W.A. Everhart, S.N. Lekakh, V.L. Richards and J.D. Smith

Department of Materials Science and Engineering

H. Li and K. Chandrashekhara

Department of Mechanical and Aerospace Engineering

H. Zhao and P.S. Nam

Department of Chemistry

Missouri University of Science and Technology, Rolla, MO 65409

ABSTRACT

The application of rigid plastic foam for large investment casting patterns with complex geometries can improve the dimensional tolerances and the surface quality of the casting. However, these pattern materials promote crack formation in investment casting shells during pattern removal using standard firing procedures. In typical investment casting shell processing, drying stages provide an aging period which can change the compatibility strains of the shell/foam assembly. In order to accurately predict shell cracking occurrence during pattern removal, the aging strain of the pattern must be considered. ASTM standard tests and independently developed experimental methods were combined with finite element modeling to predict stress development in the shell. The model takes into consideration the thermal properties of the pattern and the shell materials to determine the heat transfer to establish a thermal gradient within the materials. This is combined with mechanical properties to determine the thermal

expansion stresses developed in the shell during firing. An experimentally measured delay of the thermal expansion of the aged pattern was incorporated in a three-dimensional nonlinear finite element model and used to predict possible crack formation in the shells during pattern removal. The effect of pattern aging on crack formation in the shell was experimentally validated. Recommendations for pattern removal parameters to decrease stress and eliminate crack formation in the shell were formulated.

Key Words: ceramic shell, investment casting, crack, stress modeling, molding

INTRODUCTION

The investment casting process is generally used to produce small, thin walled castings with high detail. The process begins with the manufacture of a pattern from an easily shaped, inexpensive material. The most common material for patterns is wax but different types of polymeric foam are also used[1-2]. The pattern is dipped in slurry made of inorganic binder and oxide flour usually containing some combination of fused silica, zircon, alumina, or other ceramic material. Refractory granules referred to as stucco (usually fused silica, zircon or alumina) are then applied to the wet slurry coating. The combination of slurry and stucco makes a single coat which is allowed to dry before subsequent coats are applied. The shell building process generally consists of three different types of layers. Prime coats are designed to provide a better surface finish for the casting and are applied first, usually in one or two coats. Backup coats are designed to add strength to the shell and are applied after any prime coats; four to ten backup coats are applied. The seal coat is designed to seal the stucco of the final backup coat and is applied last[3-7]. The pattern is then removed from the unfired or green shell by melting or decomposition in an autoclave or furnace. Whether done as a part of pattern removal, or

as an additional firing process, the ceramic is sintered to increase the strength of the shell such that the pressure of liquid metal will not cause cracks. Liquid metal is then poured into the shell, which is usually preheated, to produce the casting.

Large patterns made from wax often do not have sufficient strength to hold their shape due to their higher weight, especially in situations where the pattern has unsupported extensions, leading to creep[8]. Polymeric foams were considered as pattern materials in investment casting in an attempt to overcome some of the wax deficiencies. Some of the first foams used were expanded polystyrene (EPS)[9]. This material has much lower density than wax and, despite its lower strength, doesn't suffer from the self loading creep that is common with wax patterns, especially in larger patterns. This becomes especially important to the dimensional stability of the pattern during storage. However, EPS foams are also very buoyant which causes problems when the pattern is initially dipped in the slurry. The forces on the pattern when submerged can be high enough to distort or even break the pattern. EPS foam and wax patterns also show some dimensional change when they are cooled after production. Because of these issues, stronger, higher density polymeric foams are needed. Polyurethane foams fit these requirements well and can be made in complicated shapes with high surface quality and dimensional accuracy[10]. However, polyurethane foams have high coefficients of thermal expansion and high decomposition temperatures which can cause the pattern to expand and break the shell during the pattern removal process[9].

Preliminary aging of EPS patterns to control pattern dimensions has been successfully implemented in lost foam casting[11]. The use of aging to prevent shell cracking is based on the change in pattern dimensions over time, especially at elevated

temperatures[12]. The polymeric foam aging mechanism relates to the development of crystallinity. An aged crystalline polymer has two phases: the crystalline phase and the amorphous phase[13]. Preliminary aging of the polymeric foam pattern inside the green shell may increase the ordered domain and crystallinity of the polyurethane pattern during firing leading to volume reduction. Because of this, the effect of the thermal expansion of the polyurethane could be reduced.

The objective of this research was to develop a model to predict the effect of pattern aging on shell cracking. To achieve this goal, the aging properties of the polyurethane foam were experimentally determined along with glass transition temperatures and the Young's modulus of aged foam. Additionally, samples were tested for shell cracking by firing shelled patterns in various conditions. These data were used in a finite element model to predict crack formation during pattern removal.

PROCEDURES

EXPERIMENTAL

Foam pattern properties

Polyurethane foam with density of 170 kg/m^3 was tested. Samples were cut from the center of foam blocks with a cross-section of 7000 mm2. Compression testing of the foam was used to determine the elastic modulus after aging at 100 ℃ for 24 hours. Samples had a cross-section of 2580 mm2 and a thickness of 25.4 mm or 50.8 mm (ASTM D1621)[14]. Thermal dilation during foam aging was measured using a laser assisted dilatometer. Foam samples were cut into 50 mm long 18 mm diameter cylinders. Two thin aluminum disks were placed on both ends of the foam and inserted into a quartz glass tube (19 mm diameter) submerged in an oil bath. A small hole was present in the

end of the tube to allow oil flow inside for improved heating of the sample. Another

quartz tube was placed on the upper aluminum disk. The expansion of the foam sample

was monitored through the linear movement of the upper tube using a laser proximity

probe with 1 μm precision. The average temperature of the foam samples was collected

by averaging the reading of two thermocouples inserted in the oil bath, one of which was

inserted in a spare foam sample and the other thermocouple was left exposed to the oil.

The heating rate of the foam was approximately 1 ℃/min. Samples were held at various

aging temperatures and times, cooled back to room temperature and heated aging until

softening. Additionally one sample was heated and held at different temperatures in a

stepped fashion. Differential scanning calorimetry (DSC) was done on the foam in both

the aged and un-aged condition. The samples were stabilized by first heating from room

temperature to 180 ℃ in the instrument, then immediately quenched in liquid nitrogen

and held for 1 min. The 2mg quenched sample was then tested using DSC (TA

instrument DSC Q2000) from -38 ℃ to 210 ℃ at a heating rate of 20 ℃/min in a nitrogen

gas atmosphere.

Shell construction and properties

A simple pattern (50.8 x 63.5 x 63.5 mm) was prepared to test shell cracking

during burnout (Figure 1). The slurry consisted of colloidal silica binder (Megasol BI)

and fused silica flour (-200 mesh). Slurry viscosity was measured by Brookfield DVII+

Pro Viscometer. All coatings were applied at 800 ± 100 cP viscosity which is equivalent

to 19-22 seconds on a #5 Zahn cup. The patterns were submerged in the slurry until

completely covered and then removed and suspended over the slurry for approximately

50 seconds. During this time, the pattern was rotated and allowed to drain from different

points to promote an even coating. A uniform distribution of stucco was then applied using the rainfall method. This was done by continuously rotating the pattern so that all surfaces were directly impacted by the falling stucco until no more stucco would adhere to the surface. The stucco for the prime coat was granular zircon (-100+200 mesh) and the stucco for the back-up coats was fused silica (-30+50 mesh). The seal coat used no stucco. The samples were dried for at least four hours between coats. Shells were fabricated with one prime coat, either three or five backup and one seal coat. The samples with three backup coats had five total layers (3.8 mm average thickness) and the samples with five backup coats had seven total layers (6.4 mm average thickness). After the seal coat was applied the samples dried for another 24 hours. Half of the patterns were then aged. After sample preparation the shells were fired in electrical resistance box furnace using flash firing in a furnace preheated to 600 °C.

Figure 1. Shell built around foam pattern: 50.8 x 63.5 x 63.5 mm.

The maximum stress at rupture and elastic modulus of the five and seven layer shells were determined using three point bend testing of green shells performed at room

temperature according to ASTM C1161[15]. The tip of the testing fixture had a radius of three mm. The bulk density of the shells was measured using Archimedes method in distilled water according ASTM C20 using approximately 10 g samples[16].

MODELING

A nonlinear coupled finite element model was developed to study the crack formation in the shell during pattern removal. The model accounts for both mechanical and thermal loadings and assumes a fixed interface between the pattern and shell. It is capable of simulating the complete detail of pattern and shell behavior during the firing process. To reduce computational time, one quarter of the pattern surrounded by shell has been modeled and symmetric boundary conditions are applied at the cut planes. An eight-node brick element is used to mesh the model. To mesh the pattern, all edges are initially seeded by numbers. In order to obtain higher result accuracy and save computational cost, additional seeds and biased seeds are used in critical regions and fewer seeds in regions that are less of interest, and hex mesh shape and structured mesh technique are used. The mesh of the finite element model for both the shell and foam pattern is shown in Figure 2. Finer mesh is used near the corner of ceramic shell. 19,683 brick elements were used for the model. The contact properties between the pattern and shell are defined as fixed in order to simulate the actual experimental process.
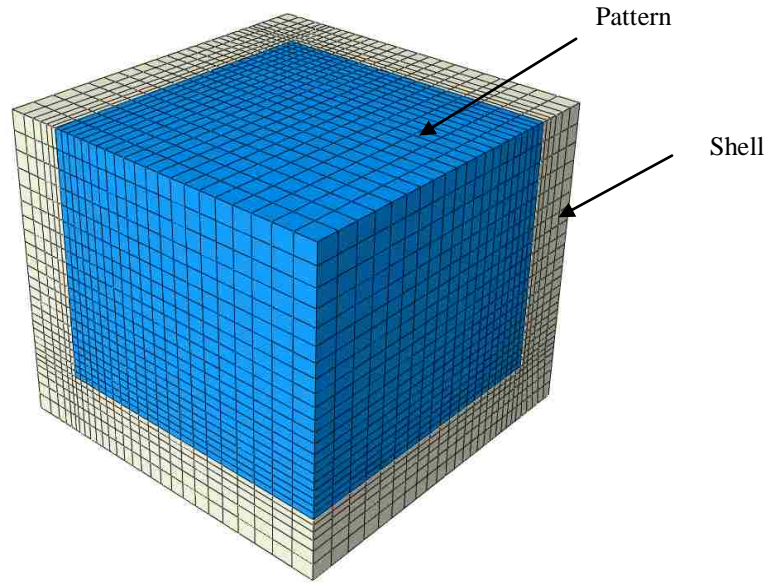
Figure 2. Mesh of finite element model for the foam pattern and ceramic shell.

The formulation for the transient mechanical analysis can be written as:

$$[M^e]\{\ddot{U}^e\} + [K^e]\{U^e\} = \{F^e\} + \{F_T^e\} \tag{1}$$

where: $[M^e] = \int_v \rho [N]^T [N] dV$

$[K^e] = \int_v [B]^T [C][B] dV$

$\{U^e\} = \{u, v, w\}^T$

$[M^e]$ is the mass matrix, $[K^e]$ is the stiffness matrix, $\{F^e\}$ and $\{F_T^e\}$ are mechanical and thermal loadings, N is shape function, B is strain-displacement function, C is elasticity matrix, ρ is the density, and $\{u, v, w\}^T$ are displacement components in a rectangular Cartesian coordinate system.

The formulation for heat transfer can be expressed as:

$$[C_T^e]\{\dot{\theta}^e\} + [K_T^e]\{\theta^e\} = \{Q^e\} \tag{2}$$

where: $[C_T^e] = \int_v \rho c_p N^T N dV$

$[K_T^e] = \int_v N^T \underline{k} N dV$

$$\{Q^s\} = \int_S N^T q \, dS + \int_V N^T r \, dV$$

$[C_T^e]$ is the heat capacitance matrix, $[K_T^e]$ is the conductivity matrix, and $\{Q^s\}$ is the external flux vector. c_p is the specific heat of the material, $\underline{k}$ is the thermal conductivity, q is the surface heat flux, and r is the body heat flux generated by plastic deformation.

A smeared crack model was used to describe the response of the ceramic material when a crack initiates. The crack model does not track individual "macro" cracks. Cracking is assumed to occur when the stress reaches a crack detection criterion surface. This failure surface is mathematical construction which is a linear relationship between the equivalent pressure stress and the von Mises equivalent deviatoric stress. When a crack has been detected its orientation is stored for subsequent calculations. Subsequent cracking at the same point is restricted to being orthogonal to this direction since stress components associated with an open crack are not included in the definition of the failure surface used for detecting additional cracks[17].

RESULTS

EFFECT OF AGING ON FOAM PROPERTIES

The effect of time and temperature on foam aging is important when this behavior benefits the process by reducing shell cracking. Appropriate aging times and temperatures can be vital when applying this method to industry. A preliminary study on the effect of aging was done with a sample that was heated and held at various temperatures in a stepping fashion (Figure 3). This test shows that the aging rate significantly increases at temperatures above approximately 80°C.
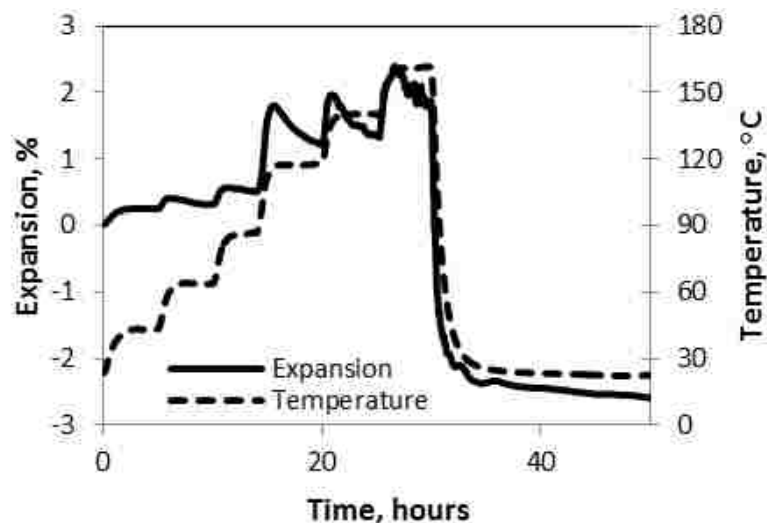
Figure 3. Thermal expansion of the stepped aging sample showing increased shrinkage above 80 ℃.

Separate samples were then aged at various temperatures for 24 hours to determine the effect of aging temperature on the maximum shrinkage, and expansion after aging (Figure 4b). These results suggest that shrinkage from aging increases at temperatures above 60 ℃. Temperatures above 100 ℃ were not tested because these temperatures are high enough to cause shell cracking from pattern expansion. Samples were also aged for various amounts of time at 100 ℃ to determine the effect of aging time on the amount of shrinkage (Figure 4). The results show that after 24 hours the amount of shrinkage does not significantly increase until the aging time is longer than 48 hours.
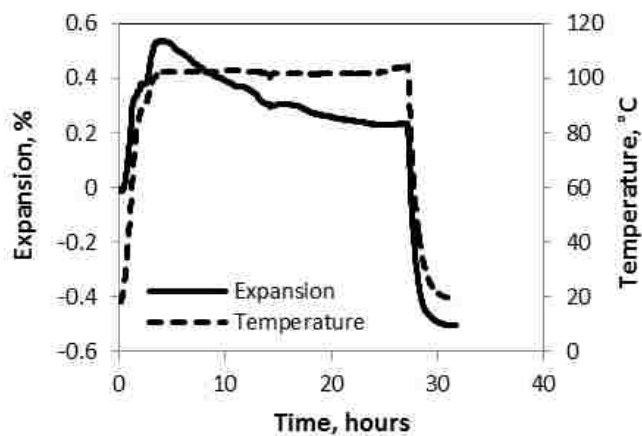
a)
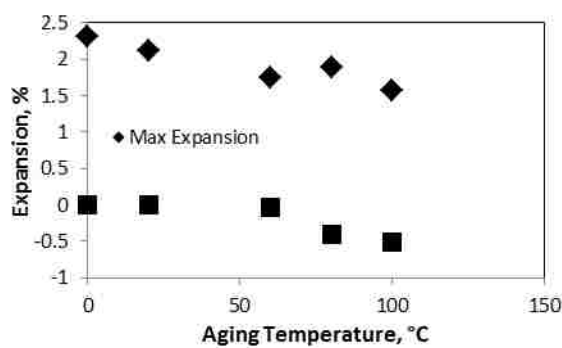
b)
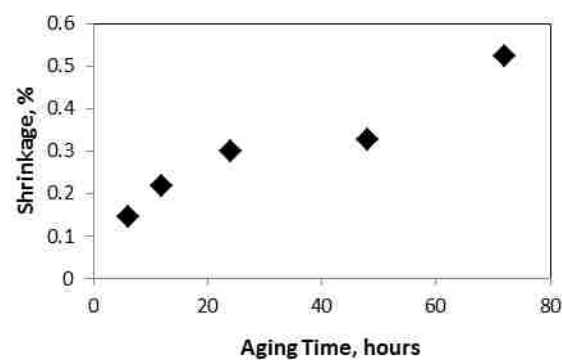
c)

Figure 4. Example of an aging test of polyurethane foam at 100 ℃ (a), maximum expansion/shrinkage of polyurethane foam after 24 hours aging at various temperatures (b) and final shrinkage of polyurethane foam after aging for various amounts of time at 100 ℃ (c).

The coefficient of thermal expansion (CTE) of an un-aged sample of polyurethane foam at temperatures below 90 ℃ is approximately 80 $\times 10^{-6}$ ℃$^{-1}$ while above that temperature the CTE increases to 400 $\times 10^{-6}$ ℃$^{-1}$. At approximately 155 ℃ the foam stops expanding and begins to soften. At this point the CTE becomes slightly negative. Aged samples showed similar CTE behavior and foam softening temperature, but because the sample had contracted during aging and did not return to its original size until it had been heated to approximately 80 ℃, the net expansion of the aged foam relative to a shell mold of fixed dimension was less (Figure 5).
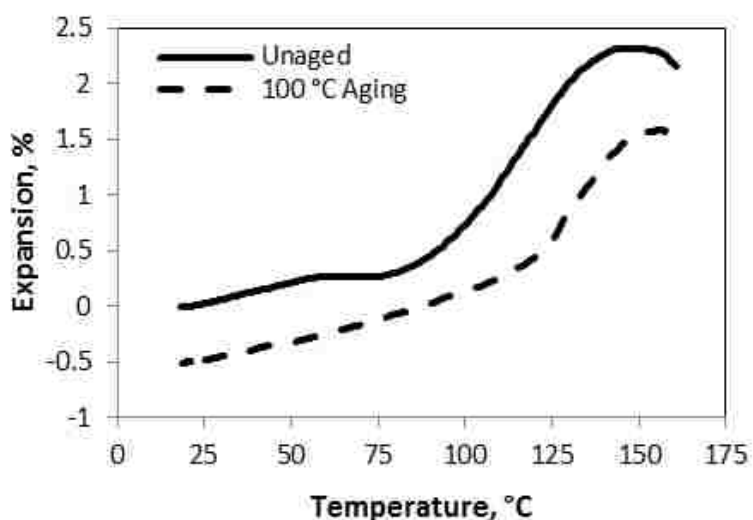
Figure 5. Comparison of the thermal expansion of an aged and un-aged sample.

To study the physico-chemical nature of polyurethane foam aging, DSC testing of the foam was performed. Results showed two endothermic peaks, indicated by changes in slope, one at approximately 60 ℃ and another at approximately 140 ℃ (Figure 6). The 60 ℃ peak is a glass transition temperature and matches well with the transition in CTE.

The 140 ℃ peak matches the foam softening temperature and is associated with the break
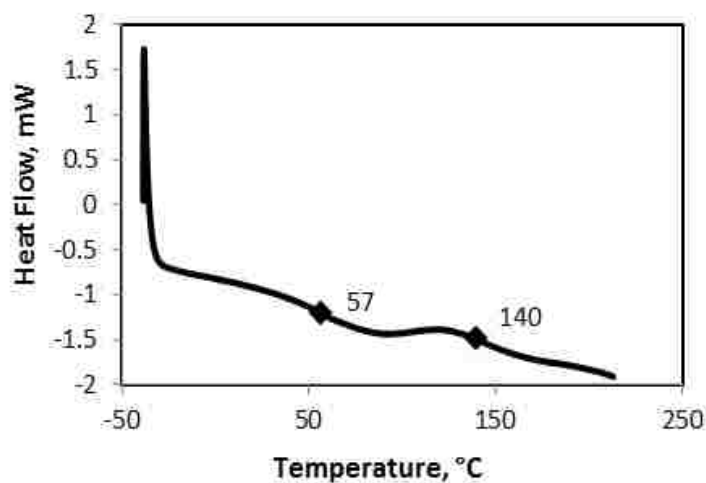
down of the crystalline structure.

Figure 6. Example DSC results of polyurethane foam showing glass transition
temperatures.

The elastic modulus is an important property of foam patterns used for investment

casting because of its impact on shell cracking. The effect of aging on the elastic

modulus of the foam was determined by comparing the results of compression testing of

aged and un-aged samples at room temperature. The average elastic modulus of un-aged

samples was 53 MPa and the average modulus of samples that were aged at 100 ℃ for 24

hours was 52 MPa. This implies that aging has no significant effect on the room

temperature mechanical properties of foam pattern. Temperature dependent values of the

elastic modulus of the foam are required to accurately simulate stress in the shell during

pattern removal. These values were determined using the known[18, 19] tendency of the

elastic modulus to degrade above the glass transition temperature. In the model the

elastic modulus begins to degrade at 80 ℃ until it is near zero at the foam softening temperature.

CERAMIC SHELL PROPERTIES

The maximum failure stress and elastic modulus of the shell were experimentally determined for shells with five and seven layers using three-point bend testing performed at room temperature. Five samples for both types of shells were tested and the calculated values are included in Table 1. The failure stress for the five layer shells was lower than the seven layer shells while the five layer shells had a higher elastic modulus. The variation in mechanical properties is likely due to a higher percentage of zircon stucco in the five layer shells.

Table 1. Strength and density of shells.

Property	5 Layer Shell	7 Layer Shell
Shell thickness, mm	3.8 ±0.3	6.4 ±0.5
Maximum stress, MPa	4.4 ±0.5	7.2 ±1.1
Elastic modulus, MPa	3411 ±518	1995 ±314
Bulk density, kg/m^3	1920 ±220	1800 ±30

MODELING RESULTS

The experimentally verified thermo-mechanical properties for the pattern and the shell were used as input into the model (Table 2). The foam is assumed to decompose when it reaches a temperature of 155 ℃. Instead of modeling the actual shrinkage that occurs during aging, the CTE from room temperature to 80 ℃ for aged samples is set to zero in the simulation. A zero CTE prevents stress development in the shell by

approximating the gap formed by aging and the subsequent free expansion of the pattern

until the pattern expands to fill the gap (Figure 7). In addition to the experimental data in

Table 1, thermal conductivity and specific heat capacity data were used[9, 20-22]. The

thermal boundary conditions for flash firing at 600 ℃ used in the simulations are shown

in Table 3. Modeling was completed for aged (100 ℃ for 24 hours) and un-aged samples

with pattern dimensions of 50.8 x 63.5 x 63.5 mm.

Table 2. Material properties for modeling[9, 20-22].

Property	Polyurethane Foam	5 Layer Shell	7 Layer Shell
Density, kg/m^3	170	1800	1800
Poisson's ratio	0	0.24	0.24
Heat capacity, J/gK	1.3	0.65	0.65
Thermal conductivity, W/mK	0.06	1	1
CTE, K^{-1}	See Figure 7	2×10^{-6}	2×10^{-6}
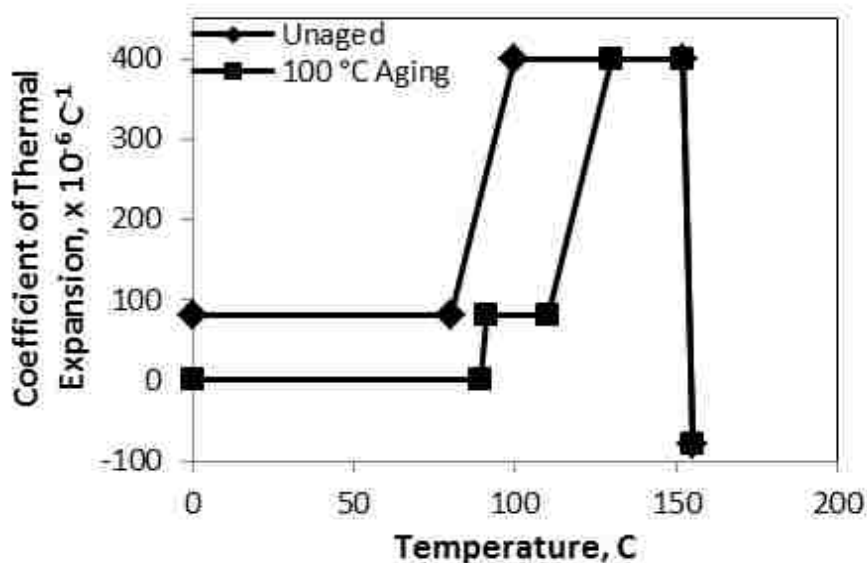
Figure 7. CTEs used in simulation for aged and un-aged samples. This shows the
assumptions made for the aged sample to approximate aging shrinkage in the model.

Table 3. Thermal boundary conditions.

Parameters	Flash Fire
Oven initial temperature	600 ℃
Shell surface convection coefficient	20 W/m^{2}K
Emissivity of the shell surface	0.3

An example of the modeling results for flash fire at 600 ℃ for aged and un-aged patterns with shell thickness of 6.4 mm is included as Figure 8. The maximum stress in the shell occurs when the boundary temperature between shell and pattern reaches the foam softening temperature. At that temperature, the applied pressure begins to decrease as a result of foam softening. This critical temperature was experimentally defined from the thermal expansion results. The maximum stress for both aged and un-aged samples occurs at the internal edges of the shell (Figure 8). Compared to aged, an un-aged sample produces a much higher stress concentration in the shell.
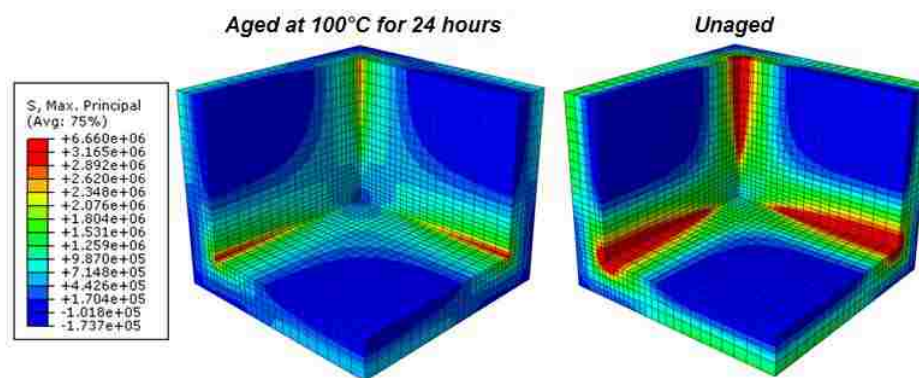

Figure 8. Maximum principal stress distribution of the shell at the end of flash firing and for aged and un-aged foam patterns.

DISCUSSION

Crack formation in the shell during rigid foam pattern removal by heat treatment depends on multiple parameters which can be divided into the following groups:

Group 1 - *foam properties*, most important of which include elastic modulus, thermal
expansion, softening temperature and aging

Group 2 - *shell properties*, most important of which include failure stress, elastic
modulus, and shell wall thickness

Group 3 - *firing regime*, continuous heating versus flash firing in high temperature
preheated furnace.

The effect of aging after shell building and before pattern removal on polyurethane foam properties and shell cracking during pattern removal was investigated. Longer aging times were shown to increase the amount of shrinkage, especially for times less than 24 hours. After approximately 20 hours the shrinkage for a pattern aged at 100°C subsides due to nearing completion of the transformation from an amorphous structure to a crystalline structure (Figure 4a).

When aging temperature is above the glass transition temperature indicated by DSC (approximately 60°C) the amount of shrinkage increases from zero to 0.5% (Figure 4b) supporting the idea that the transformation of the polyurethane foam from amorphous to crystalline is the aging mechanism. Activation energy for aging was determined from the shrinkage in Figure 3. The activation energy was approximately 600 J/mol when aging was below 80°C and 1800 J/mol when above 80°C. Foam aging was not found to increase or decrease the elastic modulus of the polyurethane foam.

During pattern removal the strain in the pattern consists of aging strain, thermal strain and elastic strain and the strain in the shell consists of thermal strain and elastic strain. The small amount of shrinkage caused by aging induces a negative strain in the pattern. This negative strain reduces the overall strain in the pattern and shell at their interface thus lowering the stress developed in the shell (Figure 9).
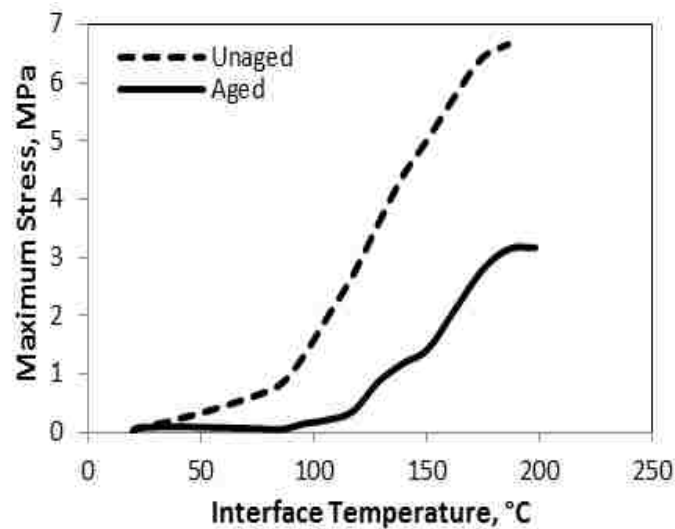

Fig. 9. Comparison of stress development in the 6.4 mm thick shell for aged and un-aged foam patterns showing significantly higher stress in un-aged patterns.

This concept was applied to a shell cracking model to show the effect of aging on the stress developed in the shell during pattern removal and specific cases were experimentally verified in the laboratory shell cracking test (Figure 10). The comparison of experimental results and prediction of crack formation in the model are given in Table 4, indicating that modeling is consistent with experimental results. Aging the patterns significantly reduced the stress in the shell during pattern removal. Aging prevented cracking of the 3.8 mm thick shells and lowered stress development in the 6.4 mm shells (Figure 9).

Table 4. Comparison of simulation and experimental results.

Case No	Shell Thickness (mm)	Aging	Shell Fail (Simulation)	Shell Fail (Experiment)
1	6.4	Not Aged	No	No
2	3.8	Not Aged	Yes	Yes
3	6.4	Aged 100 C	No	No
4	3.8	Aged 100 C	No	No

Fig. 10. Example of crack formed in the shell during pattern removal.

CONCLUSIONS

Aging reduces the stress in the shell by producing shrinkage which lowers the compatibility strain on heating and its consequent elastic stress development. A model was developed for predicting crack formation in investment casting shells due to pattern expansion. The model accurately predicts the presence of cracking during pattern removal for un-aged patterns with five layer shells. The results of the model and the experiments demonstrate that aging patterns can be an effective way to prevent shell cracking during pattern removal. To effectively prevent shell cracking it is recommended

that aging be done above the glass transition temperature (60 ℃ - 100 ℃) for at least 24 hours.

ACKNOWLEGEMENTS

REFERENCES

1. Foster, G, "Flashfire Dewax for Today's Investment Casting Foundry", Investment Casting Institute 42nd Annual Meeting, pp. 2:1-2:11, Atlanta, Georgia; USA; 25-28 September 1994.

2. Yao, W L, Leu, M C, "Analysis of Shell Cracking in Investment Casting with Laser Stereolithography Patterns", Rapid Prototyping Journal, Vol. 5, no. 1, March 1999.

3. Capadona, J A, "Slurry Process Control in Production can "Crack Down" on Shell Cracking", Incast Vol. 4, no. 4, pp. 10-12, April 1991.

4. Guerra, M, Schiefelbein, G W, "Review of Shell Components, Shell Characteristics and Properties: Refractory Selection for Primary Shell Coat", Investment Casting Institute 42nd Annual Meeting, Atlanta, Georgia; USA; 25-28 September 1994.

5. Arzt, A M, "Optimizing Control of Shell Cracking in Investment Casting", Mod. Cast. Vol. 77, no. 2, pp. 30-33. February 1987.

6. Roberts, W O, "Shell Cracking – a Complete and Detailed Compilation of Papers, Case Histories, and Discussions Presented at the AFS/CMI Symposium "Factors Affecting Shell Cracking", "Colloidal Silica", American Foundrymen's Society, Publications Department, Golf & Wolf Roads, Des Plaines, IA, 1987.

7. Schiefelbein, G W, "Ceramic Shell Production for Controlling Shell Cracking", Conference on Factors Affecting Shell Cracking, December 2-3, 1986.

8. Cannell, N, Sabau, A S, "Predicting Pattern Tooling and Casting Dimensions for Investment Casting, Phase II", Final technical report, September 2005.

9. Kline, D, Lekakh, S, Mahimkar, C, Richards, V, "Crack Formation in Ceramic Shell During Foam Pattern Firing", Technical and Operating Conference, Chicago, Illinois; USA; December 2009.

10. "Foam Patterns for Investment casting", Modern Casting, Vol. 99, no. 7, pp. 46, July 2009.

11. Smith, B V, Biederman, S, "Examining Lost Foam's 'White side'", Modern casting, Vol. 90, no. 8, August 2000.

12. Li, X ; Cao, H, Zhang, Y, "Structures and Physical Properties of Rigid Polyurethane Foams with Water as the Sole Blowing Agent", Science in China. Series B, Chemistry, Vol. 49, no. 4, pp. 363-370, 2006.

13. Ho, T, Wynne, K J, "A New Fluorinated Polyurethane: Polymerization, Characterization, and Mechanical Properties", Macromolecules, pp.3521-3527, 1992.

14. ASTM D1621, "Standard Test Method for Compressive Properties of Rigid Cellular Plastics", ASTM International, 2010.

15. ASTM C1161, "Standard Test Method for Flexural Strength of Advanced Ceramics at Ambient Temperature", ASTM International, 2002.

16. ASTM C20, "Standard Test Methods for Apparent Porosity, Water Absorption, Apparent Specific Gravity, and Bulk Density of Burned Refractory Brick and Shapes by Boiling Water", ASTM International, 2000.

17. ABAQUS Version 6.9. Manual, Dassault Systèmes, 2009.

18. Kinyanjui, J., "Thermally Induced Changes in the Chemical and Mechanical Properties of Epoxy Foam", Journal of Cellular Plastics. Vol. 46, no. 6, pp. 531-549, 2010.

19. Batallas, B., Yih, H., Singh, P., "Determining the Performance of Polyurethane Foam Pipe Insulation for High Temperature Service", Northern Area Western Conference, Calgary, Alberta, CA, 2006 (http://www.shawpipe.ca/literature/tech/TP_Polyurethane.pdf)

20. C. Mahimkar, V. L. Richards, S.N. Lekakh, "High Temperature Thermo-physical Properties of Ceramic Shell", Missouri University of Science & Technology, ICI, 2009

21. Sabau, A S, Viswanathan, S, "Thermo-physical Properties of Zircon and Fused Silica Based Shells for Investment Casting", Transactions of the American Foundry Society, Vol. 112, No. 04-081, pp 649 - 661, 2004.

22. Niknejad, A, Liaghat, GH, Moslemi, N H, Behravesh, AH, "Theoretical and Experimental Studies of the Instantaneous Folding Force of the Polyurethane Foam-filled Square Honeycombs", Materials and Design. Vol. 32, no. 1, pp. 69-75, January 2011.

APPENDIX B.

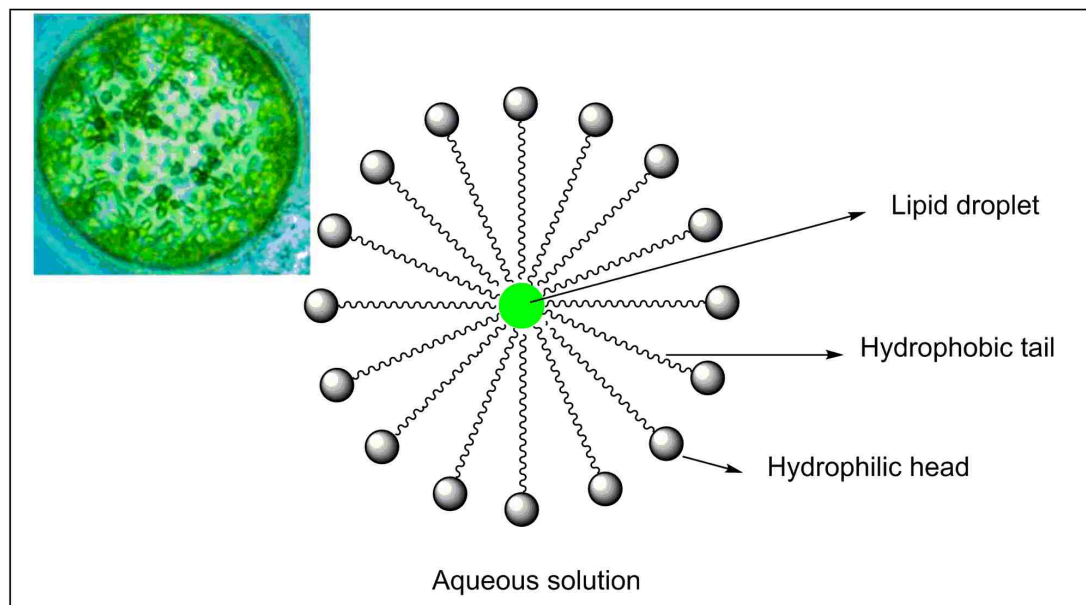**SCHEME OF MICELLE IN AN AQUEOUS SOLUTION**

Figure 1 Scheme of micelle in an aqueous solution

APPENDIX C.

GRAVIMETRIC METHOD FOR LIPIDS EXTRACTION

GRAVIMETRIC METHOD FOR LIPIDS EXTRACTION

By far the best known total lipid extraction method is the Bligh and Dyer method, which has become one of the most recommended methods for determining total lipid. 50mg of freeze-dried algae sample was weight into a vial (W_S) and a mixture of $CHCl_3$-MeOH-H_2O (volume ratio: 1/2/0.5ml) was added. The vial was sonicated for 10 minutes and then centrifuged at 2500rpm for another 10 minutes. The supernatant in the vial was transferred to a large vial. The extraction steps were repeated for 3 times. 4mL H_2O and 3mL $CHCl_3$ were added to the pooled extract in the large vial. The mixture in the vial was shook vigorously and left overnight for separation into two layers. The top layer (mainly H_2O) was removed and discarded. 5mL of H_2O was added to wash the lipid-containing bottom layer (mainly $CHCl_3$). The bottom layer was transferred to a pre-weighed vial (W_V), and 2×1 ml of $CHCl_3$ was used to transfer remaining residue. The $CHCl_3$ was evaporated with gentle heating (~45 $^{\circ}C$) for overnight. The total weight of the vial with lipid (W_{L+V}) was recorded. The percentage of lipid content in microalgae was calculated by the following equation,

Lipid % = ($W_{L+V} - W_V$)/ W_S

APPENDIX D.

SPE FRACTIONATION FOR EXTRACTED LIPIDS

2. Fractionation process

Before the fractionation, the SPE column was conditioned with 10mL chloroform and then approximately 10mg lipids dissolved in 100 μL chloroform was loaded to the column. 10mL chloroform was slowly added to the column and the analyte of non-polar lipid was eluted in a pre-weight vial with the force of gravity. After the elution of non-polar part was finished, a 10mL methanol was gradually added in the SPE column to elute the analyte of polar lipids in another pre-weight vial. The vials filled with non-polar and polar lipids were placed on a heating plate (~45 °C) to evaporate the organic solvents of chloroform and methanol, respectively. Finally the weight of lipids with vial was recorded and the weight percentages of non-polar and polar lipids from the total lipids were calculated. Each sample was performed triplicate.

APPENDIX E.

FAMES ANALYSIS

FAMES ANALYSIS

Microalgal lipids contain primarily polar structural lipids such as phospholipids and glycolipids together with neutral storage lipids such as monoglycerides (MAGs), diglycerides (DAGs) and triglycerides (TAGs). The fatty acids present in triacylglycerol (TAG) are of commercial interest due to their wide applications in transportation fuels, nutraceuticals (ω-3 fatty acids) and food commodities. The fatty acid (FA) composition may differ between lipid classes. A method to determine the content and composition of total fatty acids present in microalgae is described.

1. Lipid derivatization

It is a requirement that the sample to be analyzed should be volatile for GC analysis. Lipid must experience derivation reaction by methylation to form fatty acid methyl esters (FAMEs) in order to enable chromatographic separations. During methylation, lipids are transterified in the presence of a catalyst (alkaline or acids) and a short-chain alcohol that replaces the glycerol moiety. The methylation process was presented in Figure 3.
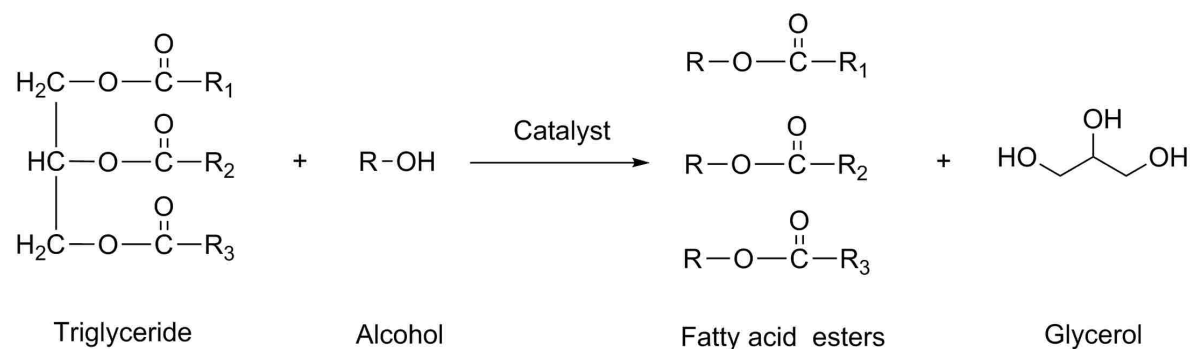

Figure 3 Methylation process of lipids

The use of alkaline catalyst would not be suitable due to the possibility of saponification reaction in the high FFA (free fatty acid) containing oils[13]. In this paper, the inorganic acid, sulphuric acid (H_2SO_4) was chosen to be as catalyst for methylation of the lipid. 5mg lipid sample was dissolved in 1mL toluene, and then 2mL 1% sulfuric acid in methanol was added. The mixture was placed in a stoppered tube and kept in a heating plate at 50 $^{\circ}$C for 24h. After the completion of methylation, 5mL aqueous sodium chloride solution (5%, wt/wt in water) was added in to the mixture and the required methyl ester were extracted with 3mL hexane. Necessary dilutions were made before injection for GC analysis.

2. GC-FID analysis

The FAMEs obtained were separated by gas chromatography (GC) and flame ionization detection (FID) (Perkin Elmer, Autosystem). A GC column of length 30m, ID 0.250mm, film 0.25 μm (J&W, Agilent Technologies) was used with the following time-temperature program: 100-200 $^{\circ}$C at 20 $^{\circ}$C/min, 200-240 $^{\circ}$C at 4 $^{\circ}$C/min, 240 $^{\circ}$C (10min). Helium was used as a carrier gas. Both of the injection and detector temperatures were set at 250 $^{\circ}$C and injection volume was 1 μL. Peak areas were quantified with the AI-450 data stations (Dionex). Standards (Restek Corporation, Bellefonte, PA) containing a total of 6 different FAMEs, including methyl palmitate (C16:0), methyl stearate (C18:0), methyl oleate (C18:1), methyl linoleate (C18:2), methyl linolenate (C18:3) and methyl arachidate (C20:0) were analyzed for provisional peak identification 0.1, 0.2, 0.4, 0.8, 1.0mg/mL of total FAMEs concentration were prepared in order to establish the calibration curve (see Figure 4).
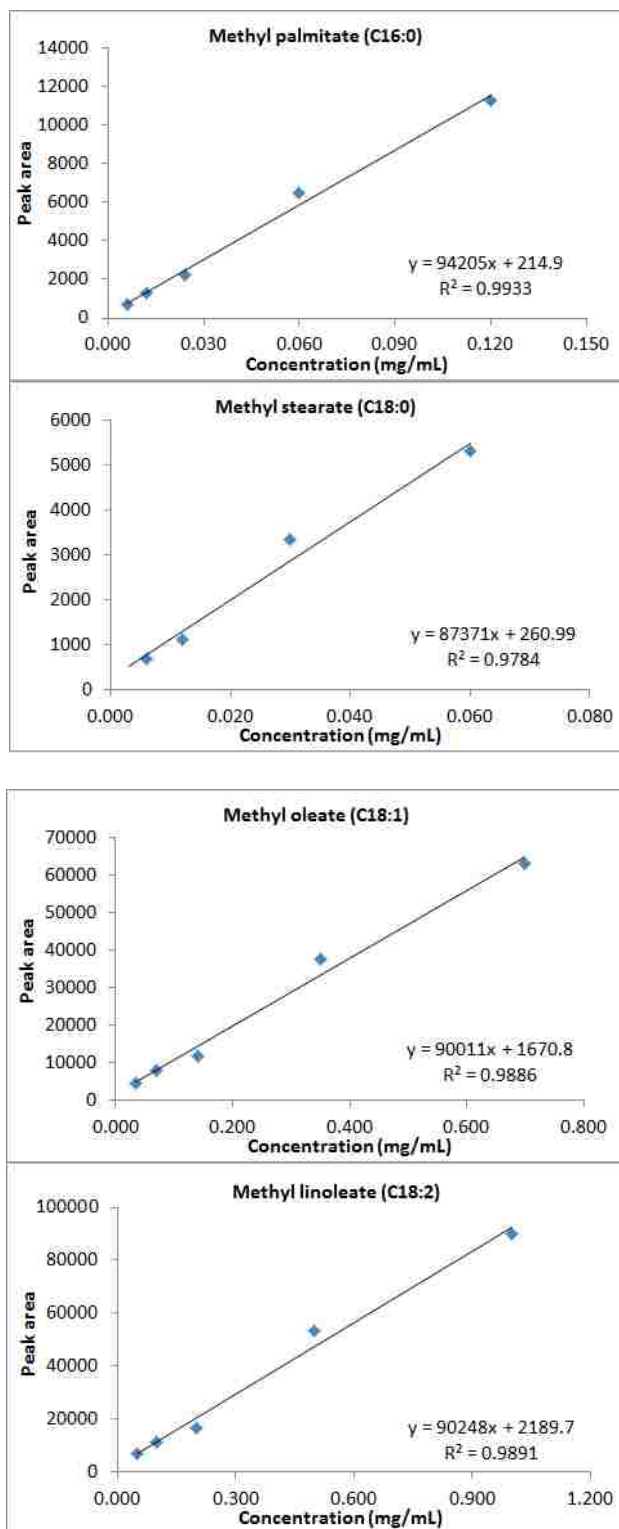
Figure 4 The calibration curves of six FAME standards. Each sample was analyzed in triplicates
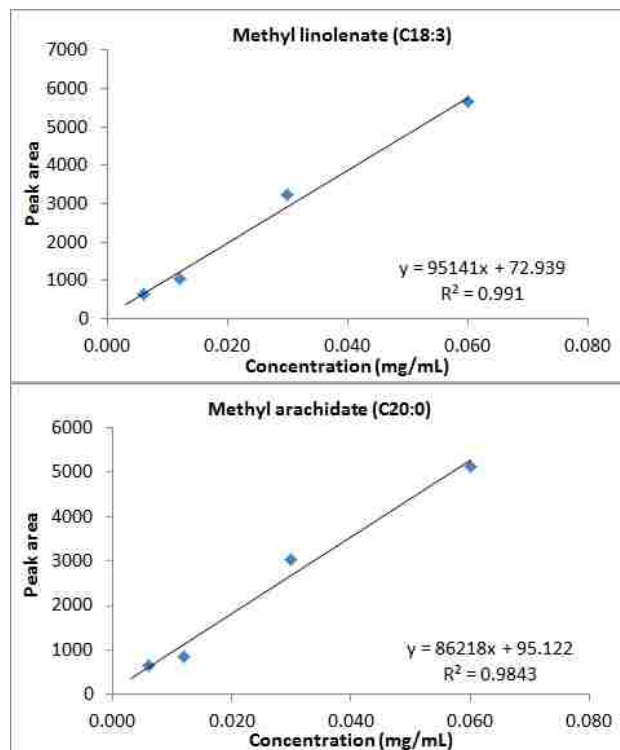
Figure 4 The calibration curves of six FAME standards. Each sample was analyzed in triplicates (cont.)

From Figure 4, there was a good rectilinear response for each individual fatty acid. All correlation coefficient values achieved linearity of greater than 0.980. The composition and content of corresponded fatty acids from the microalgal lipids can be calculated based upon the obtained calibration curves of each fatty acid.

The prepared fatty acid methyl esters were analyzed using GC-FID instrument with the same experiment conditions as for the calibration standards. The GC chromatograms of fatty acid methyl esters from the four different microalgal species were given in Figure 5. It was observed that all the fatty acid peaks were presented in sharp shape and well separated with high resolution. The calculated fatty acid composition as a percentage of total fatty acid was showed in Table 1.

Table 1 Fatty acid composition as a percentage of total fatty acids. Three replicate determinations were performed for each sample.

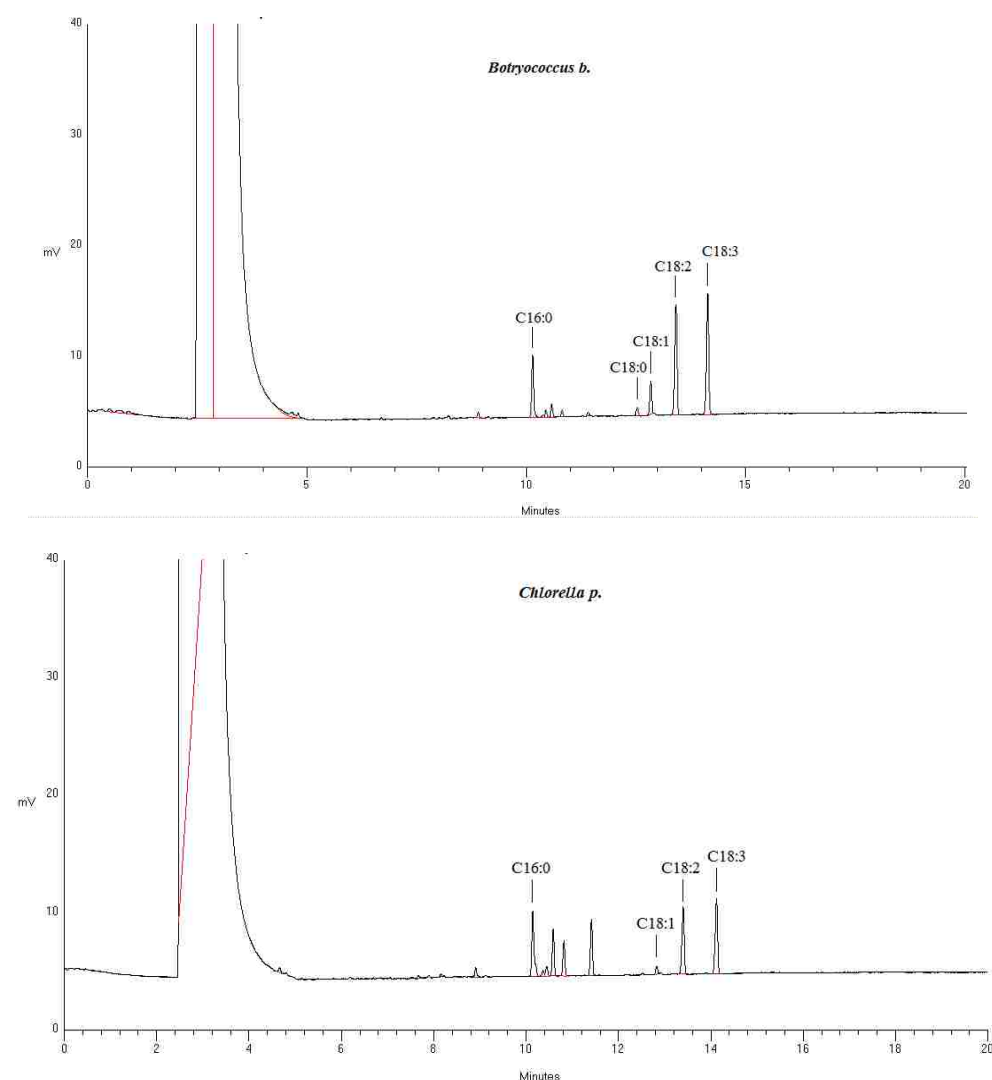|	C16:0	C18:0	C18:1	C18:2	C18:3
Botryococcus b.	9.4±1.0	1.3±0.3	4.4±0.8	19.0±2.3	21.5±1.9
Chlorella p.	4.5±0.6	-	0.1±0.0	4.3±0.3	5.6±0.9
Haemetococcus p.	10.5±0.9	0.6±0.0	3.3±0.1	10.3±1.2	4.0±0.1
Scenedesmus q.	4.6±0.4	-	1.4±0.2	2.2±0.1	8.7±0.6

Figure 5 The GC chromatograms of FAMEs of extracted lipids from microalgae. Each sample was analyzed in triplicates
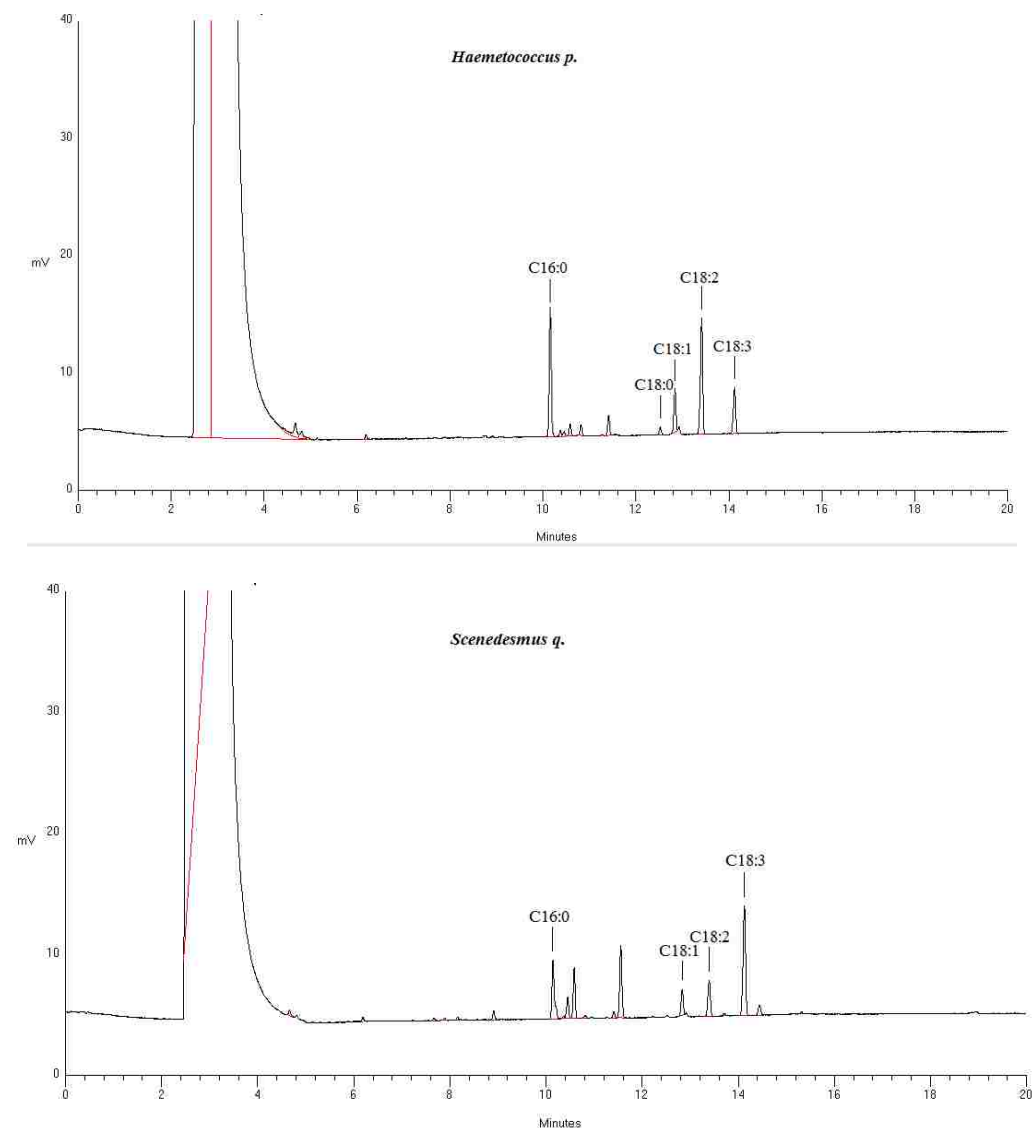
Figure 5 The GC chromatograms of FAMEs of extracted lipids from microalgae. Each sample was analyzed in triplicates (cont.)

The fatty acids C16:0, C18:0, C18:1, C18:2 and C18:3 were all found in these four microalgal species except that the content of methyl stearate (C18:0) was below the detection limit for both *Chlorella p.* and *Scenedesmus q.*. It was also found that all the microalgal species contained few methyl arachidate (C20:0) under the cultivation conditions in the lab.

The storage lipids in *Haemetococcus p.* was found to consist largely of the SAFA palmitic acid, C16:0 (10.5%) and the PUFA methyl linoleate C18:2 (10.3%). It was also revealed that 56% of the total TAGs in *Botryococcus b.* consisted of around 20% of both PUFA C18:2 and C18:3. Thereof, *Botryococcus b.* is a potential candidate resource for preparation of biopolymers, such as polyols, epoxies and polyurethanes.

APPENDIX F.

MAGMASOFT SIMULATIONS OF LOST FOAM CASTING (LFC)

MAGMASOFT SIMULATIONS OF LOST FOAM CASTING (LFC)

To investigate the effects of high temperatures and radiant heat transfer modes present in steel casting. The LFC processes were simulated by using Magmasoft-LostFoam module. The simulation processes were performed changing with two different thickness of coating and three different densities of polystyrene (Table 1). The thermophysical properties of polystyrene used for parameters inputs in the Magmasoft-LostFoam module are listed in Table 2. The steel pouring temperature is 1600 $^{\circ}$C.

Table 1 Coating thickness and polystyrene densities used for Magmasoft simulation

Coating	Thickness (mm)	Gas permeability
	0.1	0.1
	0.2	0.02
Polystyrene	Density (Kg/m^3)	
	25	
	57	
	73	

A simple geometry modeling of steel LFC is showed in Figure 1. The LFC simulation results of polystyrene with three different foam densities and two coating thickness are displayed in the Figure 2 and 3, respectively. It showed that foam densities and coating properties are the factors which can influence the filling process. The LFC process with higher density of foam needs more time to fill. The thicker coating or low permeability of coating could slow the LFC process.

Table 2 The thermophysical properties of polystyrene used for Magmasoft simulation

| Property	Value	Unit
Glass transition temperature	80	$^\circ$C
Vaporization temperature	200	$^\circ$C
Density of solid foam	25, 57, 73	Kg/m^3
Density of liquid foam	1000	Kg/m^3
Density of vapor foam	1.2	Kg/m^3
Heat Conductivity of solid	0.045	W/m K
Heat Conductivity of liquid	0.075	W/m K
Heat Conductivity of vapor	0.02	W/m K
Specific heat of solid	1700	J/kg K
Specific heat of liquid	1700	J/kg K
Specific heat of vapor	1000	J/kg K
Activation Energy	113044	J/ mol
Reaction frequency factor	6×10^8	1/s
Vaporization enthalpy	499005	J/kg
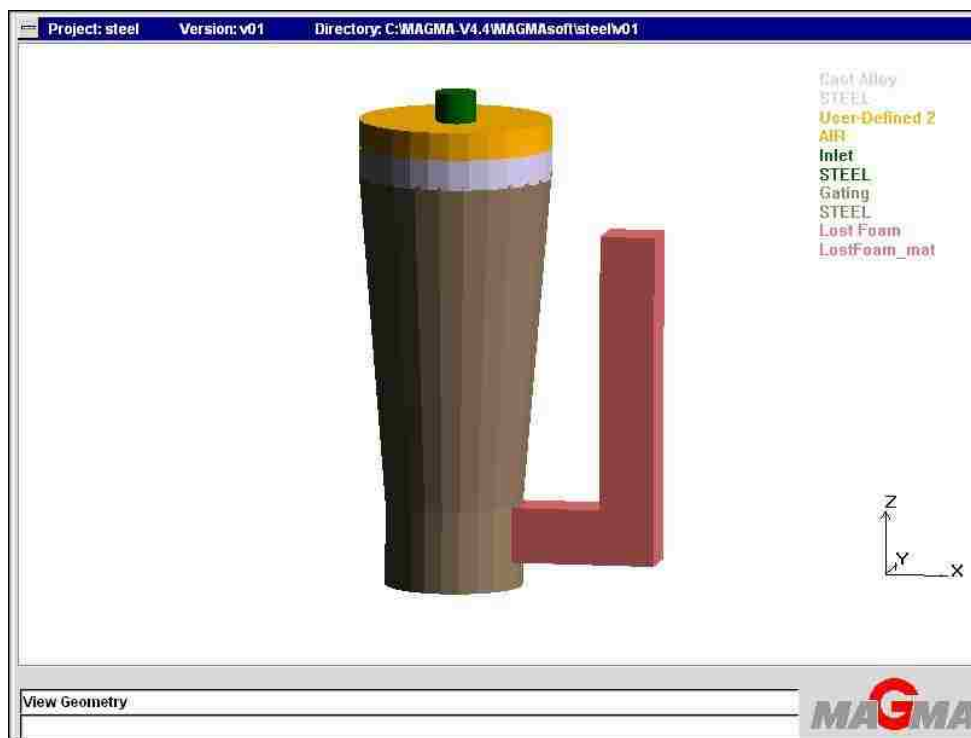
Figure 1 A simple geometry modeling of steel LFC

Figure 2 The resulting temperature distribution of the melt and receding polystyrene foam at a particular time (0.5, 1.7, 2.8, 3.9, and 5s, respectively from top to bottom). The density of polystyrene was 25, 57, and 73Kg/m^3, respectively from left to right. The coating thickness was 0.1mm.
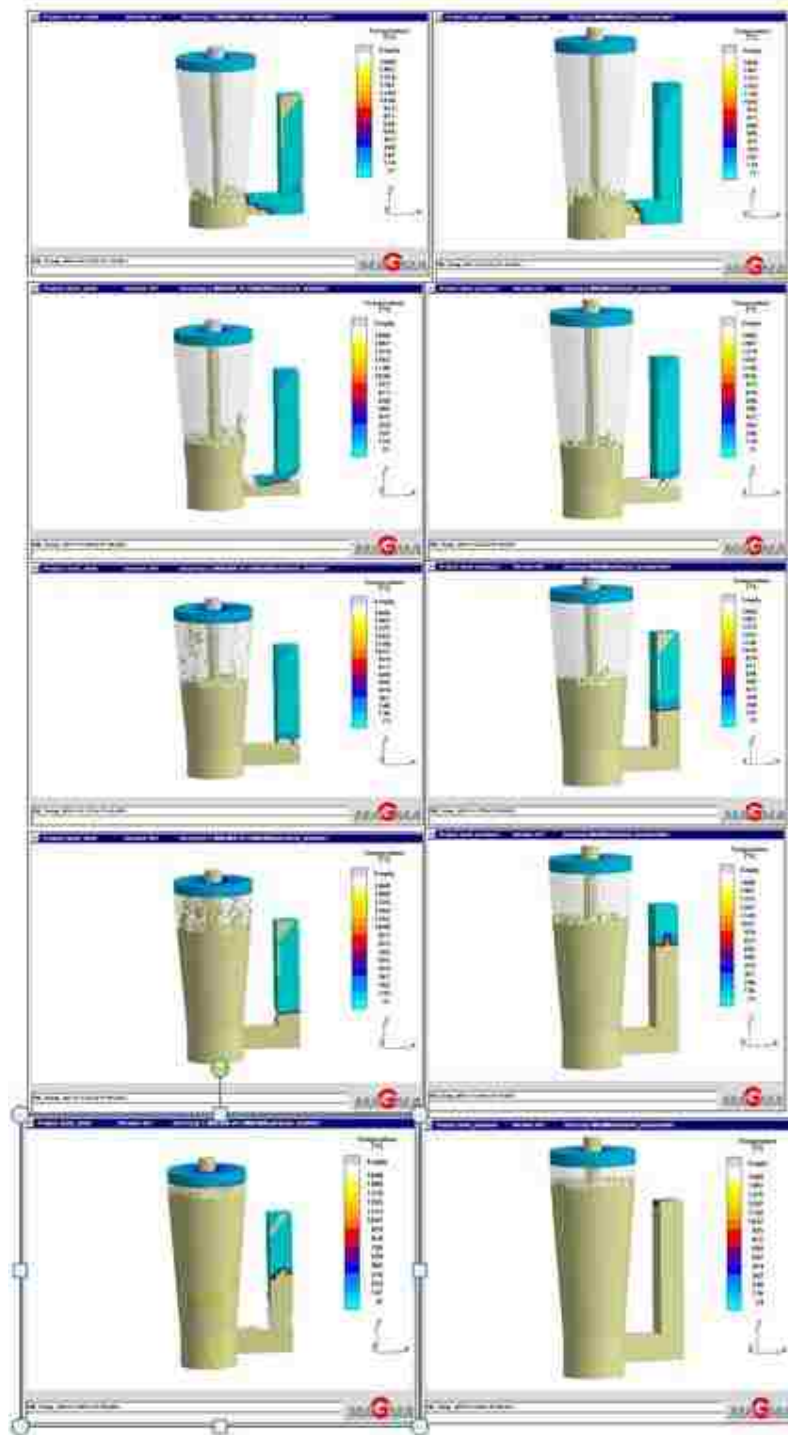
Figure 3 The resulting temperature distribution of the melt and receding polystyrene foam at a particular time (0.5, 1.7, 2.8, 3.9, and 5s, respectively from top to bottom). The density of polystyrene was 25Kg/m^3. The coating thickness was 0.2 and 0.1mm, respectively from left to right.

VITA

Hongfang Zhao was born in Baotou, Inner Mongolia, China. She received her Bachelor's degree in Chemistry from Inner Mongolia Normal University, Hohhot, China in 2005. In 2008, Hongfang obtained her Master degree in Physical Chemistry from Taiyuan University of Technology, Taiyuan, China. Upon completion, Hongfang joined Missouri University of Science and Technology to purse her PhD degree in Chemistry in January 2009 and begun her doctoral studies under the direction of Dr. Paul Nam. She interned with the Goodyear Tire and Rubber Company in the summer of 2012. Hongfang has served as a session co-chair of the 104th AOCS (American Oil Chemists' Society) Annual Meeting & Expo in Montreal, Canada in 2013. She completed her PhD requirements in chemistry in August 2014.